Department of Mathematics and Applied Mathematics

MAM5001W

University of Cape Town

Leveraging Numerical Relativity Formulations for Perturbative Analysis: Applications to quasinormal modes in general relativity

Author: Sipho Nkele

Supervisor:
Dr Bishop Mongwane

June 12, 2025

Contents

Abstract

Numerical relativity has become an essential tool for studying highly dynamic and strong-field regimes of general relativity, enabling the simulation of compact object mergers, gravitational collapse, and other nonlinear phenomena. At the same time, perturbation theory provides a powerful analytical framework for understanding small deviations from equilibrium configurations, offering insights into gravitational wave emission, stability, and fundamental mode structures of relativistic systems. Despite their complementary strengths, numerical relativity and perturbation theory are often treated as distinct approaches, with limited interaction between them. Bridging this gap is crucial for improving our ability to extract physical information from numerical simulations and for validating approximations used in perturbative studies. In this work, we study two key problems on quasinormal modes of compact objects, as a case study in unifying numerical relativity with perturbation theory.

We discuss a new approach for analyzing linearized perturbations of a Schwarzschild black hole using the characteristic formulation of numerical relativity, focusing on the computation of quasinormal modes (QNMs). Unlike traditional methods based on the Regge-Wheeler and Zerilli equations, this approach focuses on deriving the master equation governing gravitational perturbations within the characteristic formulation of numerical relativity. We analyze the singular points of this equation, and we derive series solutions with coefficients determined by three-term recurrence relations. These allow for the application of Leaver's continued fraction method, leading to the standard Schwarzschild quasinormal modes (QNMs).

In addition, we investigate linearized ADM perturbations on a Tolman-Oppenheimer-Volkoff (TOV) background solution to study radial perturbations. Within this framework, the perturbation equations take the form of three coupled partial differential equations, in contrast to the usual Sturm-Lioville problem that arises in the traditional approach. Using the Weighted Essentially Non-Oscillatory (WENO) finite difference method, we analyze three models derived from a polytropic equation of state: one stable, one marginally stable near the onset of instability, and one unstable. Our results consistent with those derived from standard methods, confirming the expected stability characteristics of these models.

Declaration

This thesis incorporates research conducted by the author at the University of Cape Town under the supervision of Dr. Bishop Mongwane. Chapter 6 is based on the listed publication:
"Quasinormal modes of a Schwarzschild black hole within the Bondi-Sachs framework"
Mongwane, Bishop and Nkele, Sipho and Duniya, Didam G. A. and Bishop, Nigel T.
Journal-ref: Phys. Rev. D 111, 044002 (2025)

I hereby certify that this thesis is my original work and has not been submitted, in the same or any other form, to this or any other university for the purpose of obtaining a degree.

Signed by candidate

2025-02-16

Acknowledgment

I am profoundly grateful to my supervisor, Dr. Bishop Mongwane, for his exceptional patience, guidance, and unwavering support throughout the completion of this Master's thesis. His dedication and commitment have been invaluable in shaping my understanding and approach to research. I am especially grateful for his in-depth lessons on key concepts in the field and scientific writing, which have greatly contributed to my academic development. I am very thankful for this opportunity and for making this an incredible experience.

I would also like to especially thank my mother, Ntombomzi Nkele, and my father Mbangiswa Nkele for their unwavering support and encouragement, as well as my siblings for always standing by me throughout this journey. Finally, I am grateful to my scholarship, Exness, for their financial support, which made this research possible.

Chapter 1

Introduction

Numerical relativity has emerged as a critical field within gravitational physics, providing tools to solve Einstein's field equations in cases where analytical solutions are not feasible [85]. These equations describe the fundamental relationship between spacetime geometry and the distribution of matter and energy, but their inherent nonlinearity and complexity necessitate numerical approaches for many realistic astrophysical phenomena [67]. Among the key areas of interest in numerical relativity are neutron stars and black holes, both of which serve as laboratories for testing the predictions of general relativity and understanding the physics of strong gravitational fields.

This work investigates two key problems in numerical relativity, the radial oscillations of relativistic stars via the ADM formalism and the QNMs of Schwarzschild black holes. The TOV equations are used as a background solution to the ADM perturbations, providing 3 Models of neutron stars necessary for studying their stability [85, 67, 4, 21, 15]. The study of black holes and neutron stars has gained significant importance, especially with the detection of gravitational waves by LIGO and Virgo [3, 2]. Quasinormal modes (QNMs) of black holes characterize the ringdown phase of black hole mergers, while QNMs of neutron stars can reveal insights into their internal structure and equation of state. Numerical relativity plays a crucial role in modeling these phenomena, allowing for precise waveform predictions that can be compared with observational data from observatories like LIGO and Virgo.

Like most other fields, numerical relativity faces its own challenges such as maintaining numerical stability during evolution, handling black hole singularities, minimizing the computational costs of 3D simulations, and ensuring that the Hamiltonian and Momentum constraints are preserved at each hypersurface. While full numerical simulations are essential for modeling mergers, perturbation

theory is also critical in providing analytical insights into the late-time behavior of compact objects, such as quasinormal modes of black hole and quasinormal modes of neutron stars. Bridging numerical relativity and perturbation theory is crucial for improving accuracy and efficiency, leading to a deeper understanding of general relativity.

Before, we focus on two of the most widely studied problems in the field (Chapter 5, Chapter 6), we will outline few key Chapters. Preliminaries Chapter 2 reviews fundamental concepts in general relativity required for the thesis. It introduces notations, conventions, and key equations, including the Einstein field equations 2.16. The Schwarzschild solution is presented and discussed as a background for later studies. Chapter 3 discusses numerical relativity formalisms used in the development of numerical codes. The ADM formulation 3.1 is introduced, along with its decomposition of spacetime into hypersurfaces. Gauge conditions are discussed, including geodesic slicing 3.2.1, maximal slicing 3.2.2, and Bona-Masso slicing 3.2.4. The BSSN formulation (see Section 3.3) is presented as an improvement over ADM for numerical stability. Finally, the characteristic formulation 3.4 is introduced, which decomposes spacetime using null hypersurfaces and leads to the Bondi-Sachs metric. Chapter 4 describe the structure of static, spherically symmetric neutron stars in general relativity. The derivation of the TOV equations 4.41 is presented, along with the role of the equation of state (EOS) 4.42 in modeling neutron star matter.

On the main chapters, the first Chapter 5 examines radial perturbations of neutron stars by linearizing the ADM equations and imposing boundary conditions. Numerical methods are used to evolve the resulting perturbation equations to compute eigenfrequencies and analyze their dependence on the equation of state (EOS). The second Chapter 6 explores the QNMs of Schwarzschild black holes. The master equation governing gravitational perturbations is derived using the characteristic formulation of numerical relativity. Leaver's continued fraction method is used to compute QNM frequencies, extracting the fundamental oscillation and damping rates. The algebraically special mode is also examined within the Bondi-Sachs framework.

Chapter 2

Preliminaries

2.1 Notations and Conventions

- We use the signature $(-,+,+,+)$ for the metric.
- We employ geometrized units such that $G = c = 1$.
- In situations where ambiguities may arise, we designate ${}^{(4)}A_{ab}$ for 4-dimensional tensors and ${}^{(3)}A_{ab}$ for 3-dimensional tensors

Commonly used Acronyms:

ADM	Arnowitt-Deser-Misner
BSSN	Baumgarte-Shapiro-Shibata-Nakamura
EFE	Einstein Field Equation
PDE	Partial Differential Equation
EOS	Equation of State
ODE	Ordinary Differential Equation
QNM	Quasinormal Mode
TOV	Tolman-Oppenheimer-Volkoff
BBH	Binary Black Hole

Tensor symmetries:

$$S_{[ab]} = \frac{1}{2}(S_{ab} - S_{ba}) \tag{2.1}$$

$$S_{(ab)} = \frac{1}{2}(S_{ab} + S_{ba}) \tag{2.2}$$

2.2 Einstein Field Equations

The Einstein Field Equations (EFE), is a set of ten nonlinear partial differential equations that form the core of Einstein's General Theory of Relativity [103, 105, 47]. Published by Einstein in 1915, these equations relate the geometry of spacetime to the distribution of matter within it [105, 20, 103, 47]. In this chapter, we provide a brief summary of some key concepts in general relativity that are utilized in this thesis. For two events in 4 dimensional spacetime the invariant interval ds^2 between them is represented by the line element [102, 35, 46, 72]

$$ds^2 = g_{ab}dx^a dx^b, \tag{2.3}$$

where g_{ab} is the 4-dimensional metric tensor. In this spacetime, we can observe how a tensor ${}^{(4)}A_{ab}$ behaves when it is parallel transported along a path. This process involves comparing the tensor's components at different points in a way that accounts for the curvature of spacetime. To formalize this comparison, we introduce the concept of the covariant derivative,

$$\nabla_c T^a{}_b = \partial_c T^a{}_b + {}^{(4)}\Gamma^a{}_{dc} T^d{}_b - {}^{(4)}\Gamma^d{}_{bc} T^a{}_d. \tag{2.4}$$

Here, ${}^{(4)}\Gamma^b{}_{ac}$ are the Christoffel symbols related to the metric g_{ab}. They describe how the basis vectors and their corresponding co-vectors change under parallel transport [35]. They are defined in terms of the metric by,

$${}^{(4)}\Gamma^b{}_{ac} = \frac{1}{2} g^{bd}(\partial_c g_{da} + \partial_a g_{dc} - \partial_d g_{ac}), \tag{2.5}$$

where g^{ab} is the inverse metric such that

$$g^{ab} g_{ab} = \delta^a{}_a. \tag{2.6}$$

For the flat spacetime the metric g_{ab} is given by the Minkowski metric

$$\eta_{ab} = \mathrm{diag}(-1, 1, 1, 1), \tag{2.7}$$

In curved spacetime, a crucial variable that describes curvature in the gravitational field is the Riemann curvature tensor ${}^{(4)}R^a{}_{bcd}$, which is defined by [20]

$${}^{(4)}R^a{}_{bcd} = \partial_c {}^{(4)}\Gamma^a{}_{bd} - \partial_d {}^{(4)}\Gamma^a{}_{bc} + {}^{(4)}\Gamma^a{}_{ec} {}^{(4)}\Gamma^e{}_{bd} - {}^{(4)}\Gamma^a{}_{ed} {}^{(4)}\Gamma^e{}_{bc}. \tag{2.8}$$

In flat space, where the metric tensor g_{ab} equals the Minkowski metric η_{ab}, the Riemann tensor ${}^{(4)}R^{a}{}_{bcd}$ vanishes. A notable property of the Riemann tensor is that the cyclic sum of its last three lowered indices equals zero,

$$ {}^{(4)}R_{abcd} + {}^{(4)}R_{adbc} + {}^{(4)}R_{acdb} = 0. \tag{2.9} $$

There is also a symmetry in the interchange of pairs of indices [20]

$$ {}^{(4)}R_{abcd} = -{}^{(4)}R_{bacd}, \qquad {}^{(4)}R_{abcd} = -{}^{(4)}R_{abdc}, \qquad {}^{(4)}R_{abcd} = {}^{(4)}R_{cdab}. \tag{2.10} $$

and the Bianchi identity

$$ \nabla_{[a}{}^{(4)}R_{bc]de} = 0. \tag{2.11} $$

Then Ricci tensor is defined by taking the trace of the Riemann tensor

$$ {}^{(4)}R_{ab} = {}^{(4)}R^{c}{}_{acb}, \tag{2.12} $$

due to the symmetries of the Riemann tensor, 2.11 is the only independent contraction. The Ricci scalar is the defined by taking the trace of the Ricci tensor,

$$ {}^{(4)}R = {}^{(4)}R^{a}{}_{a}. \tag{2.13} $$

Consider the Bianchi identity 2.10 contracted with the inverse metric g^{ec} and g^{ad}, as well as applying the anti-symmetry of the Riemann tensor on ${}^{(4)}R_{abde}$ as

$$ g^{ec}g^{ad}\left(\nabla_{a}{}^{(4)}R_{bcde} + \nabla_{b}{}^{(4)}R_{\text{cade}} + \nabla_{c}{}^{(4)}R_{abde}\right) = 0, \tag{2.14} $$

gives the equation

$$ \nabla^{a}\left(2{}^{(4)}R_{ba} - g_{ab}{}^{(4)}R\right) = 0. \tag{2.15} $$

The term within the parentheses is referred to as the Einstein tensor defined as [11]

$$ G_{ab} = {}^{(4)}R_{ab} - \frac{1}{2}g_{ab}{}^{(4)}R, \tag{2.16} $$

and its symmetry arises from the symmetry of the Ricci tensor. The Einstein field equations relate the geometry of spacetime to the matter distribution through the equation,

$$ G_{ab} = \kappa T_{ab}, \tag{2.17} $$

where G_{ab} is given by 2.15, T_{ab} is the energy momentum tensor, and κ=8π is a constant whose value is determined by the requirement that, in the weak field limit, Einstein's equations must simplify to the Poisson equation, which determines that κ is 8π in geometrized units. The local conservation equation of the energy-momentum tensor is expressed as,

$$\nabla^a T_{ab} = 0. \tag{2.18}$$

For a perfect-fluid the energy-momentum tensor is defined as

$$T_{ab} = (\rho + p)u_a u_b + p g_{ab}. \tag{2.19}$$

In this context, ρ represents the matter energy density, p denotes pressure, and the four-velocities u^a are timelike vectors. So the final form of the Einstein field equations is,

$$G_{ab} = 8\pi T_{ab}. \tag{2.20}$$

Another approach to deriving the Einstein field equations involves the use of the Einstein-Hilbert action, which is the most commonly employed method in modern treatments of general relativity. The Einstein-Hilbert action is a variational principle that expresses the action for gravity in terms of the metric tensor gab and the Ricci scalar R, given by,

$$S = \frac{1}{16\pi G} \int \sqrt{-g} R d^4x. \tag{2.21}$$

Applying the principle of least action to this action, one derives the equations of motion, which lead directly to the Einstein field equations

$$G_{ab} = \kappa T_{ab}. \tag{2.22}$$

This approach not only provides a clear derivation of the field equations but also connects them to the fundamental principles of variational mechanics. In addition, this approach is indispensable in modified gravity theories, as it allows for the systematic derivation of field equations even when the gravitational action is extended or modified to include additional terms or alternative formulations of gravity [104, 50, 47]

2.3 Schwarzschild Solution

One of the most important solutions of the field equations is the Schwarzschild solution. It is a fundamental result in general relativity, describing the spacetime geometry surrounding a static, spherically symmetric, non-rotating object. It is derived by solving Einstein's field equations under the assumption of vacuum and spherical symmetry. The Schwarzschild metric, represented in spherical coordinates (t, r, θ, ϕ), is formulated as

$$ds^2 = -\left(1 - \frac{2M}{r}\right) dt^2 + \left(1 - \frac{2M}{r}\right)^{-1} dr^2 + r^2 d\theta^2 + r^2 \sin^2\theta \, d\phi^2. \tag{2.23}$$

This solution is valid in the exterior region of any spherically symmetric spacetime, including those containing matter. Therefore, it applies to the vacuum exterior of static or spherically symmetric collapsing stars. According to Birkhoff's theorem, any spherically symmetric solution to the vacuum Einstein field equations is both static and asymptotically flat. Consequently, the Schwarzschild metric describes the gravitational field outside any spherically symmetric, non-rotating mass (such as a star or black hole), regardless of its internal structure.

Using the transformation law

$$g'_{\alpha\beta} = \frac{\partial x^\mu}{\partial x'^\alpha} \frac{\partial x^\nu}{\partial x'^\beta} g_{\mu\nu}, \tag{2.24}$$

the Schwarzschild metric can be expressed in different coordinate systems, depending on the specific problem being addressed. Other forms of the Schwarzschild metric, such as the isotropic radial coordinates, are particularly useful in numerical computations [21]. The Schwarzschild metric in its isotropic form is given by

$$ds^2 = -\left(\frac{1 - M/2\bar{r}}{1 + M/2\bar{r}}\right)^2 dt^2 + \left(1 + \frac{M}{2\bar{r}}\right)^4 \left[d\bar{r}^2 + \bar{r}^2 \left(d\theta^2 + \sin^2\theta \, d\phi^2\right)\right], \tag{2.25}$$

where the relationship between areal and isotropic radius is

$$r = \bar{r}\left(1 + \frac{M}{2\bar{r}}\right)^2. \tag{2.26}$$

In outgoing Eddington-Finkelstein coordinates, the Schwarzschild metric is transformed by replacing the Schwarzschild time coordinate t with the null coordinate u, defined as

$$u = t + r_*, \tag{2.27}$$

where r_* is the tortoise coordinate

$$r_* = r + 2M \ln \left| \frac{r}{2M} - 1 \right| . \tag{2.28}$$

The metric in outgoing Eddington-Finkelstein coordinates becomes

$$ds^2 = -\left(1 - \frac{2M}{r}\right) du^2 + 2\, du\, dr + r^2 \left(d\theta^2 + \sin^2\theta\, d\phi^2\right) . \tag{2.29}$$

This form eliminates the coordinate singularity at $r = 2M$ and is well-defined across the event horizon. Outgoing null geodesics follow constant u, making the metric particularly convenient for analyzing the causal structure and outgoing radiation in black hole spacetimes. Additionally, it is frequently used in characteristic formulations of general relativity [6]. This metric form serves as the background solution utilized in the QNM Chapter 6.

Chapter 3

3+1 and 2+1+1 Formulations

This chapter provides a concise introduction to the significant formalisms that have been developed over the years to address numerical difficulties in the field of numerical relativity. This introduction commences by discussing the initial formalism that employs the 3+1 decomposition of spacetime, followed by a concise reference to other formalisms [69, 37, 32, 37, 89].

3.1 ADM Formulation

3.1.1 Foliation of spacetime

The 3+1 formulation is a framework within numerical relativity that divides spacetime into non-intersecting space-like hypersurfaces. This approach allows for the formulation of Einstein's equations as a Cauchy problem with constraints that must be satisfied at each hypersurface [57, 20, 69, 32, 4]. Spacetime is a 4-dimensional manifold $(\mathcal{M}, g_{ab})$ where each event is characterized by a coordinate system, consisting of 1 dimension of time and 3 dimensions of space. To conduct physical simulations and take advantage of the simplicity of implementing numerical algorithms for hyperbolic partial differential equations, it is possible to divide spacetime into separate components of time and space [85, 21, 69, 8]. This concept involves dividing spacetime into a series of non-intersecting hypersurfaces Σ 3.1.

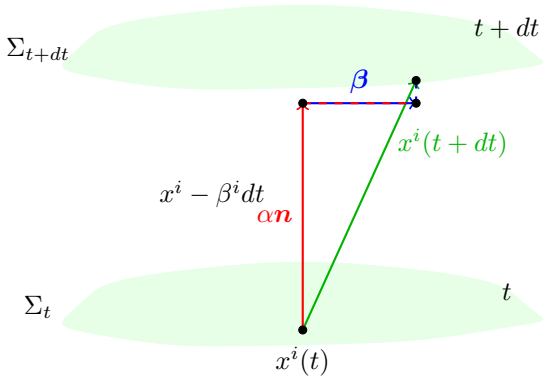

Figure 3.1: Representation of the geometric decomposition of spacetime, illustrating the evolution of a spatial hypersurface Σ_t to Σ_{t+dt}. The lapse function α governs the orthogonal separation between hypersurfaces, while the shift vector β^i accounts for the spatial displacement of coordinates. The combined motion results in the displacement from $x^i(t)$ to $x^i(t+dt)$.

Each hypersurface Σ_t is defined by a scalar function t. The initial hypersurface Σ_0 is associated with the initial data, which serves as the starting point for the spacetime. The unit normal vector n^a, resulting from the spacetime foliation, is orthogonal to each hypersurface and is related to the gradient of t, as [66, 20]

$$n^a = -\alpha g^{ab} \nabla_b t. \tag{3.1}$$

The symbol α, referred to as the lapse function, is used to normalize the gradient. This function quantifies the proper time of an orthogonal observer between two consecutive hypersurfaces. In order to normalise the vector mentioned above 3.1, it needs to be adjusted in a manner that satisfies the criterion $n^a n_a = -1$ for timelike four vectors. This condition can be achieved using the following calculations:

$$\begin{aligned} n^a n_a &= \Big(-\alpha g^{ab} \nabla_a t\Big)\Big(-\alpha g^{ab} \nabla_b t\Big) \\ &= \alpha^2 g^{ab} (\nabla_a t)(\nabla_b t) = -1. \end{aligned} \tag{3.2}$$

The expression for α can be determined as.

$$\alpha = (-g^{ab} (\nabla_a t)(\nabla_b t))^{-1/2}. \tag{3.3}$$

However, a challenge arises when constructing the normal vector and its one-form because they do not indicate the direction of the temporal derivatives. Therefore, it becomes necessary to build a new vector that will have a normalization constant of one when combined with the one-form. Subsequently, we can employ the function t discussed previously to establish the coordinate system.

Within this system, the congruent time lines that intersect the hypersurfaces Σ_t are characterised by the vector field [21, 4]

$$t^a = \alpha n^a + \beta^a. \tag{3.4}$$

In this manner, a new variable, the shift vector is introduced. The shift vector, denoted as β^a, is a spatial vector. It is used to quantify the displacement of the worldline followed by an observer between two adjacent hypersurfaces, relative to the unit normal vector n^a. The concept of orthogonality arises from tensor algebra and the presence of the metric tensor g_{ab} [21, 4, 35]. In this context, the condition $\vec{a} \cdot \vec{b} = 0$ indicates that the two vectors are orthogonal to each other. This implies that it is possible to define a projection operator that is orthogonal to a specific unit vector, denoted as $\vec{v}$. The projection operator can be expressed as follows,

$$P^a{}_b = \delta^a{}_b - v^a v_b. \tag{3.5}$$

Based on the information provided above, we can derive the spatial projection operator for the unit timelike vector as follows,

$$P^a{}_b \equiv \gamma^a{}_b = g^a{}_b + n^a n_b = \delta^a{}_b + n^a n_b. \tag{3.6}$$

A projection operator along the timelike direction can also be defined as

$$N^a{}_b = -n^a n_b = \delta^a{}_b - \gamma^a{}_b. \tag{3.7}$$

These two projection operators are orthogonal to each other, i.e

$$\begin{aligned} \gamma^a{}_b N^b{}_c &= (\delta^a{}_b + n^a n_b)(-n^b n_c) \\ &= -\delta^a{}_b n^b n_c - n^a n_b n^b n_c \\ &= -n^a n_c + n^a n_c \\ \gamma^a{}_b N^b{}_c &= 0. \end{aligned} \tag{3.8}$$

This implies that the spacetime metric g_{ab} gives rise to a spatial metric denoted by γ_{ab}. By employing the projection operator, we get the spatial metric as

$$\begin{aligned} \gamma_{ab} &= g_{ad}\gamma^d{}_b \\ &= g_{ad}\delta^d{}_b + g_{ad}n^d n_b \\ \gamma_{ab} &= g_{ab} + n_a n_b, \end{aligned} \tag{3.9}$$

and the inverse of the spatial metric is

$$\gamma^{ab} = g^{ac} g^{bd} \gamma_{cd} = g^{ab} + n^a n^b. \tag{3.10}$$

Within this formalism, a general line element is expressed as [29, 11, 20, 4, 21]

$$ds^2 = -\alpha^2 dt^2 + \gamma_{ij}(dx^i + \beta^i dt)(dx^j + \beta^j dt). \tag{3.11}$$

The spatial metric γ_{ab} quantifies the distances within each individual hypersurface in our foliated spacetime, in contrast to the spacetime metric g_{ab} which quantifies distances in the entirety of spacetime. Having established the definitions of spatial and time projection operators, we now possess the means to break down 4-dimensional tensors into distinct spatial components. An arbitrary rank-2 tensor T_{ab}, can be decomposed into solely spatial components as

$$\perp T_{ab} = \gamma_a^c \gamma_b^d T_{cd}, \tag{3.12}$$

where the equation represents the pure spatial projection, denoted by the symbol $\perp$ [4, 21]. This choice is made for convenience in order to eliminate the need for complex projections. For every vector u^a, it is possible to divide it into components that are purely spatial and components that are timelike,

$$\begin{aligned} u^a &= \delta^a_b u^b = (\gamma^a{}_b + N^a{}_b) u^b = \gamma^a{}_b u^b - n^a n_b u^b \\ &= \perp v^a - n^a n_b u^b. \end{aligned} \tag{3.13}$$

A spacetime metric on a specific manifold permits the establishment of a distinct covariant derivative. The 3-dimensional covariant derivative is a function that takes spatial tensors as input and produces spatial tensors as output. The spatial covariant derivative, denoted as D_a, is obtained by projecting all indices of the 4-dimensional covariant derivative onto a hypersurface Σ.

$$D_a T^b_c = \gamma^d_a \gamma^b_e \gamma^f_c \nabla_d T^e_f. \tag{3.14}$$

By definition, $D_a T^a_c$ is a spatial tensor that is consistent with the spatial metric γ_{ab}, meaning that $D_a \gamma_{bc} = 0$. The connection coefficient can also be defined in this context as

$${}^{(3)}\Gamma^a{}_{bc} = \frac{1}{2} \gamma^{ad} (\partial_c \gamma_{db} + \partial_b \gamma_{dc} - \partial_d \gamma_{bc}). \tag{3.15}$$

Similarly we define the 3-dimensional Riemann tensor as

$$D_a D_b V_c - D_b D_a V_c = {}^{(3)}R^d_{cba} V_d. \tag{3.16}$$

This is defined for every spatial component, but index d leaves out the time component to be defined again as ${}^{(3)}R^d_{cba} n_d = 0$. The contraction of the Riemann tensor ${}^{(3)}R^d_{adb}$ gives the 3-dimensional Ricci tensor ${}^{(3)}R_{ab}$, and Ricci scalar ${}^{(3)}R = {}^{(3)}R_{ab}\gamma^{ab}$. However, this only describes the intrinsic curvature of each hypersurface but does not provide information about how each hypersurface Σ_t is mapped into $(\mathcal{M}, g_{ab})$. To obtain this information, another tensor is introduced, known as the extrinsic curvature tensor, which is given by

$$K_{ab} = -\gamma^c_a \gamma^d_b \nabla_c n_d. \tag{3.17}$$

The tensor is symmetric on the indices a and b, and it is purely spatial, as the contraction of the tensor and the unit normal vector result in $n^a K_{ab} = -\gamma^c_a \gamma^d_b \frac{1}{2} \nabla_c (n_d n^a) = 0$. Expanding the above equation 3.17 using the spatial projection operator and the identity $n^d \bigtriangledown_c n_d = 0$ gives

$$K_{ab} = -(\delta^c_a + n_a n^c)(\delta^d_b + n_b n^d) \bigtriangledown_c n_d = -(\delta^c_a + n_a n^c)\delta^d_b \bigtriangledown_c n_d = - \bigtriangledown_a n_b - n_a a_b,$$

this can be reformulated as [110]

$$K_{ab} = -\frac{1}{2}\mathcal{L}_n \gamma_{ab}. \tag{3.18}$$

The operator $\mathcal{L}_n$ represents the Lie derivative in the direction of the normal vector n^a. The extrinsic curvature tensor measures the normal vector changes from point to point on a given hypersurface, while also measuring the rate at which the hypersurface deforms when it is carried along the normal vector, this gives an understanding of how curvature is measured as one moves from one hypersurface to the other. Finally we introduce the extrinsic curvature scalar,

$$K = \gamma^{ab} K_{ab}. \tag{3.19}$$

The quantity K represents change of the 3D volume along the normal vector n^a as one moves from a hypersurface Σ_t to the next Σ_{t+1}. With this we have all the 3-dimensional tensors that describe our hypersurface Σ_t as $\{\gamma_{ab}, {}^{(3)}\Gamma^d{}_{ab}, {}^{(3)}R^a{}_{bced}, K_{ab}, K\}$, and the covariant derivative D_a certifies the spatial metric $D_i \gamma_{ab} = 0$. To complete the mathematical background for 3+1 decomposition, we present the Gauss, Godazzi and Ricci relations, as they will enable us to write down the field equations in terms of $3+1$ quantities.

3.1.2 The equations of Gauss, Codazzi and Ricci

The primary objective is to break down the Einstein's field equations 2.19 in terms of 3+1 quantities. For this purpose, we start with the Riemann tensor and expressed it as

$$\begin{aligned}
{}^{(4)}R_{abcd} &= g^{p}{}_{a}g^{q}{}_{b}g^{r}{}_{c}g^{s}{}_{d}\,{}^{(4)}R_{pqrs} \\
&= (\gamma^{p}{}_{a} - n_a n^p)(\gamma^{q}{}_{b} - n_b n^q)(\gamma^{r}{}_{c} - n_c n^r)(\gamma^{s}{}_{d} - n_d n^s)\,{}^{(4)}R_{pqrs} \\
&= \gamma^{p}{}_{a}\gamma^{q}{}_{b}\gamma^{r}{}_{c}\gamma^{s}{}_{d}\,{}^{(4)}R_{pqrs} - \gamma^{p}{}_{a}\gamma^{q}{}_{b}\gamma^{r}{}_{c}n_d n^{s}\,{}^{(4)}R_{pqrs} + \gamma^{p}{}_{a}\gamma^{q}{}_{b}n_c n^r n_d n^{s}\,{}^{(4)}R_{pqrs} + 0. \qquad (3.20)
\end{aligned}$$

The first term in the equation is solely related to spatial factors, while in the second term one index is normally projected. The third term contains two normal indices, and due to symmetry, the fourth term is zero. This is because of the projection of ${}^{(4)}R_{pqrs}$ with the normal index. these establish the relationship between the 4-dimensional Riemann tensor and the 3-dimensional quantities R_{abcd},K_{ab}. For a 3-dimensional hypersurface, the first derivative of an arbitrary vector V^a on a given purely spatial hypersurface Σ_t ($n_a V^a = 0$) is expressed as,

$$\begin{aligned}
D_a V^b &= \gamma^{c}{}_{a}\gamma^{b}{}_{d}\nabla_c V^d \\
&= \gamma^{c}{}_{a}(g^{b}{}_{d} + n^b n_d)\nabla_c V^d \\
&= \gamma^{c}{}_{a}\nabla_c g^{b}{}_{d}V^d + \gamma^{c}{}_{a}n^b n_d \nabla_c V^d \\
&= \gamma^{c}{}_{a}\nabla_c V^b - \gamma^{c}{}_{a}n^b V^d \nabla_c n_d \\
&= \gamma^{c}{}_{a}\nabla_c V^b - n^b V^e \gamma^{c}{}_{a}\gamma^{d}{}_{e}\nabla_c n_d \\
D_a V^b &= \gamma^{c}{}_{a}\nabla_c V^b + K_{ae}n^b V^e. \qquad (3.21)
\end{aligned}$$

Taking an additional derivative of Equation 3.21 yields,

$$D_a D_b V^c = \gamma^{p}_{a}\gamma^{q}_{b}\gamma^{c}_{r}\nabla_p \nabla_q V^r - K_{ab}\gamma^{c}_{r}n^q \nabla_q V^r - K^{c}_{a}K_{bp}V^p. \qquad (3.22)$$

This equation establishes the relationship between the 3-dimensional hypersurface and the 4-dimensional spacetime. Consequently, the 3-dimensional hypersurface can be expressed as,

$$\begin{aligned} R^{dc}_{ba}V_d &= 2D_{[a}D_{b]}V^c, \\ &= 2\{\gamma^p_a\gamma^q_b\gamma^c_r\nabla_{[p}\nabla_{q]}V^r - K_{[ab]}\gamma^c_r n^q\nabla_q V^r - K_{[c}K_{b]p}V^b\}, \\ &= 2\{\gamma^p_a\gamma^q_b\gamma^{c\,(4)}_r R^{dc}_{qp}V_d - K_{[ab]}\gamma^c_r n^q\nabla_q V^r - K_{[c}K_{b]p}V^b\}, \\ R_{dcba}V^d &= \gamma^p_a\gamma^q_b\gamma^{r\,(4)}_c R_{drqp}V^d - 2K_{c[a}K_{e]d}V^d. \end{aligned} \tag{3.23}$$

Since the extrinsic curvature K_{ab} is symmetric, the term $-2K_{[ab]}\gamma^c_r n^q \bigtriangledown_p V^r$ vanishes. For any given spatial vector V^a we rewrite the above to get the following

$$R_{abcd} + K_{ac}K_{bd} - K_{ad}K_{cb} = \gamma^p_a\gamma^q_b\gamma^r_c\gamma^{r\,(4)}_d R_{pqrs}. \tag{3.24}$$

The spatial projection of the 4-dimensional Riemann tensor yields a 3-dimensional intrinsic Riemann tensor and an extrinsic curvature, as expected in this type of decomposition. This relationship is known as the Gauss equation 3.24.

Next, we consider one normal and 3 spatial projection of the 4-dimensional Riemann tensor,

$$\gamma^p_a\gamma^q_b\gamma^r_c n^{s\,(4)} R_{pqrs} = D_b K_{ac} - D_a K_{bc}. \tag{3.25}$$

The equation 3.25 is known as the Codazzi equation. After considering two normal projections and spatial projections, we obtain the following result,

$$\mathcal{L}_n K_{ab} = n^d n^c \gamma^q_a\gamma^{r\,(4)}_b R_{drcq} - \frac{1}{\alpha}D_a D_b\alpha - K^c_b K_{ac}. \tag{3.26}$$

The equation being referred to 3.26 is known as the Ricci equation. By applying contraction to the first two equations, namely the Gauss equation 3.24 and the Codazzi equation 3.25 and utilising the spatial metric γ^{ac}, we may simplify the equations further. We begin by contracting the Gauss relation,

$$R_{bd} + KK_{bd} - K^c_d K_{ab} = \gamma^{pr}\gamma^q_b\gamma^{s\,(4)}_d R_{pqrs}. \tag{3.27}$$

We have contracted the extrinsic curvature with the metric to obtain the trace of the extrinsic curvature, denoted as $K = \gamma^{ab}K_{ab} = K^a_a$. Subsequently, we have contracted the results with the

metric γ^{bd}, to obtain

$$\begin{aligned} R + K^2 - K_{ab}K^{ab} &= (g^{pr} + n^p n^r)(g^{qs} + n^q n^s)\,{}^{(4)}R_{pqrs} \\ &= g^{pr}\,g^{ps\,(4)}R_{pqrs} + 2n^p n^{r\,(4)}R_{pr} \\ &= {}^{(4)}R + 2n^p n^r (G_p + \frac{1}{2} g_{pr}\,{}^{(4)}R) \\ &= 2n^p n^r G_{pr} \\ R + K^2 - K_{ab}K^{ab} &= 16\pi n^p n^r T_{pr}, \end{aligned} \tag{3.28}$$

Using the field equations 2.19, we substitute the Einstein tensor with the energy-momentum tensor T_{ab}. Similarly, other objects, such as the stress-energy tensor, can be decomposed into their respective components, which are given by

$$\rho \equiv T_{pr} n^p n^r, \quad S_a \equiv -T_{pr} n^p \gamma^r{}_a, \quad S_{ab} \equiv T_{pr} \gamma^p{}_a \gamma^r{}_b, \quad S = \gamma^{ab} S_{ab}. \tag{3.29}$$

The quantity ρ denotes the energy density observed by an observer moving orthogonally to the hypersurface, while S_a represents the corresponding momentum density measured by the same observer. S_{ab} is the spatial stress tensor, which describes how stresses (forces per unit area) act on the hypersurface. S is the trace of the spatial stress tensor, obtained by contracting S_{ab} with the spatial metric γ^{ab}. Thus, 3.28 becomes

$$R + K^2 - K_{ab}K^{ab} = 16\pi\rho. \tag{3.30}$$

The above equation 3.30 is referred to as the Hamiltonian constraint. Similarly, by contracting the Codazzi equation 3.25, we get the outcome of the momentum constraint,

$$D_b K^b_a - D_a K = 8\pi S_a. \tag{3.31}$$

Then finally, using the Ricci equation 3.26, we obtain

$$\mathcal{L}_n K_{ab} = -\frac{1}{\alpha} D_a D_b \alpha + R_{ab} - 2K_{ac}K^c_b + K K_{ab} - 8\pi(S_{ab} - \frac{1}{2}\gamma_{ab}(S - \rho)). \tag{3.32}$$

This equation is important for studying the time evolution since it involves the time derivative along the normal vector. The observer moving along the tangent coordinate t^a is referred to as a

coordinate observer. These observers will adhere to the time evolution equation,

$$\begin{aligned}\mathcal{L}_t K_{ab} &= \alpha \mathcal{L}_n K_{ab} + \mathcal{L}_\beta K_{ab}, \\ \mathcal{L}_t K_{ab} &= -D_a D_b \alpha + \alpha \left(R_{ab} - 2K_{ac}K^c_b \right) - 8\pi\alpha \left(S_{ab} - \frac{1}{2}\gamma_{ab}(S-\rho) \right) + \mathcal{L}_\beta K_{ab}, \end{aligned} \tag{3.33}$$

and also the time evolution of the spatial metric

$$\mathcal{L}_t \gamma_{ab} = -2\alpha K_{ab} + \mathcal{L}_\beta \gamma_{ab}. \tag{3.34}$$

The coordinates for the metric so far are completely generic, which means the choice of coordinates has to be made for the evolution of these equations. From these derivations, we obtain two sets of equations: the constraint equations and the evolution equations.

Constraint equations

The constraint equations 3.30, 3.31 are given by [60, 21]

$$R + K^2 - K_{ij}K^{ij} = 16\pi\rho, \tag{3.35}$$

$$D_j K^j_i - D_i K = 8\pi S_i. \tag{3.36}$$

Evolution equations

The two evolutions equation also given as

$$\partial_t \gamma_{ij} = -2\alpha K_{ij} + D_i\beta_j + D_j\beta_i, \tag{3.37}$$

$$\begin{aligned}\partial_t K_{ij} &= \alpha(R_{ij} - 2K_{ik}K^k_j + KK_{ij}) - D_iD_j\alpha - 8\pi\alpha(S_{ij} - \frac{1}{2}\gamma_{ij}(S-\rho)) + \beta^k\partial_k K_{ij} \\ &\quad + K_{kj}\partial_{ij}\beta^k + K_{kj}\partial_i\beta^k. \end{aligned} \tag{3.38}$$

The contraction of the extrinsic curvature and the spatial metric yields,

$$\partial_t \ln \gamma^{1/2} = -\alpha K + D_i\beta^i, \tag{3.39}$$

$$\partial_t K = -\gamma^{ij} D_i D_j \alpha + \alpha(K_{ij}K^{ij} + 4\pi(\rho + S)) + \beta^i D_i K, \tag{3.40}$$

which is often useful when choosing a slicing condition. To solve these evolution equations, one must select an appropriate shift vector and lapse function to ensure that the equations form a closed system.

3.2 Gauge Conditions

Prior to commencing the numerical implementation of the above evolution equations, it is necessary to select the gauge conditions. In the context of general relativity, there is no inherent preference for one set of coordinates over another. However, we must select specific gauge variables, α and β^i, which correspond to choosing a coordinate system. These variables determine the manner in which spacetime is foliated into distinct slices. These functions are utilised to progress the field data from one hypersurface at time t to the subsequent hypersurface at time $t + \delta t$. Although we have the freedom to select our lapse function and shift vector, this is not a trivial task. In general, having a geometric understanding and physical insight into the problem we aim to model is crucial in selecting an appropriate coordinate system. Ideally, the gauge conditions should prevent the appearance of singularities, whether they are related to coordinates or physical properties. Failure to address these problems can cause numerical simulations to become unstable, leading to code crashes due to numerical overflow or underflow. When selecting a suitable coordinate system, we must consider two factors: picking a time coordinate and selecting spatial coordinates. A time coordinate choice, often referred to as time slicing, is responsible for determining the configuration of hypersurfaces Σ that collectively encompass the entire spacetime. The lapse function, in turn, governs the evolution of the shape of these slices Σ over time, along the normal vector n^a that connects one hypersurface to the next. On the other hand, the shift vector β^i is used to assign labels to spatial positions relative to the normal observer n^a on the adjacent hypersurfaces. Put simply, the shift vector allows for the selection of spatial coordinates. In the following, we present some common gauge choices [7, 4, 21].

3.2.1 Geodesic Slicing

We begin with the most basic gauge choice, geodesic slicing, which allows us to freely select the shift vector and lapse function as [21],

$$\alpha = 1, \qquad \beta^i = 0. \tag{3.41}$$

Since coordinate observers move with four-velocities $u^a = t^a = e^a_{(0)}$ and are equivalent to normal observers, meaning $u^a = n^a$, the shift vector simplifies to $\beta^i = 0$, resulting in $\alpha = 1$ throughout the evolution. Therefore, the coordinate time intervals are equivalent to the proper time intervals, and as a result, both observers experience an acceleration that is determined by,

$$a_b = D_b \ln \alpha = 0. \tag{3.42}$$

This gauge will result in any motion that is in close proximity to a black hole ultimately settling within the singularity of the black hole. For a simulation of a single black hole of mass M the singularity is reached at time $\tau = t = \pi M$. This is the point at which numerical simulations code fail.

To understand this problem, it is helpful to consider the equation governing the change of the trace of the extrinsic curvature in 3.33. Under the geodesic gauge, we get [21]

$$\partial_t K = K_{ij}K^{ij} + 4\pi\left(\rho + S\right) \geq 0. \tag{3.43}$$

Given that the term $K_{ij}K^{ij}$ is non-negative and the strong energy condition ensures $\rho + S \geq 0$, the expansion of an Eulerian observer decreases monotonically along their timelike geodesic. Consequently, the trace of the extrinsic curvature continuously increases without limit from one hypersurface to the next, indicating greater warping of hypersurfaces as we progress along the geodesic. This gauge condition impacts the spatial metric by affecting the contracted evolution equation 3.39, ultimately leading to a reduction,

$$\partial_t \ln \gamma^{1/2} = -K. \tag{3.44}$$

This indicates that our chosen gauge is not always effective, highlighting the need for a more suitable gauge condition.

3.2.2 Maximal slicing

Maximal slicing is advantageous compared to geodesic slicing, particularly in the numerical simulation of black holes. This is because maximal slicing permits longer time evolution than geodesic slicing, which is limited to $t = \pi M$. A commonly used approach for the slicing condition is to select a constant value for K in both space and time i.e

$$K = 0 = \partial_t K. \tag{3.45}$$

Then plugging this back into the evolution equation 3.40 for the extrinsic curvature results into an Elliptic equation for the lapse,

$$D^2\alpha = \alpha\left(K_{ij}K^{ij} + 4\pi\left(\rho + S\right)\right). \tag{3.46}$$

The purpose of this is to prevent K from deviating from its original value as a result of numerical inaccuracies during the process of evolution [6, 5]. The maximal slicing gauge offers geometric advantages compared to certain gauge choices. Furthermore, it is specifically designed to prevent the appearance of singularities. However, the process necessitates the computational determination of the lapse via a numerical solution of an Elliptic Partial Differential Equation (PDE) as it progresses. This computational process is considered undesirable due to the potential dominance of the computational effort by the solution of equation 3.46, particularly in the context of 3D simulations.

3.2.3 Harmonic coordinates

By contracting the 4-dimensional Christoffel connection coefficients, we obtain the following result,

$$ {}^{(4)}\Gamma^a \equiv \gamma^{bc\,(4)}\Gamma^a_{bc} = -\frac{1}{|g|^{1/2}}\partial_b(|g|^{1/2}g^{ab}). \tag{3.47} $$

Gauge conditions are determined by equating quantities ${}^{(4)}\Gamma^a$ to a predefined function H^a,

$$ {}^{(4)}\Gamma^a = H^a. \tag{3.48} $$

The function H^a has the flexibility to take on any value, including the possibility of being defined as zero. This property is particularly useful when considering harmonic coordinates defined as,

$$ {}^{(4)}\Gamma^a = 0. \tag{3.49} $$

Using the inverse metric 3.10 to insert into 3.47 then we end up with the coupled, non-linear hyperbolic equations of the lapse function and shift vector as [110]

$$ (\partial_t - \beta^j\partial_j)\alpha = -\alpha^2 K, \tag{3.50} $$

$$ (\partial_t - \beta^j\partial_j)\beta^i = -\alpha^2(\gamma^{ij}\partial_j \ln\alpha + \gamma^{jk}\Gamma^i_{jk}). \tag{3.51} $$

Currently, this condition has made the lapse function and shift vector into dynamic variables that necessitate temporal evolution in spacetime. These evolution equations are hyperbolic in nature, which are comparatively simpler to solve than the elliptic equation discussed in section 3.2.2.

3.2.4 Bona-Masso Slicing

Harmonic-slicing has resulted in other hyperbolic forms of the equations for the lapse function. These equations imitate the conditions of maximal slicing and also prevent the appearance of singularities, as demonstrated by Bona and Masso [25]. Their study showed that while harmonic slicing can avoid singularities to a certain extent, it is inferior to maximal slicing in terms of avoiding stronger singularities. This is because the lapse function of harmonic slicing collapses when approaching a singularity. Bona and Masso have conducted extensive research on the vacuum Einstein field equations in the harmonic slicing gauge. This research has resulted in a group of generalised slicing conditions known as the Bona-Masso family of slicing conditions. These conditions ensure that the lapse function satisfies the evolution equation [26],

$$\left(\partial_t - \beta^i \partial_i\right) \alpha = -\alpha^2 f(\alpha) K, \tag{3.52}$$

where $f(\alpha)$ is any positive function of α. By analysing the behaviour of the function $f(\alpha)$, we can derive many slicing conditions. Specifically, when $f = 0$ and $\alpha = 1$, we obtain the geodesic slicing condition 3.41 The case when $f = 1$ corresponds to the harmonic slicing condition 3.50. When dealing with a diverging function, such as $f(\alpha) \to \infty$, the condition acts similarly to the maximally slicing condition, resulting in the avoidance of strong singularities. Another intriguing algebraic condition that may be derived is the $1 + log$ slicing condition, which occurs when $f = 2/\alpha$. By setting the shift vector to zero, we can do integration on equation 3.52 to obtain the result [9]

$$\alpha = 1 + log\gamma, \tag{3.53}$$

by selecting the constant of integration to be equal to one. The 1 + log slicing condition is a reliable and stable algebraic condition that has demonstrated great effectiveness in the evolution of black holes in three dimensions and in strong gravitational fields in general [26, 19].

3.3 BSSN formulation

In practice, the ADM evolution equations have been found to exhibit numerical instabilities. The instability and lack of uniqueness in the system's solutions can be attributed to the presence of mixed second-order derivatives of the 3-spatial metric in the Ricci tensor [84, 21]. For hyperbolic PDEs, strong hyperbolicity is necessary for stable numerical evolutions. The BSSN formalism guarantees strong hyperbolicity by eliminating the mixed second derivatives in the Ricci tensor. In the BSSN version of the 3 + 1 equations, the spatial metric γ_{ij} is separated into a conformal metric

$\bar{\gamma}_{ij}$ with a conformal factor $\psi = e^{\phi}$ as [61]

$$\tilde{\gamma}_{ij} = e^{-4\phi}\gamma_{ij}. \tag{3.54}$$

The conformal factor is chosen to satisfy

$$\psi^4 \equiv e^{4\phi} = \det\left(\gamma_{ij}\right)^{\frac{1}{3}} = \gamma^{\frac{1}{3}}, \tag{3.55}$$

such that $\det(\tilde{\gamma}_{ij}) = 1$. In addition, we decompose the extrinsic curvature into its constituent parts: the trace K and the trace-free component A_{ij}.

$$A_{ij} = K_{ij} - \frac{1}{3}\gamma_{ij}K, \tag{3.56}$$

and subject the trace-free component to a conformal transformation, akin to the procedure employed with the metric 3.54.

$$\tilde{A}_{ij} = e^{-4\phi}A_{ij}. \tag{3.57}$$

The indices of $\tilde{A}_{ij}$ are raised and lowered using the conformal metric $\bar{\gamma}_{ij}$, resulting in $\tilde{A}^{ij} = e^{4\phi}A^{ij}$. Through this process, we arrive at the following set of BSSN evolved variables.

$$\begin{aligned}
\tilde{\gamma}_{ij} &= e^{-4\phi}\gamma_{ij} && (3.58)\\
K &= \gamma^{ij}K_{ij} && (3.59)\\
\tilde{A}_{ij} &= e^{-4\phi}A_{ij} && (3.60)\\
\phi &= \ln\psi = \frac{1}{12}\ln\gamma. && (3.61)
\end{aligned}$$

Expressed in terms of these variables 3.58, the Hamiltonian constraint 3.30 takes the form [109]

$$0 = \mathcal{H} = \tilde{\gamma}^{ij}\tilde{D}_i\tilde{D}_j e^{\phi} - \frac{e^{\phi}}{8}\tilde{R} + \frac{e^{5\phi}}{8}\tilde{A}_{ij}\tilde{A}^{ij} - \frac{e^{5\phi}}{12}K^2 + 2\pi e^{5\phi}\rho. \tag{3.62}$$

Meanwhile, the momentum constraint 3.31 becomes

$$0 = \mathcal{M}^i = \tilde{D}_j\left(e^{6\phi}\tilde{A}^{ji}\right) - \frac{2}{3}e^{6\phi}\tilde{D}^i K - 8\pi e^{6\phi}S^i. \tag{3.63}$$

The equation governing the evolution of γ_{ij}, labelled as 3.39, can be divided into two separate equations.

$$\partial_t \phi = -\frac{1}{6}\alpha K + \beta^i \partial_i \phi + \frac{1}{6}\partial_i \beta^i, \tag{3.64}$$

$$\partial_t \tilde{\gamma}_{ij} = -2\alpha \tilde{A}_{ij} + \beta^k \partial_k \tilde{\gamma}_{ij} + \tilde{\gamma}_{ik}\partial_j \beta^k + \tilde{\gamma}_{kj}\partial_i \beta^k - \frac{2}{3}\tilde{\gamma}_{ij}\partial_k \beta^k, \tag{3.65}$$

while the evolution equation 3.38 for K_{ij} splits into the two equations

$$\partial_t K = -\gamma^{ij} D_j D_i \alpha + \alpha\left(\tilde{A}_{ij}\tilde{A}^{ij} + \frac{1}{3}K^2\right) + 4\pi\alpha(\rho + S) + \beta^i \partial_i K \tag{3.66}$$

$$\begin{aligned}\partial_t \tilde{A}_{ij} = {} & e^{-4\phi}\left(-(D_i D_j \alpha)^{TF} + \alpha\left(R_{ij}^{TF} - 8\pi S_{ij}^{TF}\right)\right) + \alpha\left(K\tilde{A}_{ij} - 2\tilde{A}_{il}\tilde{A}^l{}_j\right) \\ & + \beta^k \partial_k \tilde{A}_{ij} + \tilde{A}_{ik}\partial_j \beta^k + \tilde{A}_{kj}\partial_i \beta^k - \frac{2}{3}\tilde{A}_{ij}\partial_k \beta^k,\end{aligned} \tag{3.67}$$

where TF in the last equation denotes the trace-free portion of the 3-dimensional second rank tensor, which is represented by

$$R_{ij}^{TF} = R_{ij} - \gamma_{ij} R/3. \tag{3.68}$$

Ricci tensor R_{ij} can be written in two parts,

$$R_{ij} = \tilde{R_{ij}} + R_{ij}^{\phi}. \tag{3.69}$$

The equation for the part of R_{ij} involving the logarithm of the conformal factor R_{ij}^{ϕ} is determined by,

$$R_{ij}^{\phi} = -2\tilde{D}_i \tilde{D}_j \phi - 2\tilde{\gamma_{ij}}\tilde{D}^l \tilde{D}_l \phi + 4\tilde{D}_i \phi \tilde{D}_j \phi - 4\tilde{\gamma_{ij}}\tilde{D}^l \phi \tilde{D}_l \phi. \tag{3.70}$$

To express the conformal part $\tilde{R}_{ij}$, we must first define the conformal connection functions,[4]

$$\tilde{\Gamma^i} = \tilde{\gamma}^{jk}\tilde{\Gamma}^i_{jk} = -\partial_j \tilde{\gamma}^{ij}. \tag{3.71}$$

The conformal connection function $\tilde{\Gamma^i}$ aids in removing mixed derivatives from the evolution equations. Here, we consider the Christoffel symbols associated with the metric $\tilde{\gamma}_{ij}$. In Cartesian coordinates, where $\tilde{\gamma} = 1$, this condition holds. Using this, we can express the conformal Ricci tensor $\tilde{R}_{ij}$ in terms of these conformal connection functions $\tilde{\Gamma^i}$ as follows,

$$\tilde{R_{ij}} = -\frac{1}{2}\tilde{\gamma}^{lm}\partial_l \partial_m \tilde{\gamma}_{ij} + \tilde{\gamma}_{k(i}\partial_{j)}\tilde{\Gamma}^k + \tilde{\Gamma}^k \tilde{\Gamma}_{(ij)k} + \tilde{\gamma}^{lm}(2\tilde{\Gamma}^k_{l(i}\tilde{\Gamma}_{j)km} + \tilde{\Gamma}^k_{im}\tilde{\Gamma}_{klj}). \tag{3.72}$$

It is beneficial for maintaining numerical stability to evolve the $\tilde{\Gamma}^i$ as independent variables throughout. The evolution equation can be derived directly from definition 3.71 and the evolution equation for the conformal 3-metric 3.65, by explicitly expressing the terms using Lie-derivatives. The $\tilde{\Gamma}^i$ are now regarded as independent functions that obey their own evolution equations

$$\partial_t \tilde{\Gamma}^i = -\partial_j (2\alpha \tilde{A^{ij}} - 2\tilde{\gamma^{m(j}} \partial_m \beta^{i)} + \frac{2}{3} \tilde{\gamma^{ij}} \partial_l \beta^l + \beta^l \partial_l \tilde{\gamma^{ij}}). \tag{3.73}$$

Lastly, we need the Momentum constraint 3.31 to eliminate the divergence of the extrinsic curvature. This provides the evolution equation,

$$\begin{aligned} \partial_t \tilde{\Gamma}^i = -2\tilde{A}^{ij}\partial_j \alpha + 2\alpha(\tilde{\Gamma}^i_{jk}\tilde{A}^{kj} - \frac{2}{3}\tilde{\gamma}^{ij}\partial_j K - 8\pi\tilde{\gamma}^{ij}S_j + 6\tilde{A}^{ij}\partial_j \phi) + \beta^j \partial_j \tilde{\Gamma}^i - \tilde{\Gamma}^j \partial_j \beta^i \\ + \frac{2}{3}\tilde{\Gamma}^i \partial_j \beta^j + \frac{1}{3}\tilde{\gamma}^{li}\partial_l \partial_j \beta^j + \tilde{\gamma}^{lj}\partial_j \partial_l \beta^i. \end{aligned} \tag{3.74}$$

Therefore, we have a system of evolution equations with the set of 17 independent variables $\{\phi, \tilde{\gamma_{ij}}, K, \tilde{A_{ij}}, \tilde{\Gamma_i}\}$, which are second order in space and first order in time. The BSSN system has been shown to lead to more stable evolutions when compared with the ADM system [21, 4, 35].

3.4 Characteristic formalism

The characteristic evolution system is one of the approaches used to solve the Einstein field equations. Unlike the traditional 3+1 decomposition methods, such as ADM and BSSN, which foliate 4-dimensional spacetime into 3-dimensional spatial hypersurfaces evolving along a timelike direction, this formalism instead foliates spacetime using null hypersurfaces characterized by constant retarded time $u = r - t$. Since these null hypersurfaces correspond to the characteristic structure of the Einstein equations, this approach is often referred to as the characteristic initial value problem [88]. A key advantage of this formulation is its ability to reduce the number of variables and simplify the system of equations. This formalism is based on the work by Bondi [28, 27] in studying gravitational radiation within the nonlinear regime. Over time, it has become an essential tool for analyzing gravitational waves numerically [55]. In fact, characteristic evolution methods were among the first to achieve long-term stable simulations of moving black holes in three dimensions [55]. One significant strength of this formalism is its ability to compactify the radial coordinate while maintaining numerical stability. This feature enables precise studies of gravitational waves at future null infinity, where their properties can be clearly defined [107]. Despite its strengths, the method has a notable limitation, the potential formation of coordinate singularities. These arise due to the focusing of null rays, particularly in regions of strong gravitational fields [74]. However, at

large distances from the source, extending to future null infinity, this approach provides an accurate description of the gravitational wave zone. When combined with other techniques, such as Cauchy evolution, it allows for the modeling of the entire spacetime of systems with intense gravitational fields, including binary black hole mergers [107, 19, 5, 55].

3.4.1 Bondi-Sachs metric

The Bondi-Sachs formalism relies on a specific type of metric tensor to represent the geometry of spacetime. This metric is formulated using the Bondi-Sachs coordinate system, defined as $x^\nu = (r, u, x^A)$. To solve the Einstein equations along characteristic lines, a well-structured coordinate system is essential. The Bondi coordinates [28, 71] consist of angular components x^A (where $A = 1, 2$), a radial coordinate $x^1 = r$, and a retarded time coordinate $x^0 = u = r - t$. These coordinates ensure that hypersurfaces of constant u are null, meaning that u parametrizes a family of outgoing null hypersurfaces originating from a world-tube Γ [71].

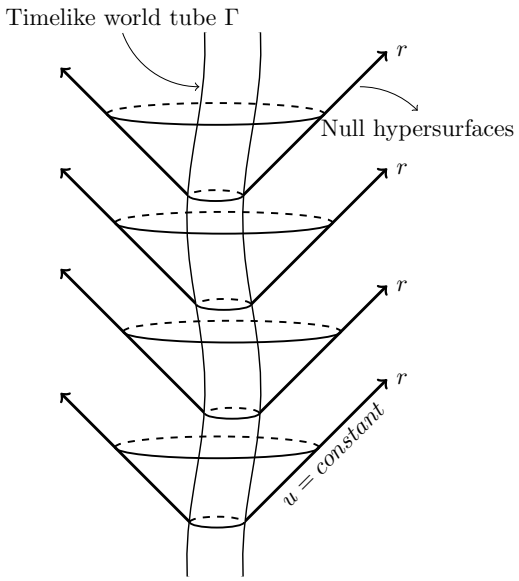

Figure 3.2: Illustration of a timelike world tube Γ surrounded by null hypersurfaces. The null hypersurfaces are depicted as slanted lines radiating outward, intersecting at constant u levels. These surfaces highlight the propagation of light rays in spacetime geometry, with r representing the radial coordinate.

The Bondi-Sachs metric tensor for a spacetime $(\mathcal{M}, g)$ in these coordinates becomes [108, 34, 33, 87],

$$ds^2 = -\left(e^{2\beta}\frac{V}{r} - r^2 h_{AB}U^A U^B\right)du^2 - 2e^{2\beta}dudr - 2r^2 h_{AB}U^B dudx^A + r^2 h_{AB}dx^A dx^B, \tag{3.75}$$

where h_{AB} with $h^{AB}h_{AC} = \delta^A{}_C$, satisfies the determinant condition

$$\det(h_{AB}) = \det(q_{AB}), \tag{3.76}$$

with q_{AB} the unit 2-sphere metric [108]. The variables V and β are functions of (r, u, x^A), and U^A represents a shift vector [108, 33]. From the above metric the non-zero contravariant components can be computed as

$$g^{rr} = e^{-2\beta}\frac{V}{r}, \quad g^{rA} = -e^{-2\beta}U^A, \quad g^{ru} = -e^{-2\beta}, \quad g^{AB} = r^{-2}h^{AB}. \tag{3.77}$$

3.4.2 2+1 decomposition of the metric

The construction of Bondi coordinates is based on out-going null hypersurfaces $u = const$, that means the normal co-vector $k_a = -\partial_a u$ satisfies $g^{ab}\partial_a u \partial_b u = 0$ which implies that

$$g^{uu} = 0. \tag{3.78}$$

The future-pointing vector $k^a = -g^{ab}\partial_b u$ are tangent to the null rays. Then the two angular coordinates x^A are given as constants along the null rays which then means $k^a \partial_a x^A = -g^{ab}(\partial_a u)\partial_b u x^A = 0$ implying

$$g^{uA} = 0. \tag{3.79}$$

The $x^1 = r$ is chosen to be a surface area coordinate and it varies along the null rays, such that

$$\det[g_{AB}] = r^4 q, \tag{3.80}$$

where $q(x^A)$ is given to be the determinate of the unit sphere metric q_{AB} with the given angular coordinates x^A, h_{AB} is the symmetric 2-tensor, which represents the conformal geometry of the 2-surfaces which we get by setting $dr = du = 0$, and these foliate the world-tube Γ, and they also represent the angular part of the spacetime metric given by the $g_{AB} = r^2 h_{AB}$, which is derived from the intrinsic metric of $r = const$ surfaces,that we get by setting $dr = 0$ in with 3.76. This $2+1$ decomposition allows for the construction of the Bondi-Sachs metric in the form [28]

$$\gamma_{ij} dy^i dy^j = -\mathrm{e}^{2\beta}\frac{V}{r} du^2 + r^2 h_{AB}\left(dy^A - U^A du\right)\left(dy^B - U^B du\right), \tag{3.81}$$

where β is scalar and measures the expansion $e^{2\beta}$ the light cone between the world-tube and the asymptotic light cone, V is the same measure as the Newtonian potential and U^A is the shift vector and the square of the lapse function is given as $\frac{e^{2\beta}V}{r}$. By making use of the condition $\det(h_{AB}) = \det(q_{AB})$ enables the 2-symmetric tensor to be fixed, such that the are only two independent components that give us two degrees of freedom which are the radiative degrees of the gravitational field equation.

3.4.3 The Einstein field equations in characteristic formulation

Using the Bondi-Sachs metric we have the following reduced Einstein field equations in vacuum $R_{ab} = 0$ to hypersurface equations and evolution equations.

Hypersurface equations

We have the four hypersurface equations which are given by, R_{rr}, R_{rA} and $h^{AB}R_{AB}$, written as

$$\beta_{,r} = \frac{1}{16} r h^{AC} h^{BD} h_{AB,r} h_{CD,r} \tag{3.82a}$$

$$\left(r^4 \mathrm{e}^{-2\beta} h_{AB} U^B{}_{,r}\right)_{,r} = 2r^4 \left(r^{-2}\beta_{,A}\right)_{,r} - r^2 h^{BC} D_C h_{AB,r} \tag{3.82b}$$

$$\begin{aligned} 2\mathrm{e}^{-2\beta} V_{,r} = {} & R - 2D^A D_A \beta - 2D^A \beta D_A \beta + r^{-2}\mathrm{e}^{-2\beta} D_A \left(r^4 U^A\right)_{,r} \\ & - \frac{1}{2} r^4 \mathrm{e}^{-4\beta} h_{AB} U^A_{,r} U^B{}_{,r}. \end{aligned} \tag{3.82c}$$

All these equations involve the metric components of only the $u = const$, hypersurfaces.

Evolution equations

Then we have the evolution equations which contain the derivative of u for the null data, these are derived from the trace-free part of the angular components of the Einstein field equations $m^A m^B G_{AB}$, where the 2-symmetric tensor $h^{AB} = 2m^{(A}\bar{m}^{B)}$.

This gives the evolution equations [106, 108],

$$\begin{aligned} & m^A m^B \Big(\big(r h_{AB,u}\big)_{,r} - \frac{1}{2r}\big(rV h_{AB,r}\big)_{,r} - \frac{2}{r} e^{\beta} D_A D_B e^{\beta} + r h_{AC} D_B \big(U^C_{,r}\big) \\ & - \frac{r^3}{2} e^{-2\beta} h_{AC} h_{BD} U^C_{,r} U^D_{,r} + 2 D_A U_B + \frac{r}{2} h_{AB,r} D_C U^C \\ & + r U^C D_C \big(h_{AB,r}\big) + r h_{AD,r} h^{CD} \big(D_B U_C - D_C U_B\big) \Big) = 0. \end{aligned} \tag{3.83}$$

The four hypersurface equations R_r,R_{rA}, $h^{AB}R_{AB}$ and the evolution equations which are the main construction of Bondi are called the main equations and together with the components $R_{u\alpha}$ or $R^r{}_\alpha$ give a complete set of the vacuum Einstein equations.

Conservation conditions

When the evolution and constraint equations are satisfied we get the trivial equation that is split from $R^r{}_\alpha$ as

$$R^r{}_r = 0, \tag{3.84}$$

which is automatically satisfied if one applies the Bianchi identities to the main equations. In addition, the supplementary equations

$$R^r{}_u = 0, \quad R^r{}_A = 0 \tag{3.85}$$

are satisfied on a complete outgoing null cone if they hold on a single spherical cross-section. Bondi's derivation identifies these equations as conservation laws for energy and angular momentum by supposing the sphere to be at infinity. We may summarise this using the constraint equations.

$$R^r{}_\alpha = 0, \quad \text{or} \quad R_{u\alpha} = 0. \tag{3.86}$$

In principle, the evolution equations 3.83 can be discretized and evolved numerically. However, it is customary to rewrite the field equations in terms of spin-weighted fields to reduce their complexity by re-expressing the angular components of some tensor variables.

3.4.4 Spin-weighted formalism

In the spin-weighted formalism, the unit sphere metric q_{AB} is represented as a dyadic product

$$q_{AB} = q_{(A}\bar{q}_{B)}, \tag{3.87}$$

where, the dyad q_A is a complex basis 2-vector, where we use an overbar i.e $\bar{q}_A$ to denote complex conjugation, and the dyad satisfies

$$q^A q_A = 0, \quad q^A \bar{q}_A = 2, \quad \text{and} \quad q_A = q_{AB} q^B. \tag{3.88}$$

It is important to note that these basis vectors are not unique and can vary by a phase transformation. For any given q_A, an alternative basis $\hat{q}_A = e^{i\alpha} q_A$ can be constructed, where α is a real phase. Using the dyad vectors q^A, rank-n tensor fields $T_{A_1 A_2 \cdots A_n}$ on the sphere can be effectively represented as scalar fields.

$$T = q^{A_1} \cdots q^{A_m} \bar{q}^{A_{m+1}} \cdots \bar{q}^{A_n} T_{A_1 \cdots A_n} \ . \tag{3.89}$$

The spin-weight s of these scalar fields is determined by the rank-n of the tensor field and is given by $s = 2m - n$, where m is the number of q^A factors and $n - m$ is the number of $\bar{q}^A$ factors present in the expression 3.89, such that the scalars transform as $T \to e^{i\alpha s} T$. So then the three spin-weighted

scalars with respective spin weights $+2$, -2 and 0 are,

$$J = \frac{1}{2} q^A q^B h_{AB}, \qquad \bar{J} = \frac{1}{2} \bar{q}^A \bar{q}^B h_{AB} \qquad \text{and} \qquad K = \frac{1}{2} q^A \bar{q}^B h_{AB}, \tag{3.90}$$

and contain all the degrees of freedom of the $2-$tensor h_{AB}. According to 3.90, the decomposition of h_{AB} is presented in an irreducible form as

$$2h_{AB} = \bar{J} q_A q_B + J \bar{q}_A \bar{q}_B + K \left(q_A \bar{q}_B + \bar{q}_A q_B \right) , \tag{3.91}$$

the inverse $2-$metric h^{AB} is given by

$$2h^{AB} = -\bar{J} q^A q^B - J \bar{q}^A \bar{q}^B + K \left(q^A \bar{q}^B + \bar{q}^A q^B \right) . \tag{3.92}$$

Furthermore, the determinant condition 3.76 implies the relationship.

$$K^2 = 1 + J\bar{J} . \tag{3.93}$$

The scalar K provides no extra information, and h_{AB} is uniquely defined by J for any Bondi-Sachs metric. Similarly, U^A and Q^A are decomposed into spin-weighted fields,

$$U = U^A q_A \qquad \bar{U} = U^A \bar{q}_A \qquad Q = Q^A q_A \qquad \bar{Q} = Q^A \bar{q}_A. \tag{3.94}$$

With respective spins of $+1$, -1, $+1$, and -1. In this spin-weighted formalism, the scalars β, V, and R are spin-0 fields.

3.4.5 Simplification of the Einstein field equations in Bondi-Sachs metric

Once we have recast these tensor quantities in terms of the spin-weighted fields and their derivative then we have the following hypersurface equations

$$\begin{aligned}
\beta_{,r} &= N_\beta, && (3.95)\\
U_{,r} &= r^{-2} e^{2\beta} Q + N_U, && (3.96)\\
(r^2 Q)_{,r} &= -r^2 (\eth J + \eth K)_{,r} + 2r^4 \eth \left(r^{-2} \beta \right)_{,r} + N_Q, && (3.97)\\
W_{,r} &= \frac{1}{2} e^{2\beta} \mathcal{R} - 1 - e^{\beta} \eth \bar{\eth} e^{\beta} + \frac{1}{4} r^{-2} \left(r^4 \left(\eth \bar{U} + \bar{\eth} U \right) \right)_{,r} + N_W, && (3.98)
\end{aligned}$$

where

$$Q \equiv q^A Q_A = r^2 \mathrm{e}^{-2\beta} q^A h_{AB} U^B{}_{,r} \tag{3.99}$$

is the new variable that obeys

$$\left(r^2 Q\right)_{,r} = 2r^4 \left(r^{-2} q^A \beta_{,A}\right)_{,r} - r^2 q^A h^{BC} D_C h_{AB,r}. \tag{3.100}$$

The Ricci scalar in equation 3.98 is given as,

$$\mathcal{R} = 2K - \eth\bar{\eth}K + \frac{1}{2}(\bar{\eth}^2 J + \eth^2 \bar{J}) + \frac{1}{4K}(\bar{\eth}\bar{J}\eth J - \bar{\eth}J\eth\bar{J}). \tag{3.101}$$

The evolution equations are also given as follows,

$$2\left(rJ\right)_{,ur} - \left(r^{-1} V \left(rJ\right)_{,r}\right)_{,r} = -r^{-1}\left(r^2 \eth U\right)_{,r} + 2r^{-1} e^{\beta} \eth^2 e^{\beta} - \left(r^{-1} W\right)_{,r} J + N_J. \tag{3.102}$$

The variables N_β, N_U, N_Q, N_W and N_J in the above equations represent the nonlinear aspherical terms [23, 74], and the form of these expressions is given in more details here defined in tensor form and covariant derivatives [23, 74, 27].

The constraint equations

The constraint equations for the spin-weighted version are obtained through the expansion of $R_{0\alpha}$ in terms of the metric and its derivatives, with the components of the metric and its derivatives expressed in terms of spin-weighted fields J, K, W, β, U. Through the contraction of the two angular components of $R_{0\alpha}$, gives the three constraint equations

$$R_{00}, \qquad R_{01}, \qquad q^A R_{0A}. \tag{3.103}$$

Just like with the Cauchy problem, these equations can be used to monitor the numerical evolution accuracy of the hypersurface equations and evolution equations, this is achieved by inserting the J, K, W, β, U into the constraint equations, if they are satisfied then that means $R_{0\alpha} = 0$ up to some error.

Chapter 4

Tolman-Oppenheimer-Volkoff (TOV) equations

4.1 Overview

In this chapter we present the solution for the static, spherically symmetric metric that will be utilized as the background solution to the linearized ADM equations in Chapter 5. This background spacetime metric is given as, [36, 21]

$$ds^2 = -e^{2\nu(r)}dt^2 + e^{2\lambda(r)}dr^2 + r^2 d\theta^2 + r^2 \sin^2\theta d\phi^2. \tag{4.1}$$

In order to obtain the TOV equations and determine the functions $\nu(r)$ and $\lambda(r)$ from the given metric g_{ab} in the line element in Eq 4.1, it is necessary to utilize the complete Einstein field equations along with the Bianchi identities. This is because we are seeking solutions that are not vacuum, meaning that the energy-momentum tensor is non-zero [82]. Therefore, we shall utilize the complete Einstein field equations [82, 36, 21].

$$G_{ab} = {}^{(4)}R_{ab} - \frac{1}{2}{}^{(4)}R g_{ab} = 8\pi T_{ab} \tag{4.2}$$

where ${}^{(4)}R_{ab}$ and R are the Ricci tensor and Ricci scalar, respectively. g_{ab} is the metric tensor with components

$$g_{ab} = \mathrm{diag}(-e^{2\nu(r)}, e^{2\lambda(r)}, r^2, r^2\sin^2\theta) \tag{4.3}$$

and T_{ab} is the energy-momentum tensor. The Bianchi identities $\nabla_a G^{ab} = 0$ implies conservation of energy-momentum i.e

$$\nabla_a G^{ab} = 0 \implies \nabla_a T^{ab}. \tag{4.4}$$

4.2 Derivation of the TOV equations

In presenting the derivation of the TOV equations, we will primarily quote the final expressions for the quantities under consideration, with the detailed steps provided in Appendix A. We start by calculating the Christoffel symbols from 4.3. Due to its symmetries, the Christoffel symbols have 40 independent components. For the line element 4.1, several of these components vanish. The non-zero Christoffel symbols,

$$\begin{aligned}
\Gamma^t_{tr} &= \partial_r \nu, && (4.5)\\
\Gamma^r_{tt} &= e^{2(\nu(r)-\lambda(r))}\partial_r \nu, && (4.6)\\
\Gamma^r_{rr} &= \partial_r \lambda, && (4.7)\\
\Gamma^\theta_{r\theta} &= \frac{1}{r}, && (4.8)\\
\Gamma^r_{\theta\theta} &= -re^{-2\lambda(r)}, && (4.9)\\
\Gamma^\phi_{r\phi} &= \frac{1}{r}, && (4.10)\\
\Gamma^r_{\phi\phi} &= -r\sin^2\theta e^{-2\lambda(r)}, && (4.11)\\
\Gamma^\theta_{\phi\phi} &= -\sin^2\theta\cos\theta, && (4.12)\\
\Gamma^\phi_{\theta\phi} &= \frac{\cos\theta}{\sin\theta}. && (4.13)
\end{aligned}$$

From the Christoffel symbols we can compute the components of the Riemann tensor 2.7. Substituting the Christoffel symbols obtained in Eqs. 4.5-4.13, the non-zero Riemann tensor components are determined to be

$$
\begin{aligned}
R^{r}_{trt} &= e^{2(\nu-\lambda)}\left[\partial_r^2\nu + (\partial_r\nu)^2 - \partial_r\nu\partial_r\lambda\right], && (4.14)\\
R^{\theta}_{t\theta t} &= \frac{1}{r}e^{2(\nu-\lambda)}\partial_r\nu, && (4.15)\\
R^{\phi}_{t\phi t} &= \frac{1}{r}e^{2(\nu-\lambda)}\partial_r\nu, && (4.16)\\
R^{t}_{rtr} &= \partial_r\nu\partial_r\lambda - \partial_r^2\lambda - (\partial_r\lambda)^2, && (4.17)\\
R^{\theta}_{r\theta r} &= \frac{1}{r}\partial_r\lambda, && (4.18)\\
R^{\phi}_{r\phi r} &= \frac{1}{r}\partial_r\lambda, && (4.19)\\
R^{t}_{\theta t\theta} &= -re^{-2\lambda}\partial_r\lambda, && (4.20)\\
R^{\phi}_{\theta\phi\theta} &= \left(1-e^{-2\lambda}\right). && (4.21)
\end{aligned}
$$

Due to the symmetries of the Ricci tensor, R_{ab} has only 10 independent components in 4 dimensions. Furthermore, since the metric is diagonal, all off-diagonal components of R_{ab} vanish. The components R_{tt}, R_{rr}, $R_{\theta\theta}$, and $R_{\phi\phi}$ can be obtained from the non-zero Riemann tensor components 4.14-4.21 as $R_{ac} = R^{c}_{acb}$. Using the above expressions, we obtain

$$
\begin{aligned}
R_{tt} &= e^{2(\nu-\lambda)}\left[\partial_r^2\nu + (\partial_r\nu)^2 - \partial_r\nu\partial_r\nu\right] + \frac{2}{r}e^{2(\nu-\lambda)}\partial_r\nu, && (4.22)\\
R_{rr} &= \partial_r\nu\partial_r\lambda - \partial_r^2\nu - (\partial_r\nu)^2 + \frac{2}{r}\partial_r\lambda, && (4.23)\\
R_{\theta\theta} &= \left\{e^{-2\lambda}\left[r\left(\partial_r\lambda - \partial_r\lambda\right) - 1\right] + 1\right\}\sin^2\theta, && (4.24)\\
R_{\phi\phi} &= \sin^2\theta R_{\theta\theta}. && (4.25)
\end{aligned}
$$

Calculating the Ricci scalar $R = g^{ab}R_{ab}$ from the Ricci tensor components above gives the expression

$$
R = 2e^{-2\lambda}\left[\partial_r^2\nu + (\partial_r\nu)^2 - \partial_r\nu\partial_r\lambda + \frac{2}{r}\left(\partial_r\nu - \partial_r\lambda\right) + \frac{1}{r^2}\left(1-e^{2\lambda}\right)\right]. \quad (4.26)
$$

The Einstein tensor components from 4.2 are constructed using the above Ricci tensor components

and Ricci scalar as

$$G_{\theta\theta} = r^2 e^{-2\lambda}[\partial_r^2\nu + (\partial_r\nu)^2 - \partial_r\nu\partial_r\lambda + \frac{1}{r}(\partial_r\nu - \partial_r\lambda)], \tag{4.27}$$

$$G_{\phi\phi} = e^{-2\lambda}\sin^2(\theta)[r\partial_r\nu - \partial_r\lambda + r^2\partial_r^2\nu + r^2(\partial_r\nu)^2 - r^2\partial_r\nu\partial_r\lambda], \tag{4.28}$$

$$G_{rr} = \frac{2}{r}\partial_r\nu + \frac{1}{r^2}(1 - e^{2\lambda}), \tag{4.29}$$

$$G_{tt} = \frac{1}{r^2}e^{2(\nu-\lambda)}[2\partial_r\lambda r - (1 - e^{2\lambda})]. \tag{4.30}$$

We need to define the energy-momentum tensor for a perfect fluid, [77, 102]

$$T_{ab} = (\epsilon + p)u_a u_b + p g_{ab}. \tag{4.31}$$

The energy density ϵ and pressure (p) are both dependent on the radial coordinate r and g_{ab} is the spacetime metric. The components of the energy-momentum tensor are determined by

$$T_{ab} = \mathrm{diag}(e^{2\nu}\epsilon, e^{2\lambda}p, r^2 p, r^2 p\sin^2\theta). \tag{4.32}$$

We have utilised the four-velocity vector u^a with $g^{ab}u_a u_b = -1$. The four-velocity vector has the components,

$$u_a = (e^{\nu}, 0, 0, 0). \tag{4.33}$$

The $\theta\theta$ and $\phi\phi$ components of the field equations do not yield any new information. As a result, we restrict to the tt and rr components. By utilising these components and the energy momentum tensor, we get the expression for the rr component of the field equations

$$\frac{1}{r^2}e^{-2\lambda}\left(2r\partial_r\nu + 1 - e^{2\lambda}\right) = 8\pi p. \tag{4.34}$$

For the tt component we have

$$\frac{1}{r^2}e^{-2\lambda}\left(2r\partial_r\lambda - 1 + e^{2\lambda}\right) = 8\pi\epsilon. \tag{4.35}$$

One can define a new function $m(r)$ as

$$e^{-2\lambda} = 1 - \frac{2m(r)}{r}. \tag{4.36}$$

Then, the integral of the tt equation gives

$$M(r) = 4\pi \int_0^R \epsilon(r) r^2 dr, \tag{4.37}$$

so that M is the total mass of the star and $m(r)$ is the mass inside a radius. With the above definition, an alternate form for metric 4.1.

$$ds^2 = -e^{2\nu} dt^2 + \left(1 - \frac{2m(r)}{r}\right)^{-1} dr^2 + r^2 d\theta^2 + r^2 \sin^2\theta d\phi^2. \tag{4.38}$$

The condition for hydrostatic equilibrium is derived from the conservation of the stress-energy tensor 2.17 which gives,

$$\frac{dp}{dr} = -\frac{(\epsilon + p)(m(r) + 4\pi r^3 p)}{r(r - 2m(r))}. \tag{4.39}$$

Utilising the rr component, the equation for $\frac{d\nu}{dr}$ can be expressed as,

$$\frac{d\nu}{dr} = \frac{(4\pi p r^3 + m(r))}{(r - 2m(r))}. \tag{4.40}$$

Then the mass function 4.36 used in the tt component of the Einstein tensor, along with equations 4.40 and 4.39, form the Tolmann-Oppenheimer-Volkov (TOV) equations [90, 21],

$$\frac{dp}{dr} = -\frac{(\epsilon + p)(m(r) + 4\pi r^3 p)}{r(r - 2m(r))}, \tag{4.41a}$$

$$\frac{d\nu}{dr} = \frac{(4\pi p r^3 + m(r))}{(r - 2m(r))}, \tag{4.41b}$$

$$\frac{dm}{dr} = 4\pi r^2 \epsilon. \tag{4.41c}$$

4.3 Equation of state

For a general equation of state there are no analytic solutions for the TOV equations. Nevertheless, one can find an analytic solution when the assumption of constant density star is made. Equilibrium requirements places a restriction on M/R. There are a number of realistic equations of state used in the literature [42] than the one used here. In this work, we use the most commonly used equation of state. This equation of state provides a straightforward relationship between pressure and density, offering a simplicity often absent in more complex equations of state. Moreover, it serves as a reasonable approximation for cold equations of state. Compared to more realistic EOSs, such as tabulated nuclear EOSs, the polytropic form significantly reduces computational complexity, enabling studies like those presented in this Chapter and Chapter 5 without the challenges typically

associated with tabulated EOSs. The polytropic equation is given as, [76].

$$\epsilon = \left(\frac{p}{K}\right)^{1/\Gamma} + \frac{K\rho^{\Gamma}}{\Gamma - 1}. \tag{4.42}$$

Since we are evolving pressure, 4.41a then the value of the EOS 4.42 is calculated and substituted in equations 4.41c and 4.41a. At the star's center, the initial conditions are defined as $P(0) = P_c$ and $M(0) = 0$, where P_c represents the central pressure and $M(0)$ denotes the mass at $r = 0$. The pressure becomes zero at the surface of the star to define the boundary condition $r = R$, and so given the central density of a neutron star we can uniquely determine the mass M and radius R.

4.4 Numerical results

The TOV equations can be used to find the interior properties of a neutron star, such as mass, densities and their relationships for $r \leq R$ where R is the surface of the star. Because of Birkhoff's theorem[1], for values of r greater than R, the Schwarzschild metric is the appropriate vacuum solution. The radius R represents the boundary separating the interior of the star from the exterior.

At the centre of the star, where $r = 0$, the TOV equations cannot be specified because 4.41c is not regular at $r = 0$. In the code, the solution is found by setting the initial value of r to an extremely small value, specifically $r = 10^{-20}$. Upon reaching the star's surface, we proceeded to restrict the metric to a Schwarzschild metric in order to seamlessly connect the internal solution with the outer. Thus, the metric functions are given by the Schwarzschild solution,

$$m(R) = M, \tag{4.43a}$$

$$p(R) = 0, \tag{4.43b}$$

$$\nu(R) = \frac{1}{2}\ln\left(1 - 2\frac{m(R)}{R}\right), \tag{4.43c}$$

$$\lambda(R) = -\frac{1}{2}\ln\left(1 - 2\frac{m(R)}{R}\right). \tag{4.43d}$$

The conditions above 4.43 are satisfied automatically except the equation 4.43c. The value of ν was set to be equal to $\nu = 1$ initially.

At the end of the integration ν adjusted separately from the rest of the values by imposing the condition that at the surface of the star ν must be consistent with eq. 4.43c. Numerically, this

is accomplished as follows,

$$C = \nu_{\text{analytical}}(R) - \nu_{\text{numerical}}(R) \quad (\text{ at } r = R), \tag{4.44a}$$

$$\nu_{\text{numerical}}(r) = \nu_{\text{numerical}}(r) + C \quad \text{loop this through all values of } r. \tag{4.44b}$$

This treatment for ν is consistent since ν only appears as a derivative in the TOV equations, so it can be specified up to a constant.

The TOV equations were solved using the code for three initial densities (see Table 4.1), for Model 1 we have the central density $\rho_c = 5.87 \times 10^{-4}\text{km}^{-2}$ which corresponds to the mass $M = 1.4M_\odot$ and the radius $R = 14.15\text{km}$. Model 2 has the central density of $\rho_c = 1.373795 \times 10^{-3}\text{km}^{-2}$, and Model 3 has the central density of $\rho_c = 4.232772 \times 10^{-3}\text{km}^{-2}$, these models use the polytropic equation of state with $K = 217.858$ and $\Gamma = 2$. Model 1 represents a stable configuration, Model 2 is stable, but very close to the unstable branch, and Model 3 is unstable. In the figure 4.1a, 4.1b, 4.1c, 4.1d below we show the results for Model 1, for pressure p, mass m and energy density ρ as well the speed of sound c_s as a function of radius r and x, where x is transformation of the $r-$coordinate $\frac{dr}{dx} = c_s$ and c_s is the speed of sound. The general definition for the speed of sound is,

$$c_s^2 = \frac{\partial p}{\partial \rho}, \tag{4.45}$$

whose expression for the polytropic equation of state is given by

$$c_s = \sqrt{\frac{\Gamma p}{\rho + p}}. \tag{4.46}$$

This solution gives the background solution that is used to solve the radial perturbation of the ADM equations in the chapter 5. The data generated as a function of the radius r is used to solve the Sturm-Liouville problem to get the eigenfrequencies, while the x coordinate generated data is used to find solutions to the three partial differential equations for h, s and u (see chapter 5 for details on the linearized equations).

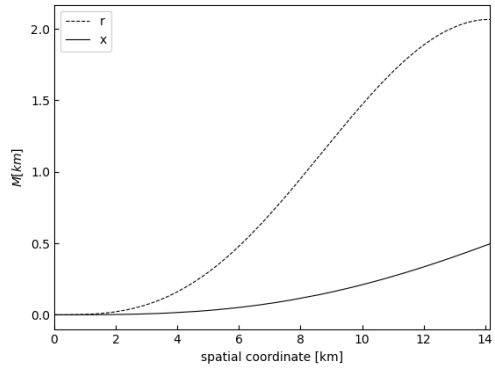

(a) Figure showing mass m as the function of r and x for the central density $\rho_c = 5.87 \times 10^{-4}\text{km}^{-2}$

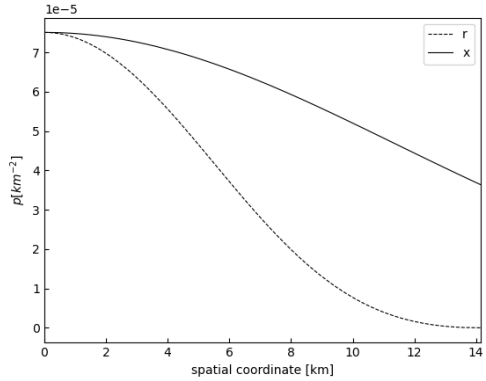

(b) Figure showing pressure p as the function of radius r and x for the Model 1

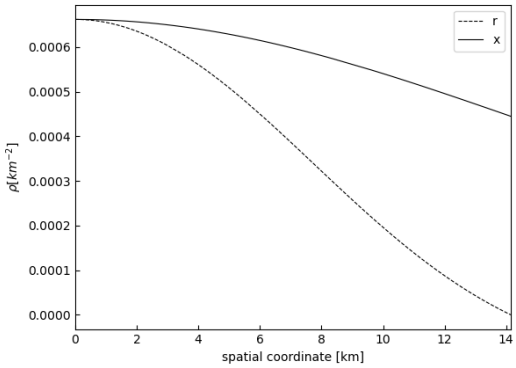

(c) Figure showing the energy density as the function of radius r and x for Model 1

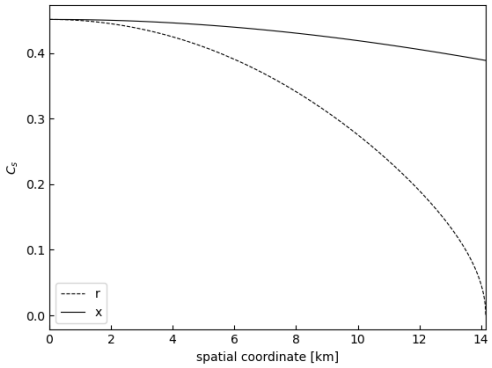

(d) Figure showing the speed of sound as the function of both radius r and x for Model 1

The transformation from radius r to x plays a crucial in the convergence of the numerical solutions for the perturbed equations. It can be noted that the pressure and density approach zero as one approaches the surface of the star which creates problems in the calculation of the speed of sound 4.1d. These quantities appear in the denominator of the linearized equations hence the transformation is essential to avoid division by zero. The numerical results of solving the TOV equations for the 3 models above is

Polytropic stellar models ($\Gamma = 2, \kappa = 217.858\,\text{km}^2$)

Model	ρ_c [1/km^2]	M [$M_\odot$]	R [km]	M/R
1	$5.87{\cdot}10^{-4}$	2.07	14.15	0.15
2	$1.37{\cdot}10^{-3}$	2.42	11.47	0.21
3	$4.23{\cdot}10^{-3}$	2.06	8.30	0.25

Table 4.1: List of the used polytropic stellar models and their physical parameters.

Chapter 5

Radial Oscillations of Neutron Stars: ADM Linear perturbations

5.1 Overview

Radial oscillations of neutron stars were first analyzed within the framework of General Relativity by Chandrasekhar [38], who developed his approach by directly perturbing the Tolman–Oppenheimer–Volkoff (TOV) equations 4.41. This method formulated the problem as a Sturm–Liouville eigenvalue equation and was subsequently adopted by several others [86, 41, 52]. An alternative approach employs a numerical relativity formulation (ADM) [86, 95]. The perturbation of the metric tensor expressed as,

$$g_{ab} = \bar{g}_{ab} + \delta g_{ab}. \tag{5.1}$$

The symbol $\bar{g}_{ab}$ denotes the background metric, while δg_{ab} denotes a small perturbation on the background metric. Indices for both the background and first order quantities are raised and lowered using the inverse of the zeroth order metric $\bar{g}^{ab}$. We ignore products that involve more than one first-order quantity because they introduce higher-order terms. In radial perturbations, we require the perturbation variables to retain the spherical symmetry of the spacetime, such that δg_{ab} is a function only of r and t. This differs from the more general non-radial perturbation where δg_{ab} depends on (t, r, θ, α), thus introducing angular dependence which breaks spherical symmetry. In this work, we focus on the most basic type of oscillation mode known as radial modes. These modes are considered simple because they do not interact with gravitational waves, making the equations involved in their study straightforward to handle.

From the perturbation of the metric, one can write down perturbations of the Christoffel symbols

and perturbations of the Ricci tensor. This will allow us to write down the ADM equations in terms of the perturbed metric. Components of the background metric $\bar{g}_{ab}$ can be read from the TOV metric 4.1 as

$$\bar{g}_{ab} = \text{diag}(-e^{2\nu}, e^{2\lambda}, r^2, r^2 \sin^2\theta). \tag{5.2}$$

Recall that from the 3+1 formalism (see chapter 3, eq. 3.11), the general form of the line element is given by [99, 86, 4, 21],

$$ds^2 = -(\alpha^2 - \beta_k\beta^k)dt^2 + 2\beta_i dt dx^i + \gamma_{ij}dx^i dx^j. \tag{5.3}$$

By comparing this with the line element of a spherically symmetric spacetime 4.1, we can write down the following zeroth order quantities for the ADM variables.

$$\alpha = \sqrt{-g_{00}} = e^{\nu}, \tag{5.4a}$$

$$\beta^i = 0, \tag{5.4b}$$

$$\gamma_{ij} = \text{diag}(e^{2\lambda}, r^2, r^2 \sin^2(\theta)). \tag{5.4c}$$

Because 5.4c has no time dependence, the extrinsic curvature given as

$$K_{ij} = 0, \tag{5.5}$$

where we have used equation 3.37 to express K_{ij} in terms of time derivatives of the metric. In equations 5.4-5.5 α represents the lapse function, β^k represents the shift vector, γ_{ij} represents the 3-metric, and K_{ij} represents the extrinsic curvature. The shift vector β^k vanishes along with the extrinsic curvature of all the hypersurfaces of constant time t since the background metric is static.

Now, we proceed to derive the evolution and constraint equations for the perturbations. Perturbing the energy-momentum tensor ensures the perturbation of the star's matter, with the pressure perturbation being determined by

$$\delta p = \frac{dp}{d\epsilon}\delta\epsilon = \frac{p'}{\epsilon'}\delta\epsilon = c_s^2\delta\epsilon. \tag{5.6}$$

The variable c_s represents the speed at which sound propagates in a fluid. By considering $k_{ij} = \delta K_{ij}$

and $h_{ij} = \delta g_{ij}$, we can linearize the ADM system (Eqs 3.37, 3.38) [92]

$$\begin{aligned}
\partial_t h_{ij} &= \beta^k \partial_k \gamma_{ij} + \gamma_{ki}\partial_j \beta^k + \gamma_{kj}\partial_i \beta^k - 2e^{\nu} k_{ij}, && (5.7)\\
\partial_t k_{ij} &= -\partial_i \partial_j \alpha + \Gamma^k{}_{ij}\partial_k \alpha + \delta\Gamma^k{}_{ij}\partial_k e^{\nu} + \alpha\left[R_{ij} + 4\pi(p\ -\epsilon)\gamma_{ij}\right] \\
&\quad + e^{\nu}\left[\delta R_{ij} + 4\pi\left((p-\epsilon)h_{ij} + \delta\epsilon\left(c_s^2\ \ -1\right)\gamma_{ij}\right)\right]. && (5.8)
\end{aligned}$$

Where $\delta\Gamma^k{}_{ij}$ is the perturbation of the Christoffel symbols, given in terms of the perturbed metric as

$$\delta\Gamma^k{}_{ij} = \frac{1}{2}\gamma^{kl}(\partial_j h_{li} + \partial_i h_{lj} - \partial_l h_{ij}), \tag{5.9}$$

and $\Gamma^k{}_{ij}$ represent the background spatial Christoffel symbols. From this, we may determine the Ricci tensor perturbations, [92]

$$\begin{aligned}
\delta R_{ij} =& \delta\Gamma^k{}_{ij;k} - \delta\Gamma^k{}_{ik;j} \\
=& \partial_k \delta\Gamma^k{}_{ij} - \partial_j \delta\Gamma^k{}_{ik} - \delta\Gamma^k{}_{mk}\Gamma^m{}_{ij} + \delta\Gamma^m{}_{ij}\Gamma^k{}_{mk}\ \ - \delta\Gamma^k{}_{mj}\Gamma^m{}_{ik} - \delta\Gamma^m{}_{ik}\Gamma^k{}_{mj}.
\end{aligned} \tag{5.10}$$

Similarly, the Hamiltonian 3.35 and Momentum constraint 3.36 are linearlized to [92, 18]

$$\gamma_{ij}\delta R_{ij} - h^{ij}R_{ij} = 16\pi\delta\epsilon, \tag{5.11}$$

$$\gamma^{jk}\left(\partial_i k_{jk} - \partial_j k_{ik} - \Gamma^l_{ik}k_{jl} + \Gamma^l{}_{ik}k_{il}\right) = -8\pi(p+\epsilon)\delta u_i. \tag{5.12}$$

The evolution equations for δu_i and $\delta\epsilon$ may be derived from the linearized energy momentum conservation equations $\delta T^{ab}{}_{;b}$.

Throughout this study, we use the polytropic equation of state 4.42. In our case, we only need to consider the resolution within the star's interior, for radial oscillations, the boundary of the numerical grid is placed at the edge of the star, so there is no need to consider the exterior. In the following, we will present the evolution equations that we use for the radial modes.

5.2 Linear perturbations of ADM equations

In order to establish the evolution equations, we employ the 3+1 formalism, which is the prevailing paradigm for numerical relativity. Below is the procedure for obtaining the evolution equations through the 3+1 decomposition. As previously mentioned, we are specifically examining radial oscillations which correspond to the $l = 0$ mode. This means that our spherical harmonic, denoted as Y_{00}, is simply equal to $1/\sqrt{4\pi}$. This value highlights that there are no angular dependencies, as

the derivatives of Y_{00} with respect to θ and ϕ will be zero. Since Y_{00} is a scalar, we can incorporate it into the perturbation variables, which are functions of t and r only. Following [86], the first order expansion of these variables along with the extrinsic curvature are given by

$$\alpha = e^{\nu} S_1(t,r), \tag{5.13a}$$

$$\beta_r = r e^{2\lambda} S_2(t,r), \tag{5.13b}$$

$$h_{ij} = \text{diag}\left(r e^{2\lambda} S_3(t,r), r^2 T(t,r), r^2 \sin^2\theta T(t,r)\right), \tag{5.13c}$$

$$k_{ij} = -e^{-\nu}\text{diag}\left(e^{2\lambda} K_1(t,r), \frac{1}{2} r^2 K_2(t,r), \frac{1}{2} r^2 \sin^2\theta K_2(t,r)\right). \tag{5.13d}$$

The prefactors in the variables are conveniently chosen to yield a simpler, more tractable set of equations. The components of the perturbed Christoffel symbols up to the first order are

$$\delta\Gamma^{r}{}_{rr} = \frac{1}{2} S_3 + \frac{1}{2} r \partial_r S_3, \tag{5.14}$$

$$\delta\Gamma^{r}{}_{\theta\theta} = r e^{-2\lambda}\left(r S_3 - T - \frac{r}{2}\partial_r T\right), \tag{5.15}$$

$$\delta\Gamma^{r}{}_{\phi\phi} = r e^{-2\lambda}\sin^2(\theta)\left(r S_3 - T - \frac{r}{2}\partial_r T\right), \tag{5.16}$$

$$\delta\Gamma^{\theta}{}_{r\theta} = \frac{1}{2}\partial_r T, \tag{5.17}$$

$$= \delta\Gamma^{\theta}{}_{\theta r}, \tag{5.18}$$

$$\delta\Gamma^{\phi}{}_{r\phi} = \frac{1}{2}\partial_r T, \tag{5.19}$$

$$= \delta\Gamma^{\phi}{}_{\phi r}. \tag{5.20}$$

Plugging in the expressions for the Christoffel symbols to find the Ricci tensor components results in

$$\delta R_{rr} = -\partial_{rr} T + \left(\partial_r \lambda - \frac{2}{r}\right)\partial_r T + \frac{S_3}{r} + \partial_r S_3, \tag{5.21}$$

$$\delta R_{\theta\theta} = -\frac{1}{2} e^{-2\lambda}\left[r^2 \partial_{rr} T + \left(4r - r^2\partial_r\lambda\right)\partial_r T + 2\left(1 - r\partial_r\lambda\right) T + \left(2r^2\partial_r\lambda - 3r\right) S_3 - r^2 S_3\right], \tag{5.22}$$

$$\delta R_{\phi\phi} = \sin^2(\theta)\delta R_{\theta\theta}. \tag{5.23}$$

Next, we proceed to define the matter perturbations, which consist of velocity perturbations in the r direction and the energy density perturbation $\delta\epsilon$. These perturbations are expressed as

$$\delta\epsilon = \rho(t,r), \tag{5.24a}$$

$$\delta u_r = -e^{\nu} u(t,r). \tag{5.24b}$$

Plugging back the perturbation of the extrinsic curvature metric 5.13c and perturbations 5.13d of the spatial 3-metric into the perturbed ADM equations 5.7, 5.8 we get the following four evolution equations

$$\frac{\partial S_3}{\partial t} = 2\left(\frac{\partial S_2}{\partial r} + \left(\lambda' + \frac{1}{r}\right) S_2 + \frac{K_1}{r}\right), \tag{5.25a}$$

$$\frac{\partial T}{\partial t} = 2S_2 + K_2, \tag{5.25b}$$

$$\begin{aligned}\frac{\partial K_1}{\partial t} = {} & e^{2\nu-2\lambda}\left[\frac{\partial^2 T}{\partial r^2} + \frac{\partial^2 S_1}{\partial r^2} + \left(\frac{2}{r} - \lambda'\right)\frac{\partial T}{\partial r} + \left(2\nu' - \lambda'\right)\frac{\partial S_1}{\partial r}\right. \\ & \left. - \left(\frac{1}{2}r\nu' + 1\right)\frac{\partial S_3}{\partial r} + \left(\lambda' - \frac{3}{2}\nu' + \frac{e^{2\lambda}-2}{r}\right) S_3\right] \\ & + 4\pi e^{2\nu}\left(1 - c_s^2\right)\rho,\end{aligned} \tag{5.25c}$$

$$\begin{aligned}\frac{\partial K_2}{\partial t} = {} & e^{2\nu-2\lambda}\left[\frac{\partial^2 T}{\partial r^2} + \left(\nu' - \lambda' + \frac{4}{r}\right)\frac{\partial T}{\partial r} + \frac{2}{r}\frac{\partial S_1}{\partial r} - \frac{\partial S_3}{\partial r}\right. \\ & \left. + 2\frac{e^{2\lambda}}{r^2}T + \left(2\lambda' - 2\nu' - \frac{3}{r}\right) S_3\right] \\ & + 8\pi e^{2\nu}\left(1 - c_s^2\right)\rho,\end{aligned} \tag{5.25d}$$

along with the Hamiltonian and the momentum constraints respectively given as

$$8\pi e^{2\lambda}\rho = -\frac{\partial^2 T}{\partial r^2} + \left(\lambda' - \frac{3}{r}\right)\frac{\partial T}{\partial r} - \frac{e^{2\lambda}}{r^2}T + \frac{\partial S_3}{\partial r} + 2\left(\frac{1}{r} - \lambda'\right) S_3, \tag{5.26}$$

$$8\pi(p+\epsilon)e^{2\nu}u = -\frac{\partial K_2}{\partial r} + \left(\nu' - \frac{1}{r}\right) K_2 + \frac{2}{r}K_1. \tag{5.27}$$

Before we can explore numerical solutions, we need to specify the gauge conditions, which entails selecting the lapse function and shift vector. The shift vector is selected as $S_2(t,r) = 0$. Furthermore, we select the value of T to be $T(t,r) = 0$ at the initial hypersurface $t = 0$. After substituting these values into the evolution equations 5.25, we obtain the simplified equations.

$$\frac{\partial S_3}{\partial t} = \frac{2}{r}K_1, \tag{5.28a}$$

$$\frac{\partial T}{\partial t} = K_2, \tag{5.28b}$$

$$\begin{aligned}\frac{\partial K_1}{\partial t} = {} & e^{2\nu-2\lambda}\left[\frac{\partial^2 S_1}{\partial r^2} + \left(2\nu' - \lambda'\right)\frac{\partial S_1}{\partial r} - \left(\frac{1}{2}r\nu' + 1\right)\frac{\partial S_3}{\partial r}\right. \\ & \left. + \left(\lambda' - \frac{3}{2}\nu' + \frac{e^{2\lambda}-2}{r}\right) S_3\right] + 4\pi e^{2\nu}\left(1 - c_s^2\right)\rho,\end{aligned} \tag{5.28c}$$

$$\frac{\partial K_2}{\partial t} = e^{2\nu-2\lambda}\left[\frac{2}{r}\frac{\partial S_1}{\partial r} - \frac{\partial S_3}{\partial r} + \left(2\lambda' - 2\nu' - \frac{3}{r}\right) S_3\right] + 8\pi e^{2\nu}\left(1 - c_s^2\right)\rho, \tag{5.28d}$$

the Hamiltonian constraint reduces to

$$8\pi e^{2\lambda}\rho = \frac{\partial S_3}{\partial r} + 2\left(\frac{1}{r} - \lambda'\right) S_3. \tag{5.29}$$

Note that although we have chosen $T(r,t) = 0$ initially, we still have an evolution equation for $T(r,t)$ 5.28b. To eliminate this equation, we will utilise the final remaining gauge flexibility of the lapse function. This is accomplished by solving the Hamiltonian constraint 5.29 for $\frac{\partial S_3}{\partial r}$ and substituting the result into equation 5.28d, leading to,

$$\frac{\partial K_2}{\partial t} = e^{2\nu-2\lambda}\left(\frac{2}{r}\frac{\partial S_1}{\partial r} - \left(2\nu' + \frac{1}{r}\right) S_3\right) - 8\pi e^{2\nu} c_s^2 \rho. \tag{5.30}$$

The idea above is equivalent to choosing the radial gauge [17, 56] hence [1]

$$T(0,r) = S_2(0,r) = K_2(0,r) = 0. \tag{5.31}$$

Next, the lapse function S_1 is selected in such a way that the right-hand side of equation 5.30 is equal to zero. This leads to the equation for S_1

$$\frac{\partial S_1}{\partial r} = \left(r\nu' + \frac{1}{2}\right) S_3 + 4\pi r e^{2\lambda} c_s^2 \rho. \tag{5.32}$$

This process is equivalent to choosing the polar slicing[2] [56]. The above set of equations 5.28 can be supplemented by the conservation law $D_\nu T^{\mu\nu} = 0$. It is convenient to recast the energy density perturbation in terms of a new variable

$$H(t,r) = \frac{c_s^2}{p+\epsilon}\rho(t,r). \tag{5.33}$$

This definition, along with the conservation equations leads to the system

$$\frac{\partial H}{\partial t} = e^{2\nu-2\lambda} c_s^2 \frac{\partial u}{\partial r} + e^{2\nu-2\lambda}\left(c_s^2\left(2\nu' - \lambda' + \frac{2}{r}\right) - \nu'\right) u - c_s^2 K_1, \tag{5.34}$$

$$\frac{\partial u}{\partial t} = \frac{\partial H}{\partial r} + \frac{\partial S_1}{\partial r}. \tag{5.35}$$

[1] For the radial gauge, the radial coordinate r is chosen in such a way that the proper area of spheres of constant r is always $4\pi r^2$, meaning the metric is such that $T = 0$.

[2] Polar slicing: Obtained by the requirement that the trace of the extrinsic curvature is zero,

$$\operatorname{tr} K = K^r{}_r \Leftrightarrow K^\theta{}_\theta + K^\phi{}_\phi = 0.$$

It is important to observe that in the aforementioned form of the matter equations (equations 5.34 and 5.35), we have already implemented the requirements $T = S_2 = K_2 = 0$. Furthermore, in equation 5.34, we can eliminate K_1 by using the Momentum constraint eqn. 5.27 as,

$$K_1 = 4\pi r e^{2\nu}(p+\epsilon)u = e^{2(\nu-\lambda)}(\lambda' + \nu')u. \tag{5.36}$$

Lastly, we can eliminate S_1 from 5.35 by using 5.32. With these steps, we now have a closed system of equations,

$$\frac{\partial H}{\partial t} = e^{2\nu-2\lambda}\left[c_s^2\frac{\partial u}{\partial r} + \left(c_s^2\left(\nu' - 2\lambda' + \frac{2}{r}\right) - \nu'\right)u\right], \tag{5.37a}$$

$$\frac{\partial u}{\partial t} = \frac{\partial H}{\partial r} + \left(\nu' + \lambda'\right)H + \left(r\nu' + \frac{1}{2}\right)S_3, \tag{5.37b}$$

$$\frac{\partial S_3}{\partial t} = 8\pi(p+\epsilon)e^{2\nu}u, \tag{5.37c}$$

with H and S_3 satisfying the hamiltonian constraint 5.29

$$8\pi e^{2\lambda}\frac{p+\epsilon}{c_s^2}H = \frac{\partial S_3}{\partial r} + 2\left(\frac{1}{r} - \lambda'\right)S_3. \tag{5.38}$$

5.3 Initial and Boundary conditions

As initial data, we use a Gausian pulse for u, with H and S_3 initially set to zero,

$$u(r,0) = A\exp\left[\left(\frac{r-\mu}{\sigma}\right)^2\right], \tag{5.39}$$

$$H(r,0) = 0, \tag{5.40}$$

$$S_3(r,0) = 0. \tag{5.41}$$

Another, equally valid option is to initialise $S_3(r,0)$ with a Gaussian profile, then use the Hamiltonian constraint Eq 5.38 to obtain $H(r,0)$, with the variables $u(r,0)$ independently set. The constants μ and σ control the shape and position of the profile relative to the origin, and have no impact on the numerical solutions. On the other hand, the amplitude A is important and controls the linearity of the perturbations. In this work, we use $A = 0.001$.

To be able to find a physical solution for the set of partial differential equations 5.37, boundary conditions are imposed at the origin of the neutron star and at the surface. First it is needed

that at the origin the perturbation variables are regular [86]

$$H(t,r) = H^0(t) + O(r^2), \tag{5.42}$$

$$u(t,r) = u^0(t)r + O(r^3), \tag{5.43}$$

$$S_3(t,r) = S_3^0(t)r + O(r^3). \tag{5.44}$$

At the stellar surface it is required that the Lagrangian pressure perturbation Δp vanishes [38, 72]. This condition involves the concept of radial displacement, $\xi(t,r)$, which represents the displacement of a fluid element from its equilibrium position as a function of both time and position. For the radial case, the connection between ξ and δu_r is expressed as follows,

$$\frac{\partial \xi}{\partial t} = e^{\nu - 2\lambda}\delta u_r. \tag{5.45}$$

The normalised displacement is then defined as,

$$\zeta := r^2 e^{-\nu}\xi. \tag{5.46}$$

The Lagrangian pressure perturbation can finally be written as

$$r^2 \Delta p = -(p+\epsilon)c_s^2 e^{-\nu}\frac{\partial \zeta}{\partial r}. \tag{5.47}$$

Eq 5.47 is satisfied whenever $c_s^2(p+\epsilon) = 0$ or $\left(\frac{\partial \xi}{\partial r}\right) = 0$. If $(p+\epsilon)c_s^2$ does not become zero at the surface, which is true for most cold EOS such as the polytropic model considered here, then

$$\frac{\partial \zeta}{\partial r}(R) = 0. \tag{5.48}$$

In order to apply this boundary condition to our system of evolution equations 5.37, we need to convert it into a condition for u. This may be achieved by using Eq 5.24b in Eq 5.49 to find,

$$\frac{\partial \xi}{\partial t} = -e^{2(\nu-\lambda)}u(t,r). \tag{5.49}$$

Therefore,

$$0 = \left(\frac{\partial \zeta}{\partial t}\right)'_{r=R} = \left(r^2 e^{-\nu}\frac{\partial \xi}{\partial t}\right)'_{r=R} = \left(-r^2 e^{-\nu}e^{2(\nu-\lambda)}u\right)'_{r=R} = -\left(r^2 e^{\nu-2\lambda}u\right)'_{r=R}. \tag{5.50}$$

Therefore, at the boundary $r = R$, we have

$$u'(R) = \left(2\lambda'(R) - \nu'(R) - \frac{2}{R}\right) u(R). \tag{5.51}$$

For the variables H, we note that, at the boundary, Eq 3.18 reduces to an ODE since $c_s^2 = 0$, and since there are no S_3 spatial derivatives in the system 5.37, boundary conditions for S_3 are not needed. However, for consistency in the code, we set $S_3(R) = 0$ at the boundary.

5.4 Comparison with the Eigenvalue problem

The standard eigenvalue problem is often formulated in terms of a Sturm–Liouville equation [63]

$$0 = \frac{d}{dr}\left(P\frac{d\chi}{dr}\right) + \left(Q + \omega^2 W\right)\chi, \tag{5.52}$$

where

$$W = (p+\epsilon)e^{3\lambda+\nu}r^{-2}, \tag{5.53}$$

$$P = (p+\epsilon)c_s^2 e^{\lambda+3\nu}r^{-2}, \tag{5.54}$$

$$Q = e^{\lambda+3\nu}(p+\epsilon)\left(\left(\nu'\right)^2 + 4\frac{\nu'}{r} - 8\pi e^{2\lambda}p\right)r^{-2}. \tag{5.55}$$

The variable $\chi(r)$ is related to the displacement via

$$\zeta(t,r) = e^{iwt}\chi(r). \tag{5.56}$$

To numerically solve the eigenvalue problem 5.52, we express it as a system of two first-order equations with χ and $\eta := P\chi'$ [18].

$$\frac{d\chi}{dr} = \frac{\eta}{P}, \tag{5.57a}$$

$$\frac{d\eta}{dr} = -\left(\omega^2 W + Q\right)\chi. \tag{5.57b}$$

To compute the eigenvalues, we integrate Eq 5.57 from the origin $r = 0$ to the stellar surface at $r = R$, ensuring the boundary condition $\chi'(R) = 0$ is met. This process is done via the shooting method (see section 5.5.2).

5.5 Numerical methods

5.5.1 WENO Finite Differencing

We use finite difference WENO scheme for the spatial derivatives in 5.37. WENO schemes are a class of high-order accurate numerical methods designed to solve hyperbolic partial differential equations (PDEs) and other convection-dominated problems [94, 112, 16, 44]. These schemes are particularly effective in handling problems with both strong discontinuities and complex smooth solution structures. The key benefit of WENO schemes is their capacity to provide high-order accuracy in smooth areas while ensuring stability, non-oscillatory behavior, and sharp transitions at discontinuities.

Finite Difference WENO Formulation

Consider the scalar conservation law

$$\frac{\partial u}{\partial t} + \frac{\partial f(u)}{\partial x} = 0, \tag{5.58}$$

where $u(x,t)$ is the conserved quantity, and $f(u)$ is the flux. The goal is to approximate the spatial derivative $\frac{\partial f}{\partial x}$. The domain is discretized using uniform grid points $x_i = i\Delta x$, with spacing Δx. The flux is split into positive and negative components [93],

$$f(u) = f^+(u) + f^-(u),$$

where $f^+(u)$ and $f^-(u)$ satisfy,

$$\frac{\partial f^+}{\partial u} \geq 0, \quad \frac{\partial f^-}{\partial u} \leq 0.$$

This ensures upwind-biased discretization for stability.

WENO Reconstruction

To approximate the flux derivative $\frac{\partial f}{\partial x}$ at a point x_i, the WENO scheme reconstructs the flux $f_{i+1/2}$ at the midpoints between grid points using weighted stencils. For a fifth-order WENO scheme, three overlapping stencils are used,

$$S_0 = \{x_{i-2}, x_{i-1}, x_i\}, \quad S_1 = \{x_{i-1}, x_i, x_{i+1}\}, \quad S_2 = \{x_i, x_{i+1}, x_{i+2}\}.$$

On each stencil S_k, a third-order polynomial $p_k(x)$ is constructed to approximate the flux,

$$p_k(x) = \text{combination of grid values in } S_k.$$

The smoothness of each stencil is measured using smoothness indicators β_k [93, 59, 91],

$$\beta_k = \sum_{r=1}^{2} \Delta x^{2r-1} \int_{x_{i-1/2}}^{x_{i+1/2}} \left(\frac{\partial^r p_k(x)}{\partial x^r} \right)^2 dx.$$

Larger β_k values indicate more oscillatory stencils. The nonlinear weights ω_k are computed as,

$$\omega_k = \frac{\alpha_k}{\sum_m \alpha_m}, \quad \alpha_k = \frac{d_k}{(\epsilon + \beta_k)^2},$$

where d_k are the linear weights for optimal accuracy, ϵ prevents division by zero ($\epsilon \sim 10^{-6}$) [93]. The flux at the midpoint is obtained by combining the candidate fluxes:

$$f_{i+1/2} = \sum_{k=0}^{2} \omega_k f_k.$$

Final Derivative Approximation

Once $f_{i+1/2}$ and $f_{i-1/2}$ are reconstructed, the flux derivative is approximated as,

$$\frac{\partial f}{\partial x}\Big|_{x_i} \approx \frac{f_{i+1/2} - f_{i-1/2}}{\Delta x}. \tag{5.59}$$

5.5.2 Shooting Method

As mentioned in section 5.4, we use the shooting method to solve the system 5.57. The shooting method is a numerical approach used to solve boundary value problems (BVPs) for ordinary differential equations (ODEs) [30, 78]. It involves converting the BVP into an initial value problem (IVP) and iteratively adjusting initial conditions to satisfy the boundary conditions at the other end of the interval. Given the ODE,

$$y''(x) = f(x, y, y'), \quad a \le x \le b, \tag{5.60}$$

with boundary conditions,

$$y(a) = \alpha, \quad y(b) = \beta, \tag{5.61}$$

it can be converted into an IVP by assuming an initial guess for $y'(a)$, the derivative at the starting point. The ODE is then solved as an IVP using the guessed initial conditions $y(a) = \alpha$ and $y'(a) =$ guess. After solving the IVP, the boundary condition at $x = b$ is checked by comparing the computed value $y(b)$ with the required boundary condition β. The guess for $y'(a)$ is adjusted using numerical root-finding methods, such as the bisection method, Newton-Raphson method, or secant method [97, 14], to minimize the difference $|y(b) - \beta|$. Iterations are stopped when $|y(b) - \beta|$ is within a specified tolerance. For the system 5.37, we use the shooting method in conjunction with a 4th-order Runge-Kutta method for solving the IVP and the bisection method for root-finding [81, 12].

5.6 Numerical Results

In Chapter 4, we introduced three models (see Table 4.1), as well as the polytropic equation of state. The background data obtained from integrating the TOV equations in Chapter 4 is used as input to solve both the Sturm-Liouville eigenvalue problem 5.57 and the system of equations 5.37. For Model 1 and 2, we expect a periodic time evolution with the signal being the superposition of multiple eigenmodes. On the other hand model 3 is unstable against radial collapse, hence exponential growth is expected.

Figure 5.1 depicts the results for the Model 1 time evolution and Fourier transformation. Table 5.1 contains the first 5 modes obtained from the Sturm-Liouville problem (frequency domain) compared with the frequencies obtained from the linearized ADM equations (time domain),

Table 5.1: Time and Frequency Domain Data

Normal mode	Time Domain	Frequency Domain
F	1.44260	1.44326
H1	3.95684	3.95480
H2	5.93526	5.91594
H3	7.79003	7.77513
H4	9.60358	9.58933

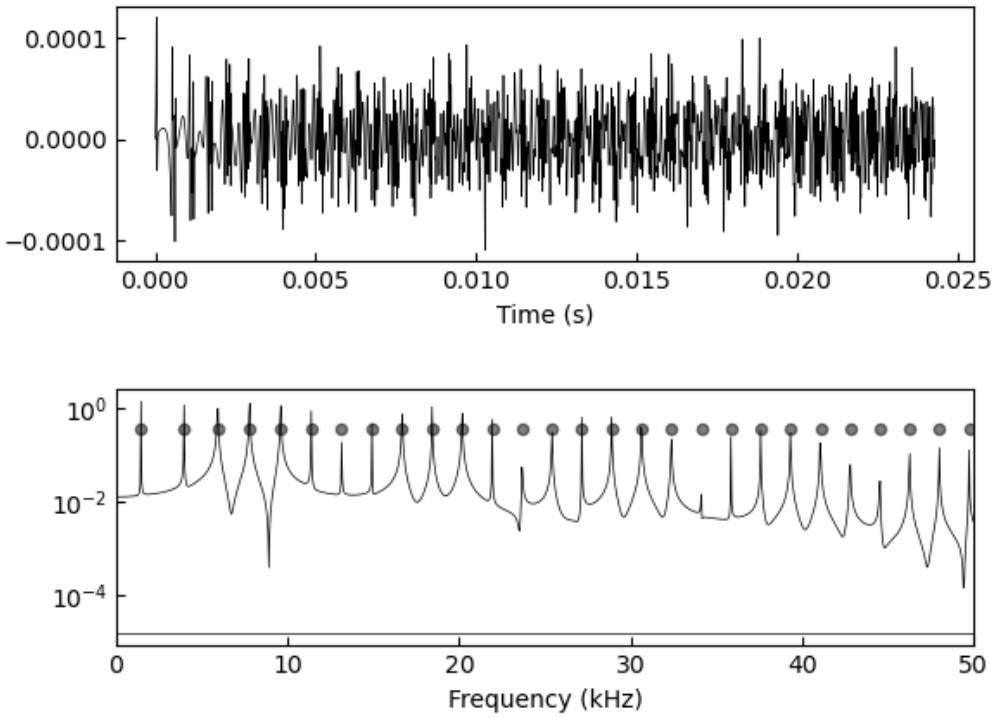

Figure 5.1: The time evolution and power spectrum of h for stellar model 1 and a central density of $\rho_c = 5.87 \times 10^{-4}\text{km}^{-2}$,where the power spectrum has clearly defined eigenmodes with the black dots obtained from solving equation 5.57.

When solving the PDE system 5.37, at each point in time, we compute the integral

$$h = \frac{1}{R}\int_0^R H dr, \tag{5.62}$$

via numerical quadrature. The top panel of figure 5.1 shows the time evolution of h. The signal demonstrates a periodic pattern, indicating the dominance of characteristic oscillation modes in the system. The bottom panel represents the Fourier transform of the time-evolved data. Sharp peaks corresponding to discrete eigenfrequencies are clearly visible, which align with the expected eigenmodes derived from the Sturm-Liouville formulation 5.57. As expected, the results from the perturbed ADM system are consistent with those obtained from the Sturm-Liouville equation, showcasing its effectiveness in capturing the discrete eigenmodes and their dynamic evolution.

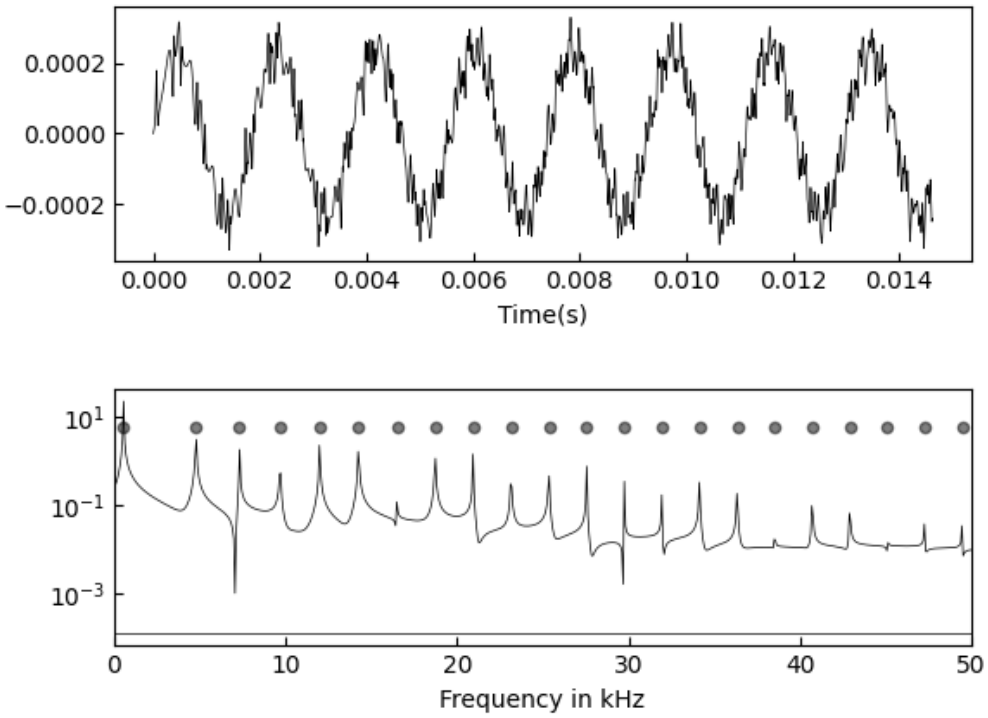

Figure 5.2: The time evolution and power spectrum of h for stellar model 2 and a central density of $\rho_c = 1.37 \times 10^{-3}\text{km}^{-2}$,where the power spectrum has clearly defined eigenmodes with the black dots obtained from solving equation 5.57.

Then, we consider Model 2 and plot the time evolution of h in the figure below 5.2, and we can see that both models 1 and 2 are similar as we see that the top panel of figure 5.2 shows the time evolution of the system's 5.37 central observable with the signal demonstrating a periodic pattern. However the bottom panel for the power spectrum of the time-evolved data, obtained via Fourier transform for Model 2 shows lower peaks for higher overtones compared to the eigenfrequencies found in the Sturm-Liouville problem, and the fundamental frequency is gradually approaching zero. From the power spectrum, once can deduce that the fundamental mode is around $v1 = 0.54$kHz. In general, one requires longer integration time to be able to resolve smaller frequncies. On the other hand, one needs higher spatial resolution to be able to resolve the larger frequencies. This presents a trade-off: because of the CFL stability condition, the time step is set proportional to the spatial step (we use $dt = 0.25dx$). It becomes computationally costly to perform long term evolutions with a small step size.

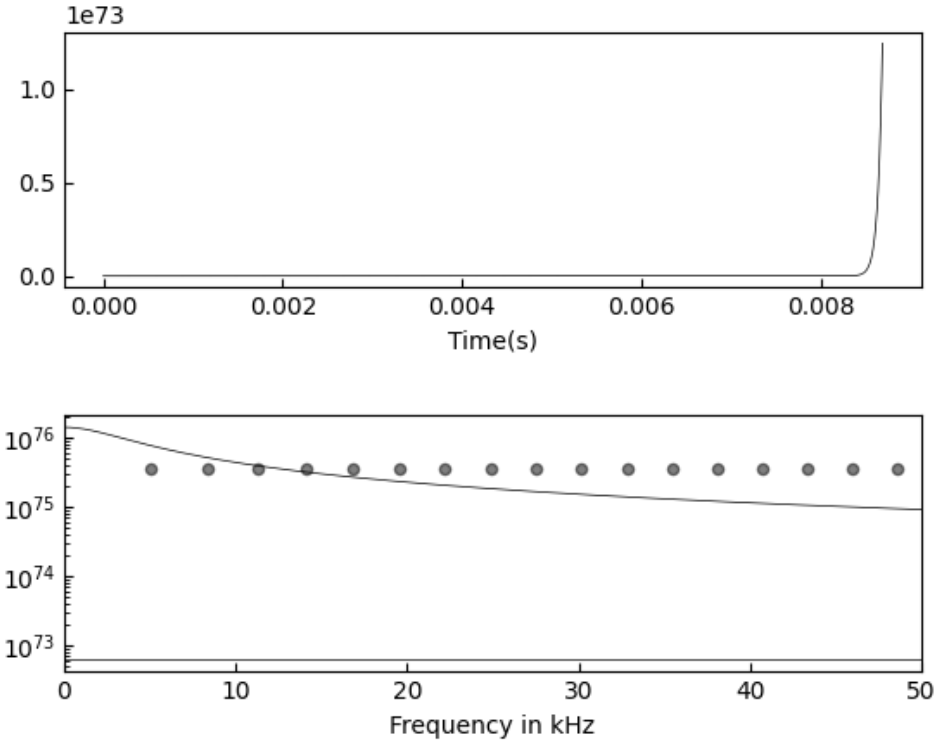

Figure 5.3: The time evolution and power spectrum of h for stellar model 3 and a central density of $\rho_c = 4.23 \times 10^{-3}\text{km}^{-2}$,where the power spectrum has clearly defined eigenmodes with the black dots obtained from solving equation 5.57.

Finally, Figure 5.3 illustrates that Model 3 is unstable, causing the neutron star to collapse into a black hole. In general, as the central density of a model increases, the star approaches its stability limit [24, 100]. The frequency of the lowest mode begins to fall toward zero. The presence of a zero-frequency eigenmode defines the stability limit. At this point, the total mass M as a function of central density reaches a local maximum [98].

Chapter 6

Quasinormal modes of a Schwarszchild black hole

In this chapter, we study the QNMs of a Schwarzschild black hole, a topic that originated with the work of Regge and Wheeler [83], who first analyzed the stability of the Schwarzschild singularity. It was then further developed by Vishveshwara [101] who first identified the characteristic ring down in the gravitational wave signal from a perturbed black hole. These results indicate that the damping time-scale nd ringing frequency form a characteristic signature of a black hole, uniquely determined by its mass, charge, and angular momentum. This is consistent with the NoHair Conjecture, which asserts that all black hole properties are fully described by these three parameters, with no additional distinguishing features [102, 58, 31, 51]. The characteristic oscillations of the black holes were termed QNMs and the frequencies associated with them are called the quasinormal frequencies. Over the years, much effort has focused on developing numerical and analytical approaches to compute QN frequencies. The beginning of this work was looking at the non-spherical metric perturbations of the Schwarzschild solution. Throughout the 1970s a number of studies were carried out and this period would usher in some of the greatest contributions to the area of perturbed spherical and rotating black holes. Among the contributions to the study of quasinormal modes and their analysis, as identified by Press [79] and Chandrasekhar [40], was Zerilli's work on even-parity perturbations [111]. Additionally, Moncrief introduced a gauge-invariant formulation for describing metric perturbations [73]. In this work, we revisit the computation of quasinormal modes Schwarzschild black hole using the characteristic formalism of numerical relativity. This formalism is reviewed in 3.4.

6.1 Linearized field equations

The starting point in deriving the master equation governing linear gravitational perturbations in the characteristic formalism is to write the Bondi-Sachs metric (Eq 3.75) in linearized form, where the spacetime is almost Schwarzschild. In outgoing null coordinates, the background metric

$$ds^2 = -\left(1 - \frac{2M}{r}\right) \mathrm{d}u^2 - 2\ \mathrm{d}u\ \mathrm{d}r + r^2 q_{AB}\ \mathrm{d}x^A\ \mathrm{d}x^B, \tag{6.1}$$

is the Eddington-Finkelstein form of the Schwarzschild metric 2.28. The line element (Eq 6.1) correspond to the Bondi-Sachs metric with $U = 0 = J = \beta$ and $W = -2M$. Then the following quantities and their derivatives are designate as first order,

$$J, \bar{J}, U, \bar{U}, w, \beta = \mathcal{O}(\epsilon), \tag{6.2}$$

where $W = -2M + w$. Applying this linearization procedure to equations 3.95-3.98, we discard terms that are second order $\mathcal{O}(\epsilon^2)$ or higher which leads to setting the non-linear quantities $N_\beta = N_U = N_Q = N_W = N_J = 0$. This leads to the linearized equations

$$\beta_{,r} = 0, \tag{6.3}$$

$$r^3 U_{,rr} + 4r^2 U_{,r} + r\bar{\eth} J_{,r} + 4\eth\beta - 2r\eth\beta_{,r} = 0, \tag{6.4}$$

$$4\beta - 2\eth\bar{\eth}\beta + \frac{1}{2}\left(\bar{\eth}^2 J + \eth^2 J\right) + \frac{1}{2r^2}\left[r^4(\eth\bar{U} + \bar{\eth}U)\right]_{,r} - 2w_{,r} = 0, \tag{6.5}$$

$$2r(rJ)_{,ur} - 2\eth^2\beta + 2r\eth U + r^2\eth U_{,r} - 2(r-M)J_{,r} - r^2\left(1 - \frac{2M}{r}\right)J_{,rr} = 0. \tag{6.6}$$

Because we are dealing with the vacuum case the following are the constraint equations in this instance

$$\frac{1}{2r^3}\Big(r(r-2M)w_{,rr} + \eth\bar{\eth}w + 2(r-2M)\eth\bar{\eth}\beta - Mr(\eth\bar{U} + \bar{\eth}U)$$
$$-4r(r-2M)\beta_{,u} - r^3(\eth\bar{U} + \bar{\eth}U)_{,u} + 2rw_{,u}\Big) = 0, \tag{6.7}$$

$$\frac{1}{4r^2}\Big(2rw_{,rr} + 4\eth\bar{\eth}\beta - (r^2\eth\bar{U} + r^2\bar{\eth}U)_{,r}\Big) = 0, \tag{6.8}$$

$$\frac{1}{4r^2}\Big(2r\eth w_{,r} - 2\eth w + 2r^2(r-2M)(4U_{,r} + rU_{,rr}) + 4r^2U + r^2(\eth\bar{\eth}U - \eth^2\bar{U})$$
$$+2r^2\bar{\eth}J_{,u} - 2r^4U_{,ur} - 4r^2\eth\beta_{,u}\Big) = 0. \tag{6.9}$$

For the purposes of our applications, we do not need the expressions for the constraint equations; we provide them here for completeness.

6.2 Eigenfunction decomposition and Spin weighted harmonics

The metric quantities (Eqs 6.2) can be expressed as eigenfunctions of the $\eth$ and $\bar{\eth}$ operators, which is more convenient. Without loss of generality, we assume that the linearized variables can be expressed as

$$\beta = \beta_0(r)\,\mathrm{Re}\left(e^{i\nu u}\right) Z_{\ell m}, \tag{6.10a}$$

$$w = w_0(r)\,\mathrm{Re}\left(e^{i\nu u}\right) Z_{\ell m}, \tag{6.10b}$$

$$U = U_0(r)\,\mathrm{Re}\left(e^{i\nu u}\right) \partial Z_{\ell m}, \tag{6.10c}$$

$$J = J_0(r)\,\mathrm{Re}\left(e^{i\nu u}\right) \partial^2 Z_{\ell m}. \tag{6.10d}$$

In our equations 6.10, equation 6.11 is used, and we have used the convention that whenever $s = 0$ we omit the subscript, i.e. ${}_0Z_{\ell m} = Z_{\ell m}$. As basis functions, it is convenient to use the spin-weighted harmonics ${}_sZ_{\ell m}$ rather than the usual ${}_sY_{\ell m}$, in order to avoid mode couplings in terms involving $\eth$ and $\bar{\eth}$, particularly from terms such as $\left(\bar{\eth}^2 J + \eth^2 J\right), (\eth\bar{U} + \bar{\eth}U)$ and similar. These basis functions are given as

$${}_sZ_{\ell m} = \begin{cases} \dfrac{i}{\sqrt{2}}\left[(-1)^m {}_sY_{\ell m} + {}_sY_{\ell\,-m}\right] & \text{for } m < 0 \\ {}_sY_{\ell m} & \text{for } m = 0 \\ \dfrac{1}{\sqrt{2}}\left[(-1)^m {}_sY_{\ell m} + {}_sY_{\ell\,-m}\right] & \text{for } m > 0 \end{cases} \tag{6.11}$$

The ${}_sY_{\ell m}$ are the standard spin-weighted spherical harmonics [54, 71]

$${}_sY_{\ell m} = \begin{cases} \sqrt{\dfrac{(\ell-s)!}{(\ell+s)!}}\eth^s Y_{\ell m} & \text{for } s \geq 0 \\ \\ (-1)^s\sqrt{\dfrac{(\ell-s)!}{(\ell+s)!}}\eth^{-s} Y_{\ell m} & \text{for } s < 0 \end{cases} \tag{6.12}$$

The following properties are useful in handling the angular derivatives in the field equations [70],

$$\eth({}_sY_{\ell m}) = \sqrt{(\ell-s)(\ell+s+1)}\,{}_{s+1}Y_{\ell m}, \tag{6.13}$$

$$\bar{\eth}({}_sY_{\ell m}) = -\sqrt{(\ell+s)(\ell-s+1)}\,{}_{s-1}Y_{\ell m}, \tag{6.14}$$

$$\begin{aligned}\bar{\eth}\eth({}_sY_{\ell m}) &= \eth\bar{\eth}({}_sY_{\ell m}) \\ &= -(\ell-s)(\ell+s+1)\,{}_sY_{\ell m},\end{aligned} \tag{6.15}$$

$$\eth^2({}_sY_{\ell m}) = [(\ell-s)(\ell+s+1)]\,{}_{s+2}Y_{\ell m}, \tag{6.16}$$

$$\bar{\eth}^2({}_sY_{\ell m}) = [(\ell+s)(\ell-s+1)]\,{}_{s-2}Y_{\ell m}, \tag{6.17}$$

$$\begin{aligned}\bar{\eth}^2\eth^2({}_sY_{\ell m}) &= \bar{\eth}^2\eth^2({}_sY_{\ell m}) \\ &= (\ell-s-1)(\ell-s)(\ell+s+1)(\ell+s+2)\,{}_sY_{\ell m}.\end{aligned} \tag{6.18}$$

6.3 Master equation

With the ansatz in Eqs 6.10, the linearized equations are now ODEs in r

$$\beta_{,r} = 0, \tag{6.19}$$

$$r^3U_{,rr} + 4r^2U_{,r} + r(\ell+2)(\ell-1)J_{,r} + 4\beta - 2r\beta_{,r} = 0, \tag{6.20}$$

$$4\beta + 2\ell(\ell+1)\beta + \ell(\ell-1)(\ell+1)(\ell+2)J - \frac{1}{r^2}\left[r^4\ell(\ell+1)U\right]_{,r} - 2w_{,r} = 0, \tag{6.21}$$

$$2r(rJ)_{,ur} - 2\beta + 2rU + r^2U_{,r} - 2(r-M)J_{,r} - r^2\left(1-\frac{2M}{r}\right)J_{,rr} = 0. \tag{6.22}$$

For convenience we will introduce a complex frequency variable $\rho = i\nu$ and will also drop the zero subscripts on Eqs 6.10 as well, and from these we can then write down the master equation for the variable J which was first introduced in [23] as

$$\begin{aligned}&r^3(r-2M)J_{,rrrr} - 2r^2\left(\rho r^2 - 4r + 5M\right)J_{,rrr} - r\left[14\rho r^2 - 12r - \ell(\ell+1)r + 4M\right]J_{,rr} \\ &- 2\left[\rho r^2 - \ell(\ell+1)r - 2M\right]J_{,r} = 0.\end{aligned} \tag{6.23}$$

In [23] the investigation was only for $\ell = 2$ case and the independent variable was $x = 1/r$ variable. To simplify the analysis of the Master equation we introduce a new auxilliary variable $\mathcal{J} = r^3(rJ(r)_{,rr})$ as a transformation, to reduce the fourth order Ordinary differential (ODE) 6.23 given above into the second order ODE

$$r^3(r-2M)\mathcal{J}_{,rr} - 2r\left(\rho r^2 + r - 5M\right)\mathcal{J}_{,r} - \left[2\rho r^2 + \left(\ell^2+\ell-2\right)r + 16M\right]\mathcal{J} = 0. \tag{6.24}$$

With this simplification we can now focus on the regular singular points, one at $r = 0$ and the other at $r = 2M$, and the irregular singular point at $r = \infty$. For the regular singular point at $r = 0$, the master equation solution 6.24 when expressed around this singular point, in the form

$$\lim_{r\to 0} \mathcal{J} = r^{k_i}, \tag{6.25}$$

then the exponents assume the two values $k_1 = 4$ and $k_2 = 2$. For the second regular singular point at $r = 2M$, the solution to the master equation 6.24 around this point takes the form

$$\lim_{r\to 2M} \mathcal{J} = (r - 2M)^{s_i}, \tag{6.26}$$

where the exponents s_i in this form take the values $s_1 = 0$ and $s_2 = 4\rho M - 2$. From our sign conventions used in this work, $s_2 = 4\rho M - 2$ is the outgoing solution and $s_1 = 0$ is a static solution. At $r = \infty$ we have an irregular singular point. The asymptotic solutions of the master equation 6.24 become

$$\mathcal{J} = \frac{1}{r} \quad \text{and} \quad \mathcal{J} = r^{3+4\rho M} e^{2\rho r}. \tag{6.27}$$

Recall that frequency ν is complex with the imaginary part responsible for the growth and decay of the perturbation field $\mathcal{J}$. For negative imaginary parts of the complex frequency, the mode will decay and thus the black hole is stable under perturbation. Again with our sign conventions the solution $\mathcal{J} = r^{3+4\rho M} e^{2\rho r}$ serves as the outgoing mode.

6.3.1 Quasinormal modes

Now we turn our attention to the black hole Quasinormal modes which are typically defined as solutions to the master equation with purely ingoing boundary conditions at the horizon and purely outgoing wave conditions at infinity. For our purpose, we will be imposing the purely outgoing condition at infinity. However for the boundary condition at the horizon, our only requirement is that there is no information leak within this point[1]. Based on the behavior of modes outlined in Eqs 6.26 and 6.27, our boundary conditions can be specified as

$$\mathcal{J} \xrightarrow{r\to 2M} (r - 2M)^0 \quad \text{and} \quad \mathcal{J} \xrightarrow{r\to\infty} r^{4\rho M+3} e^{2\rho r}. \tag{6.28}$$

[1]This treatment at the horizon is necessary since there are no ingoing modes within this formalism; the traditional boundary condition of ingoing at the horizon and outgoing at infinity is not possible

This behavior can be achieved by seeking power series solutions of the form

$$\mathcal{J} = r^{4\rho M+3} e^{2\rho(r-2M)} \sum_{n=0}^{\infty} a_n \left(\frac{r-2M}{r}\right)^n . \tag{6.29}$$

Using the Power series 6.29 in the master equation 6.24 results in the three term recurrence relation which determines the expansion coeffients a_n

$$\alpha_0 a_1 + \beta_0 a_0 = 0 \tag{6.30}$$

$$\alpha_n a_{n+1} + \beta_n a_n + \gamma_n a_{n-1} = 0 \quad \text{for } n = 1, 2, \cdots \tag{6.31}$$

where the functions a_n, b_n and γ_n are given by

$$\alpha_n = -n^2 + (4M\rho - 4)n + 4M\rho - 3 \tag{6.32}$$

$$\beta_n = 2n^2 - (16M\rho - 2)n + 32M^2\rho^2 - 8M\rho - 3 + \ell(\ell+1) \tag{6.33}$$

$$\gamma_n = -n^2 + (8M\rho + 2)n - 16M^2\rho^2 - 8M\rho \tag{6.34}$$

The recurrence relations above can be used to derive an infinite continued fraction equation for the QNM eigenfrequencies

$$0 = \beta_0 - \frac{\alpha_0\gamma_1}{\beta_1 -}\frac{\alpha_1\gamma_2}{\beta_2 -}\frac{\alpha_2\gamma_3}{\beta_3 -}\cdots \tag{6.35}$$

However this same equation can be inverted an arbitrary number of times with the nth inversion given by [65]

$$\left[\beta_n - \frac{\alpha_{n-1}\gamma_n}{\beta_{n-1} -}\frac{\alpha_{n-2}\gamma_{n-1}}{\beta_{n-2} -}\cdots\frac{\alpha_0\gamma_1}{-\beta_0}\right] = \frac{\alpha_n\gamma_{n+1}}{\beta_{n+1} -}\frac{\alpha_{n+1}\gamma_{n+2}}{\beta_{n+2} -}\frac{\alpha_{n+2}\gamma_{n+3}}{\beta_{n+3} -}\cdots \tag{6.36}$$

The form 6.35 and 6.36 are equivalent for $n > 0$, but for practical computation, the form 6.36 will be used instead, where the nth overtone is computed as the root of the nth inversion.

6.3.2 Algebraically special mode

As highlighted in [39], algebraically special perturbations are those that excite gravitational waves that are either purely ingoing or purely outgoing. The Bondi-Sachs formalism is well suited to tackle these kinds of modes. In the following, we consider the purely outgoing modes in the master equation 6.24. In this case, we impose the following boundary conditions

$$\mathcal{J} \xrightarrow{r\to 2M} (r-2M)^{4\rho M-2} \qquad \text{and} \qquad \mathcal{J} \xrightarrow{r\to\infty} r^{4\rho M+3}\, e^{2\rho\, r} . \tag{6.37}$$

The appropriate series, satisfying these conditions at the boundary, can be constructed in the form

$$\mathcal{J} = (r-2M)^{4\rho M-2} r^5 \, e^{2\rho(r-2M)} \sum_{n=0}^{\infty} a_n \left(\frac{r-2M}{r}\right)^n \, . \tag{6.38}$$

Now, after substituting 6.38 into the master equation 6.24, the sequence of expansion coefficients a_n is determined by the three term recurrence relation

$$\alpha_0 a_1 + \beta_0 a_0 = 0 \, , \tag{6.39a}$$

$$\alpha_n a_{n+1} + \beta_n a_n + \gamma_n a_{n-1} = 0 \qquad n = 1, 2, \cdots \tag{6.39b}$$

with

$$\alpha_n = -(n+1)(n-1+4\rho M) \, , \tag{6.40}$$

$$\beta_n = 2n^2 - 6n + 1 + \ell(\ell+1) \, , \tag{6.41}$$

$$\gamma_n = -(n-2)(n-4) \, . \tag{6.42}$$

The root equation determining ν takes the same form as 6.36. Numerical results for $n = 1$ and $n = 3$

ℓ	$2M\nu$ $(n=1)$	$2M\nu$ $(n=3)$
2	$3.56 \times 10^{-25} - 4i$	$1.69 \times 10^{-35} + 4i$
3	$-1.55 \times 10^{-23} - 20i$	$-2.79 \times 10^{-33} + 20i$
4	$-4.20 \times 10^{-23} - 60i$	$6.23 \times 10^{-48} + 60i$
5	$-2.06 \times 10^{-22} - 140i$	$1.00 \times 10^{-38} + 140i$
6	$-6.41 \times 10^{-23} - 280i$	$-5.47 \times 10^{-32} + 280i$

Table 6.1: Eigenfrequencies determined from Eqs 6.39a, for the cases $n = 1$ and $n = 3$.

are given in Table 6.1. There are other roots corresponding to other n values. Nevertheless, the roots corresponding to $n = 1$ and $n = 3$ are noteworthy; they converge to a high degree of accuracy, suggesting that they may in fact be exact solutions. This is indeed the case, as can be verified as follows. One can impose conditions under which the infinite series 6.38 terminates, resulting in a finite number of equations for the a_i coefficients, see e.g. [68]. From the structure of the recurrence relations 6.39, this will be so if both $\gamma_{n+1} = 0$ and $a_{n+1} = 0$ for some n. If this holds, then $a_n = 0$ for all $n > m$. Now, solving $\gamma_{n+1} = 0$ leads to

$$\gamma_{n+1} = -(n-1)(n-3) = 0 \, , \tag{6.43}$$

with the solutions $n = 1$ and $n = 3$. If in addition we impose $a_{n+1} = 0$, we have the following cases

- Case $n = 1$

  Imposing the condition $a_2 = 0$ in 6.39 results in

$$\alpha_0 a_1 + \beta_0 a_0 = 0 \,, \tag{6.44a}$$

$$\beta_1 a_1 + \gamma_1 a_0 = 0 \,. \tag{6.44b}$$

  This 6.44 can be simplified to

$$\alpha_0 \gamma_1 = \beta_0 \beta_1 \,, \tag{6.45}$$

  which is equivalent to the solution

$$\rho = \frac{(\ell-1)\ell(\ell+1)(\ell+2)}{12M} \,. \tag{6.46}$$

- Case $n = 3$

  Imposing $a_{n+1} = 0$ leads to $a_4 = 0$, and the truncated recurrence relations become

$$\alpha_0 a_1 + \beta_0 a_0 = 0 \,, \tag{6.47a}$$

$$\alpha_1 a_2 + \beta_1 a_1 + \gamma_1 a_0 = 0 \,, \tag{6.47b}$$

$$\alpha_2 a_3 + \beta_2 a_2 + \gamma_2 a_1 = 0 \,, \tag{6.47c}$$

$$\beta_3 a_3 + \gamma_3 a_2 = 0 \,. \tag{6.47d}$$

  In this case, the coefficients a_i $(i = 1, 2, 3)$ can be computed explicitly from Eqs 6.47a-6.47c

$$a_1 = -\frac{\beta_0}{\alpha_0} a_0 \,, \tag{6.48}$$

$$a_2 = \left[\frac{\beta_1}{\alpha_1}\frac{\beta_0}{\alpha_0} + \frac{\gamma_1}{\alpha_1}\right] a_0 \,, \tag{6.49}$$

$$a_3 = \left[-\frac{\beta_2}{\alpha_2}\frac{\beta_1}{\alpha_1}\frac{\beta_0}{\alpha_0} - \frac{\beta_2}{\alpha_2}\frac{\gamma_1}{\alpha_1} + \frac{\gamma_2}{\alpha_2}\frac{\beta_0}{\alpha_0}\right] a_0 \,. \tag{6.50}$$

  One can then solve 6.47d

$$\left[-\frac{\beta_2}{\alpha_2}\frac{\beta_1}{\alpha_1}\frac{\beta_0}{\alpha_0} - \frac{\beta_2}{\alpha_2}\frac{\gamma_1}{\alpha_1} + \frac{\gamma_2}{\alpha_2}\frac{\beta_0}{\alpha_0}\right] \beta_3 + \left[\frac{\beta_1}{\alpha_1}\frac{\beta_0}{\alpha_0} + \frac{\gamma_1}{\alpha_1}\right] \gamma_3 = 0 \,, \tag{6.51}$$

  which yields

$$\rho = -\frac{(\ell-1)\ell(\ell+1)(\ell+2)}{12M} \,. \tag{6.52}$$

Taken together, Eqs 6.46 and 6.52, give the algebraically special mode as,

$$2M\nu = \pm i\frac{(\ell-1)\ell(\ell+1)(\ell+2)}{12M}\,. \tag{6.53}$$

6.4 Lentz Algorithm for Continued Fractions

Lentz algorithm is a robust numerical technique for evaluating continued fractions. It provides a systematic approach to compute continued fractions of the form:

$$f(x) = b_0 + \cfrac{a_1}{b_1 + \cfrac{a_2}{b_2 + \cfrac{a_3}{b_3 + \dots}}} \tag{6.54}$$

The most preferred form of the above is given as the following,

$$f(x) = b_0 + \frac{a_1}{b_1+}\frac{a_2}{b_2+}\frac{a_3}{b_3+}\frac{a_4}{b_4+}\frac{a_5}{b_5+}\cdots \tag{6.55}$$

where a_n and b_n are the coefficients of the fraction and these themselves can be functions of x. This algorithm is especially useful in applications involving special functions or iterative processes and often converges much more rapidly than power series expansion. In detail, the modified Lentz's algorithm is,

- Set $f_0 = b_0$; if $b_0 = 0$, set $f_0 = \text{tiny}$.
- Set $C_0 = f_0$.
- Set $D_0 = 0$.
- For $j = 1, 2, \dots$

  Set $D_j = b_j + a_j D_{j-1}$.
  If $D_j = 0$, set $D_j = \text{tiny}$.
  Set $C_j = b_j + \frac{a_j}{C_{j-1}}$.
  If $C_j = 0$, set $C_j = \text{tiny}$.
  Set $D_j = \frac{1}{D_j}$.
  Set $\Delta_j = C_j D_j$.
  Set $f_j = f_{j-1}\Delta_j$.
  If $|\Delta_j - 1| < \text{eps}$, then exit.

Here, eps denotes the floating-point precision, for example, 10^{-7} or 10^{-15}. The tiny parameter should be smaller than typical values of $\text{eps}|b_j|$, such as 10^{-30}. The algorithm above assumes that the continued fraction evaluation can be stopped when $|f_j - f_{j-1}|$ becomes sufficiently small.

6.5 Numerical results

The continued fraction equations 6.36 is computed via Lentz' algorithm (see section 6.4). This presents us with a standard root finding problem for each multipole number ℓ. Moreover, for each ℓ, the continued fraction equation has an infinite number of roots which are characterized by the overtone number n. The root finding methods employed here require initial guesses for each n. When $n > 2$, we set the guess for ρ via linear extrapolation from the previous roots. For $n = 1$ and $n = 2$, we initially do not have any data to extrapolate from. For that case, the initial guess is obtained via an expansion for the frequency in inverse powers of $L = \ell + 1/2$. In the notation of [43], this gives ρ as

$$-i\rho_{\ell n} = \varpi_{-1}^{(n)} L + \varpi_0^{(n)} + \varpi_1^{(n)} L^{-1} + \varpi_2^{(n)} L^{-2} + \cdots \tag{6.56}$$

The expressions of the $\varpi_i^{(n)}$ are given in [43],

$$\varpi_{-1}^{(n)} = \frac{1}{\sqrt{27}}, \tag{6.57}$$

$$\varpi_0^{(n)} = \frac{-iN}{\sqrt{27}}, \tag{6.58}$$

$$\varpi_1^{(n)} = \frac{1}{\sqrt{27}}\left[\frac{\beta}{3} - \frac{5N^2}{36} - \frac{115}{432}\right], \tag{6.59}$$

$$\varpi_2^{(n)} = \frac{-iN}{\sqrt{27}}\left[\frac{\beta}{9} + \frac{235N^2}{3888} - \frac{1415}{15552}\right], \tag{6.60}$$

$$\varpi_3^{(n)} = \frac{1}{\sqrt{27}}\left[-\frac{\beta^2}{27} + \frac{204N^2+211}{3888}\beta + \frac{854160N^4 - 1664760N^2 - 776939}{40310784}\right], \tag{6.61}$$

$$\varpi_4^{(n)} = \frac{iN}{\sqrt{27}}\left[\frac{\beta^2}{27} + \frac{1100N^2-2719}{46656}\beta + \frac{11273136N^4 - 52753800N^2 + 66480535}{2902376448}\right]. \tag{6.62}$$

where $N = n + 1/2$. In principle, one could do away with the extrapolation step by using an asymptotic expansion for the modes $\rho_{\ell n}$ as initial guesses. For the Schwarszchild case, the asymptotic expression is known to be [48]

$$-i\rho_{\ell n} = \frac{\ell + \frac{1}{2} - (n + \frac{1}{2})i}{\sqrt{27}M}\,. \tag{6.63}$$

However, since we are interested in further applying this technique to other scenarios where simple asymptotic expansions may not be readily available, we restrict our approach here to using linear extrapolation for the initial guesses.

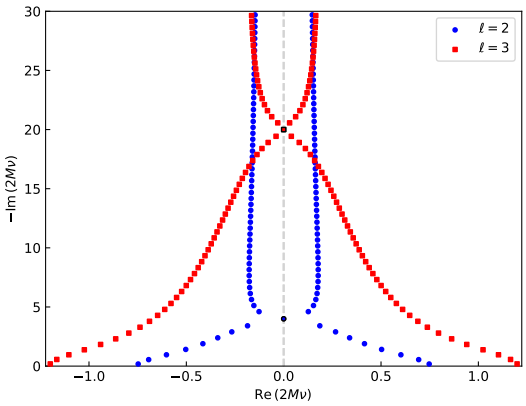

Figure 6.1: The first 60 Schwarzschild quasinormal frequencies for $\ell = 2$ and $\ell = 3$. The algebraically special modes have black outlines over them.

In Fig 6.1, we plot the first 60 modes for $\ell = 2$ and $\ell = 3$. In each case, the results are consistent with the standard quasinormal modes of the Schwarszchild black hole. The real part ($\mathrm{Re}(2M\nu)$) of the frequencies increases with increasing values of ℓ, indicating higher oscillation frequencies. The imaginary part ($\mathrm{Im}(2M\nu)$) is negative, consistent with decaying oscillations, and becomes more negative with higher overtones, reflecting faster damping for these modes. Modes with $l = 3$ have higher oscillation frequencies ($\mathrm{Re}(2M\nu)$) compared to $l = 2$ for corresponding overtones. Similarly, $l = 3$ modes show slightly faster damping, as indicated by their more negative $\mathrm{Im}(2M\nu)$ values. Lower overtones (smaller absolute $\mathrm{Im}(2M\nu)$) dominate the gravitational wave signals as they decay more slowly and persist longer. Higher overtones cluster toward the higher end of the imaginary axis, indicating their short-lived contribution to black hole spectrum. These results are consistent when compared against the standard quasinormal modes of the Schwarzschild black hole [22, 62, 64, 75].

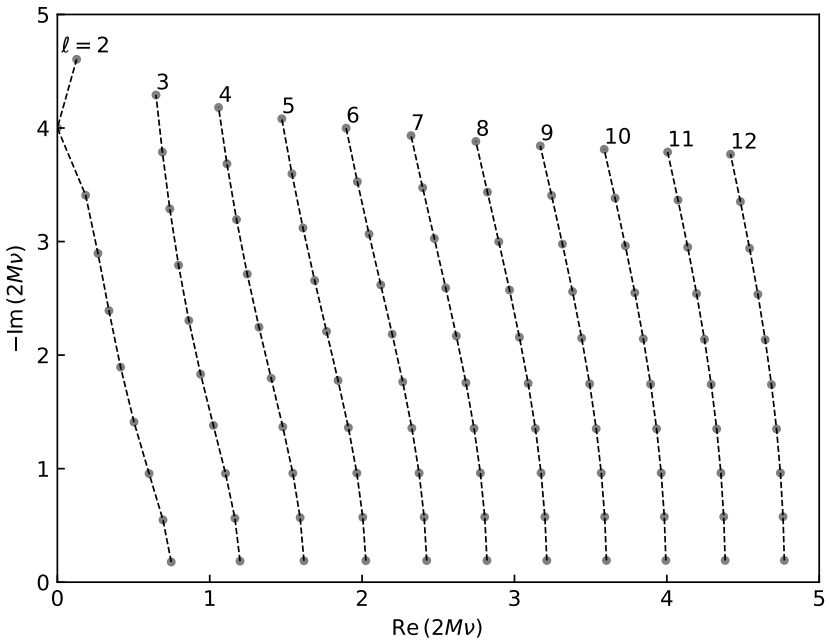

Figure 6.2: : First 10 Schwarzschild quasinormal frequencies for $\ell = 2$ through $\ell = 12$. The dashed lines connect different overtones of the modes corresponding to the same value of ℓ

We computed the eigenfrequencies of Schwarzschild black hole quasinormal modes (QNMs) for angular momentum quantum numbers $l = 2$ to $l = 12$. The results are illustrated in Figure 6.2. For $l = 2$, the mode exhibits the lowest frequency and slowest decay, making it the most prominent in astrophysical observations of gravitational wave signals. Modes with $l > 2$ contribute less significantly due to their rapid decay, with eigenfrequencies clustering further from the origin. These results are consistent with theoretical expectations for black hole QNMs, confirming the dependence of oscillation frequency and damping on angular momentum.

Chapter 7

Conclusions and Future Work

This thesis investigates the bridge between perturbation theory and numerical relativity by studying the stability of neutron stars, their radial oscillations, and the quasinormal modes (QNMs) of Schwarzschild black holes. The results provide valuable insights into how perturbative methods and full numerical simulations can complement each other, particularly within formalisms such as the ADM decomposition (Section 3.1) and the characteristic formulation (Section 3.4).

The numerical solution of the TOV equations 4.41 established the mass-radius relationship for neutron stars, revealing the transition between stable and unstable configurations based on the fundamental mode frequency. The study of radial oscillations using the linearized ADM formulation Eq 5.37 demonstrated that stable neutron stars exhibit periodic oscillations (see Figures 5.1 and 5.2), while unstable stars undergo exponential growth in perturbations, leading to collapse (see Figure 5.3). This stability transition is evident in the vanishing of the fundamental mode frequency, consistent with expectations from perturbation theory and confirmed by both time-domain and frequency-domain methods.

The characteristic formulation of numerical relativity was employed to compute the QNM spectrum of Schwarzschild black holes (Chapter 6, Eq 6.24), reproducing known frequencies (see Figures 6.1 and 6.2). This approach naturally imposes outgoing boundary conditions at future null infinity (Section 6.3.1), making it particularly well-suited for extracting QNM frequencies with high precision. The computation of Schwarzschild QNMs using the characteristic formulation successfully reproduced known mode frequencies, demonstrating the utility of this approach in perturbation studies.

The consistency of quasinormal mode results for black holes and neutron stars with those in literature reinforces the effectiveness of these formulations in compact object studies and demonstrates that it is possible to use numerical relativity to study perturbation theory, providing a bridge between analytical and computational methods. This work highlights the significance of the ADM and characteristic formulations in studying compact objects and their ability to be applied to perturbation theory, while limited to non-rotating and spherically symmetric configurations.

Future work should explore neutron stars in modified gravity theories like $f(R)$ gravity [49, 10, 13]. Investigating alternative gauge conditions can improve the numerical performance of ADM-based radial oscillation studies, particularly near instability thresholds [96]. Further work on radial oscillations in $f(R)$ gravity and boson stars can refine our understanding of compact object stability [53, 80, 45]. Additionally, the new approach on quasinormal modes (QNMs) computation of black holes can be extended to Schwarzschild black holes in $f(R)$ gravity, charged black holes, and Kerr black holes, as well as N-dimensional black holes, to deepen insights into gravitational wave astronomy and strong-field gravity.

Appendix A

Einstein Field equations components

A.1 Christoffel Symbols

$$
\begin{aligned}
\Gamma^t_{tr} &= \frac{1}{2} g^{td} \left(\partial_t g_{dr} + \partial_r g_{td} - \partial_\sigma g_{tr} \right) \\
&= \frac{1}{2} g^{td} \left(\partial_r g_{td} \right) \\
&= \frac{1}{2} g^{tt} \left(\partial_r g_{tt} \right) \\
&= \frac{1}{2} \left(-e^{-2\nu(r)} \right) \left(\partial_r \left(-e^{2\nu(r)} \right) \right) \\
&= \frac{1}{2} \left(-e^{-2\nu(r)} \right) \left(-2e^{2\nu(r)} \partial_r \nu \right) \\
\Gamma^t_{tr} &= \partial_r \nu
\end{aligned}
$$

$$
\begin{aligned}
\Gamma^r_{tt} &= \frac{1}{2} g^{rd} \left(\partial_t g_{dt} + \partial_t g_{td} - \partial_d g_{tt} \right) \\
&= \frac{1}{2} g^{rr} \left(\partial_t g_{rt} + \partial_t g_{tr} - \partial_r g_{tt} \right) \\
&= \frac{1}{2} \left(e^{-2\lambda(r)} \right) \left(-\partial_r \left(-e^{2\nu(r)} \right) \right) \\
&= \frac{1}{2} \left(e^{-2\lambda(r)} \right) \left(2e^{2\nu(r)} \right) \partial_r \nu \\
\Gamma^r_{tt} &= e^{2(\nu(r) - \lambda(r))} \partial_r \nu
\end{aligned}
$$

$$
\begin{aligned}
\Gamma^r_{rr} &= \frac{1}{2} g^{rd} \left(\partial_r g_{dr} + \partial_r g_{rd} - \partial_d g_{rr} \right) \\
&= \frac{1}{2} g^{rr} \left(\partial_r g_{rr} + \partial_r g_{rr} - \partial_r g_{rr} \right) \\
&= \frac{1}{2} g^{rr} \left(\partial_r g_{rr} \right) \\
&= \frac{1}{2} \left(e^{-2\lambda(r)} \right) \partial_r \left(e^{2\lambda(r)} \right) \\
&= \frac{1}{2} \left(e^{-2\lambda(r)} \right) (2) e^{2\lambda(r)} \partial_r \lambda \\
\Gamma^r_{rr} &= \partial_r \lambda
\end{aligned}
$$

$$
\begin{aligned}
\Gamma^\theta_{r\theta} &= \frac{1}{2} g^{\theta d} \left(\partial_r g_{d\theta} + \partial_\theta g_{rd} - \partial_d g_{r\theta} \right) \\
&= \frac{1}{2} g^{\theta\theta} \left(\partial_r g_{\theta\theta} + \partial_\theta g_{r\theta} - \partial_\theta g_{r\theta} \right) \\
&= \frac{1}{2} \left(r^{-2} \right) \partial_r \left(r^2 \right) = \frac{1}{2} \left(r^{-2} \right) (2r) \\
\Gamma^\theta_{r\theta} &= \frac{1}{r}
\end{aligned}
$$

$$
\begin{aligned}
\Gamma^r_{\theta\theta} &= \frac{1}{2} g^{rd} \left(\partial_\theta g_{d\theta} + \partial_\theta g_{\theta d} - \partial_d g_{\theta\theta} \right) \\
&= \frac{1}{2} g^{rT} \left(\partial_\theta g_{r\theta} + \partial_\theta g_{\theta r} - \partial_r g_{\theta\theta} \right) \\
&= \frac{1}{2} g^{rr} \left(0 + 0 - \partial_r g_{\theta\theta} \right) \\
&= \frac{1}{2} g^{rr} \left(-\partial_r g_{\theta\theta} \right) \\
&= \frac{1}{2} \left(e^{-2\beta(r)} \right) \left(-\partial_r r^2 \right) \\
&= -\frac{1}{2} \left(e^{-2\beta(r)} \right) (2r) \\
\Gamma^r_{\theta\theta} &= -r e^{-2\lambda(r)}
\end{aligned}
$$

$$
\begin{aligned}
\Gamma^{\phi}_{r\phi} &= \frac{1}{2} g^{\phi d} \left(\partial_r g_{d\phi} + \partial_\phi g_{rd} - \partial_d g_{r\phi} \right) \\
&= \frac{1}{2} g^{\phi\phi} \left(\partial_r g_{\phi\phi} + \partial_\phi g_{r\phi} - \partial_\phi g_{r\phi} \right) \\
&= \frac{1}{2} g^{\phi\phi} \left(\partial_r g_{\phi\phi} \right) \\
&= \frac{1}{2} g^{\phi\phi} \left(\partial_r g_{\phi\phi} \right) \\
&= \frac{1}{2} \left(r^2 \sin^2\theta \right)^{-1} \partial_r \left(r^2 \sin^2\theta \right) \\
&= \frac{1}{2} \left(r^2 \sin^2\theta \right)^{-1} \left(2r \sin^2\theta \right) \\
\Gamma^{\phi}_{r\phi} &= \frac{1}{r}
\end{aligned}
$$

$$
\begin{aligned}
\Gamma^{r}_{\phi\phi} &= \frac{1}{2} g^{rd} \left(\partial_\phi g_{d\phi} + \partial_\phi g_{\phi d} - \partial_d g_{\phi\phi} \right) \\
&= \frac{1}{2} g^{rr} \left(\partial_\phi g_{r\phi} + \partial_\phi g_{\phi r} - \partial_r g_{\phi\phi} \right) \\
&= \frac{1}{2} g^{rr} \left(-\partial_r g_{\phi\phi} \right) = \frac{1}{2} g^{rr} \left(\partial_r g_{\phi\phi} \right) \\
&= \frac{1}{2} \left(e^{-2\lambda(r)} \right) \left(-\partial_r \left(r^2 \sin^2\theta \right) \right) \\
&= \frac{1}{2} \left(e^{-2\lambda(r)} \right) \left(-2r \sin^2\theta \right) \\
\Gamma^{r}_{\phi\phi} &= -r \sin^2\theta e^{-2\lambda(r)}
\end{aligned}
$$

$$
\begin{aligned}
\Gamma^{\theta}_{\phi\phi} &= \frac{1}{2} g^{\theta\sigma} \left(\partial_\phi g_{d\phi} + \partial_\phi g_{\phi d} - \partial_d g_{\phi\phi} \right) \\
&= \frac{1}{2} g^{\theta\theta} \left(\partial_\phi g_{\theta\phi} + \partial_\phi g_{\phi\theta} - \partial_\theta g_{\phi\phi} \right) \\
&= \frac{1}{2} g^{\theta\theta} \left(-\partial_\theta g_{\phi\phi} \right) \\
&= \frac{1}{2} \left(r^2 \right)^{-1} \left(-\partial_\theta \left(r^2 \sin^2\theta \right) \right) \\
\Gamma^{\theta}_{\phi\phi} &= -\sin^2\theta \cos\theta
\end{aligned}
$$

$$
\begin{aligned}
\Gamma^{\phi}_{\theta\phi} &= \frac{1}{2} g^{\phi d} \left(\partial_\theta g_{d\phi} + \partial_\phi g_{\theta d} - \partial_d g_{\theta\phi} \right) \\
&= \frac{1}{2} g^{\phi\phi} \left(\partial_\theta g_{\phi\phi} + \partial_\phi g_{\theta\phi} - \partial_\phi g_{\theta\phi} \right) \\
&= \frac{1}{2} g^{\phi\phi} \left(\partial_\theta g_{\phi\phi} \right) \\
&= \frac{1}{2} \left(r^2 \sin^2\theta \right)^{-1} \partial_\theta \left(r^2 \sin^2\theta \right) \\
&= \frac{1}{2} \left(r^2 \sin^2\theta \right)^{-1} \left(2r^2 \sin\theta \cos\theta \right) \\
\Gamma^{\phi}_{\theta\phi} &= \frac{\cos\theta}{\sin\theta}
\end{aligned}
$$

A.2 Riemann tensor

$$
\begin{aligned}
R^r_{trt} &= \partial_r \Gamma^r_{tt} - \partial_t \Gamma^r_{rt} + \Gamma^r_{r\lambda}\Gamma^\lambda_{tt} - \Gamma^r_{t\lambda}\Gamma^\lambda_{rt} \\
&= \partial_r \Gamma^r_{tt} + \Gamma^r_{rr}\Gamma^r_{tt} + \Gamma^r_{r\theta}\Gamma^\theta_{tt} + \Gamma^r_{r\phi}\Gamma^\phi_{tt} - \Gamma^r_{tt}\Gamma^t_{rt} - \Gamma^r_{tr}\Gamma^r_{rt} - \Gamma^r_{t\theta}\Gamma^\theta_{rt} - \Gamma^r_{t\phi}\Gamma^\phi_{rt} \\
&= \partial_r \left(e^{2(\nu-\lambda)} \partial_r \nu \right) + \partial_r \lambda e^{2(\nu-\lambda)} \partial_r \nu - e^{2(\nu-\lambda)} \partial_r \nu \partial_r \nu \\
&= \partial_r^2 \nu e^{2(\nu-\lambda)} + \partial_r \nu \partial_r \left(e^{2(\nu-\lambda)} \right) + \partial_r \nu \partial_r \lambda e^{2(\nu-\lambda)} - e^{2(\nu-\lambda)} \left(\partial_r \nu \right)^2 \\
&= \partial_r^2 \nu e^{2(\nu-\lambda)} + \left(2e^{2(\nu-\lambda)} \partial_r \nu - 2e^{2(\nu-\lambda)} \partial_r \lambda \right) \partial_r \nu + \partial_r \nu \partial_r \lambda e^{2(\nu-\lambda)} - e^{2(\nu-\lambda)} \left(\partial_r \nu \right)^2 \\
&= e^{2(\nu-\lambda)} \left[\partial_r^2 \nu + 2 \left(\partial_r \nu \right)^2 - 2 \partial_r \nu \partial_r \lambda + \partial_r \nu \partial_r \nu - \left(\partial_r \nu \right)^2 \right] \\
R^r_{trt} &= e^{2(\nu-\lambda)} \left[\partial_r^2 \nu + \left(\partial_r \nu \right)^2 - \partial_r \nu \partial_r \lambda \right]. \qquad \text{(A.1)}
\end{aligned}
$$

$$
\begin{aligned}
R^\theta_{t\theta t} &= \partial_\theta \Gamma^\theta_{tt} - \partial_t \Gamma^\theta_{\theta t} + \Gamma^\theta_{\theta\lambda}\Gamma^\lambda_{tt} - \Gamma^\theta_{t\lambda}\Gamma^\lambda_{\theta t} \\
&= \Gamma^\theta_{\theta t}\Gamma^t_{tt} + \Gamma^\theta_{\theta r}\Gamma^r_{tt} + \Gamma^\theta_{\theta\theta}\Gamma^\theta_{tt} + \Gamma^\theta_{\theta\phi}\Gamma^\phi_{tt} - \Gamma^\theta_{tt}\Gamma^t_{\theta t} - \Gamma^\theta_{tr}\Gamma^r_{\theta t} - \Gamma^\theta_{t\theta}\Gamma^\theta_{\theta t} - \Gamma^\theta_{t\phi}\Gamma^\phi_{\theta t} \\
&= \Gamma^\theta_{\theta r}\Gamma^r_{tt} \\
R^\theta_{t\theta t} &= \frac{1}{r} e^{2(\nu-\lambda)} \partial_r \nu. \qquad \text{(A.2)}
\end{aligned}
$$

$$
\begin{aligned}
R^\phi_{t\phi t} &= \partial_\phi \Gamma^\phi_{tt} - \partial_t \Gamma^\phi_{\phi t} + \Gamma^\phi_{\phi\lambda}\Gamma^\lambda_{tt} - \Gamma^\phi_{t\lambda}\Gamma^\lambda_{\phi t} \\
&= \Gamma^\phi_{\phi\lambda}\Gamma^\lambda_{tt} - \Gamma^\phi_{t\lambda}\Gamma^\lambda_{\phi t} \\
&= \Gamma^\phi_{\phi t}\Gamma^t_{tt} + \Gamma^\phi_{\phi r}\Gamma^r_{tt} + \Gamma^\phi_{\phi\theta}\Gamma^\theta_{tt} + \Gamma^\phi_{\phi\phi}\Gamma^\phi_{tt} - \Gamma^\phi_{tt}\Gamma^t{}_{\phi t} - \Gamma^\phi_{tr}\Gamma^r_{\phi t} - \Gamma^\phi_{t\theta}\Gamma^\theta{}_{\phi t} - \Gamma^\phi_{t\phi}\Gamma^\phi_{\phi t} \\
&= \Gamma^\phi_{\phi r}\Gamma^r_{tt} \\
R^\phi_{t\phi t} &= \frac{1}{r} e^{2(\nu-\lambda)} \partial_r \nu. \qquad \text{(A.3)}
\end{aligned}
$$

$$
\begin{aligned}
R^t_{rtr} &= \partial_t\Gamma^t_{rr} - \partial_r\Gamma^t_{tr} + \Gamma^t_{t\lambda}\Gamma^\lambda_{rr} - \Gamma^t_{r\lambda}\Gamma^\lambda_{tr} \\
&= -\partial_r\Gamma^t_{tr} + \Gamma^t_{tt}\Gamma^t_{rr} + \Gamma^t_{tr}\Gamma^r_{rr} + \Gamma^t_{t\theta}\Gamma^\theta_{rr} + \Gamma^t_{t\phi}\Gamma^\phi_{rr} - \Gamma^t_{rt}\Gamma^t_{tr} - \Gamma^t_{rr}\Gamma^r_{tr} - \Gamma^t_{r\theta}\Gamma^\theta_{tr} - \Gamma^t_{r\phi}\Gamma^\phi_{tr} \\
&= -\partial_r\left(\partial_r\nu\right) + \partial_r\nu\partial_r\lambda - \partial_r\nu\partial_r\nu \\
R^t_{rtr} &= \partial_r\nu\partial_r\lambda - \partial_r^2\lambda - \left(\partial_r\lambda\right)^2 .
\end{aligned} \tag{A.4}
$$

$$
\begin{aligned}
R^\theta_{r\theta r} &= \partial_\theta\Gamma^\theta_{rr} - \partial_r\Gamma^\theta_{\theta r} + \Gamma^\theta_{\theta\lambda}\Gamma^\lambda_{rr} - \Gamma^\theta_{r\lambda}\Gamma^\lambda_{\theta r} \\
&= -\partial_r\left(\frac{1}{r}\right) + \Gamma^\theta_{\theta t}\Gamma^t_{rr} + \Gamma^\theta_{\theta r}\Gamma^r_{rr} + \Gamma^\theta_{\theta\theta}\Gamma^\theta_{rr} + \Gamma^\theta_{\theta\phi}\Gamma^\phi_{rr} - \Gamma^\theta_{rt}\Gamma^t_{\theta r} - \Gamma^\theta_{rr}\Gamma^r_{\theta r} - \Gamma^\theta_{r\theta}\Gamma^\theta_{\theta r} - \Gamma^\theta_{r\phi}\Gamma^\phi_{\theta r} \\
&= \frac{1}{r^2} + \frac{1}{r}\partial_r\nu - \frac{1}{r}\frac{1}{r} \\
R^\theta_{r\theta r} &= \frac{1}{r}\partial_r\lambda.
\end{aligned} \tag{A.5}
$$

$$
\begin{aligned}
R^\phi_{r\phi r} &= \partial_\phi\Gamma^\phi_{rr} - \partial_r\Gamma^\phi_{\phi r} + \Gamma^\phi_{\phi\lambda}\Gamma^\lambda_{rr} - \Gamma^\phi_{r\lambda}\Gamma^\lambda_{\phi r} \\
&= -\partial_r\left(\frac{1}{r}\right) + \Gamma^\phi_{\phi t}\Gamma^t_{rr} + \Gamma^\phi_{\phi r}\Gamma^r_{rr} + \Gamma^\phi_{\phi\theta}\Gamma^\theta_{rr} + \Gamma^\phi_{\phi\phi}\Gamma^\phi_{rr} - \Gamma^\phi_{rt}\Gamma^t_{\phi r} - \Gamma^\phi_{rr}\Gamma^r_{\phi r} - \Gamma^\phi_{r\theta}\Gamma^\theta_{\phi r} - \Gamma^\phi_{r\phi}\Gamma^\phi_{\phi r} \\
&= \frac{1}{r^2} + \frac{1}{r}\partial_r\lambda - \frac{1}{r}\frac{1}{r} \\
R^\phi_{r\phi r} &= \frac{1}{r}\partial_r\lambda.
\end{aligned} \tag{A.6}
$$

$$
\begin{aligned}
R^t_{\theta t\theta} &= \partial_t\Gamma^t_{\theta\theta} - \partial_\theta\Gamma^t_{t\theta} + \Gamma^t_{t\lambda}\Gamma^\lambda_{\theta\theta} - \Gamma^t_{\theta\lambda}\Gamma^\lambda_{t\theta} \\
&= \Gamma^t_{tt}\Gamma^t_{\theta\theta} + \Gamma^t_{tr}\Gamma^r_{\theta\theta} + \Gamma^t_{t\theta}\Gamma^\theta_{\theta\theta} + \Gamma^t_{t\phi}\Gamma^\phi_{\theta\theta} - \Gamma^t_{\theta t}\Gamma^t_{t\theta} - \Gamma^t_{\theta r}\Gamma^r_{t\theta} - \Gamma^t_{\theta\theta}\Gamma^\theta_{t\theta} - \Gamma^t_{\theta\phi}\Gamma^\phi_{t\theta} \\
&= \partial_r\nu\left(-re^{-2\lambda}\right) \\
R^t_{\theta t\theta} &= -re^{-2\lambda}\partial_r\lambda.
\end{aligned} \tag{A.7}
$$

$$
\begin{aligned}
R^\phi_{\theta\phi\theta} &= \partial_\phi\Gamma^\phi_{\theta\theta} - \partial_\theta\Gamma^\phi_{\phi\theta} + \Gamma^\phi_{\phi\lambda}\Gamma^\lambda_{\theta\theta} - \Gamma^\phi_{\theta\lambda}\Gamma^\lambda_{\phi\theta} \\
&= -\partial_\theta\Gamma^\phi_{\phi\theta} + \Gamma^\phi_{\phi t}\Gamma^t_{\theta\theta} + \Gamma^\phi_{\phi r}\Gamma^r_{\theta\theta} + \Gamma^\phi_{\phi\theta}\Gamma^\theta_{\theta\theta} + \Gamma^\phi_{\phi\phi}\Gamma^\phi_{\theta\theta} - \Gamma^\phi_{\theta t}\Gamma^t_{\phi\theta} - \Gamma^\phi_{\theta r}\Gamma^r_{\phi\theta} - \Gamma^\phi_{\theta\theta}\Gamma^\theta_{\phi\theta} - \Gamma^\phi_{\theta\phi}\Gamma^\phi_{\phi\theta} \\
&= -\partial_\theta(\cot\theta) + \frac{1}{r}\left(-re^{-2\lambda}\right) - \cot^2\theta \\
R^\phi_{\theta\phi\theta} &= \left(1 - e^{-2\lambda}\right).
\end{aligned} \tag{A.8}
$$

A.3 Ricci tensor

$$\begin{aligned} R_{tt} &= R^{\lambda}_{t\lambda t} = R^{r}_{trt} + R^{\theta}_{t\theta t} + R^{\phi}_{t\phi t} \\ R_{tt} &= R^{\lambda}_{t\lambda t} = R^{r}_{trt} + R^{\theta}_{t\theta t} + R^{\phi}_{t\phi t} \\ &= e^{2(\nu-\lambda)}\left[\partial_r^2\nu + (\partial_r\nu)^2 - \partial_r\nu\partial_r\nu\right] + \frac{2}{r}e^{2(\nu-\lambda)}\partial_r\nu \end{aligned} \tag{A.9}$$

$$\begin{aligned} R_{rr} &= R^{\lambda}_{r\lambda r} = R^{t}_{rtr} + R^{\theta}_{r\theta r} + R^{\phi}_{r\phi r}. \\ R_{rr} &= \partial_r\nu\partial_r\lambda - \partial_r^2\nu - (\partial_r\nu)^2 + \frac{1}{r}\partial_r\lambda + \frac{1}{r}\partial_r\lambda. \\ R_{rr} &= \partial_r\nu\partial_r\lambda - \partial_r^2\nu - (\partial_r\nu)^2 + \frac{2}{r}\partial_r\lambda \end{aligned} \tag{A.10}$$

$$\begin{aligned} R_{\theta\theta} &= R^{\lambda}_{\theta\lambda\theta} = R^{t}_{\theta t\theta} + R^{r}_{\theta r\theta} + R^{\phi}_{\theta\phi\theta} \\ &= -re^{-2\lambda}\partial_r\lambda + re^{-2\lambda}\partial_r\lambda + \left(1 - e^{-2\lambda}\right) \\ &= e^{-2\lambda}\left[r\left(\partial_r\lambda - \partial_r\lambda\right) - 1\right] + 1 \\ &= -re^{-2\lambda}\sin^2\theta\partial_r\lambda + re^{-2\lambda}\sin^2\theta\partial_r\lambda + \left(1 - e^{-2\lambda}\right)\sin^2\theta \\ R_{\theta\theta} &= \left\{e^{-2\lambda}\left[r\left(\partial_r\lambda - \partial_r\lambda\right) - 1\right] + 1\right\}\sin^2\theta. \end{aligned} \tag{A.11}$$

$$R_{\phi\phi} = \sin^2\theta R_{\theta\theta} \tag{A.12}$$

A.4 Ricci Scalar

$$
\begin{aligned}
R &= -e^{-2\nu}e^{2(\nu-\lambda)}[\partial_r^2\nu - \partial_r\lambda - \partial_r\nu\partial_r\lambda + \frac{2}{r}\partial_r\nu] + e^{-2\lambda}[-\partial_r^2\nu - (\partial_r\nu)^2 + \partial_r\nu\partial_r\lambda] + \frac{2}{r}\partial_r\lambda] \\
&\quad + \frac{1}{r^2}\{e^{-2\lambda}[r\partial_r\lambda - r\partial_r\nu - 1] + 1\} + \frac{1}{r^2\sin^2}(\theta)\{e^{-2\lambda}[r\partial_r\lambda - r\partial_r\nu - 1] + 1\}\sin^2(\theta) \\
&= e^{-2\lambda}\left[-\partial_r^2\nu - (\partial_r\nu)^2 + \partial_r\nu\partial_r\lambda - \frac{2}{r}\partial_r\nu - \partial_r^2\nu - (\partial_r\nu)^2 + \partial_r\nu\partial_r\lambda + \frac{2}{r}\partial_r\lambda\right] + \\
&\quad \frac{2}{r^2}\left\{e^{-2\lambda}\left[r\left(\partial_r\lambda - \partial_r\nu\right) - 1\right] + 1\right\} \\
&= 2e^{-2\lambda}\left[-\partial_r^2\nu - (\partial_r\nu)^2 + \partial_r\nu\partial_r\lambda - \frac{1}{r}\left(\partial_r\nu - \partial_r\lambda\right)\right] + 2e^{-2\lambda}\left[\frac{1}{r}\left(\partial_r\lambda - \partial_r\nu\right) - \frac{1}{r^2}\right] + \frac{2}{r^2} \\
&= -2e^{-2\lambda}\left[-\partial_r^2\nu - (\partial_r\nu)^2 + \partial_r\nu\partial_r\lambda - \frac{2}{r}\left(\partial_r\nu - \partial_r\lambda\right) - \frac{1}{r^2}\right] + \frac{2}{r^2} \\
&= -2e^{-2\lambda}\left[\partial_r^2\nu + (\partial_r\nu)^2 - \partial_r\nu\partial_r\lambda + \frac{2}{r}\left(\partial_r\nu - \partial_r\lambda\right) + \frac{1}{r^2}\left(1 - e^{2\lambda}\right)\right] \\
R &= 2e^{-2\lambda}\left[\partial_r^2\nu + (\partial_r\nu)^2 - \partial_r\nu\partial_r\lambda + \frac{2}{r}\left(\partial_r\nu - \partial_r\lambda\right) + \frac{1}{r^2}\left(1 - e^{2\lambda}\right)\right] \qquad \text{(A.13)}
\end{aligned}
$$

A.5 Einstein tensor

$$
\begin{aligned}
G_{tt} &= R_{tt} - \frac{1}{2}g_{tt}R \\
&= e^{2(\nu-\lambda)}[\partial_r^2\nu + (\partial_r\nu)^2 - \partial_r\nu\partial_r\lambda + \frac{2}{r}\nu] - \frac{1}{2}(-2e^{2\nu})(-2e^{-2\lambda})[\partial_r^2\nu + \partial_r\nu - \partial_r\nu\partial_r\lambda \\
&\quad + \frac{2}{r}(\partial_r\nu - \partial_r\lambda) + \frac{1}{r2}(1 - e^{e\lambda})] \\
&= e^{2(\nu-\lambda)}[\partial_r^2\nu + (\partial_r\nu)^2 - \partial_r\nu\partial_r\lambda - \frac{2}{r}(\partial_r\nu - \partial_r\lambda) - \frac{1}{r^2}(1 - e^{2\lambda})] \\
&= e^{2(\nu-\lambda)}[\frac{2}{r}\partial_r\lambda - \frac{1}{r^2}(1 - e^{2\lambda})] \\
&= \frac{1}{r^2}e^{2(\nu-\lambda)}[2\partial_r\lambda r - (1 - e^{2\lambda})] \qquad \text{(A.14)}
\end{aligned}
$$

$$
\begin{aligned}
G_{rr} &= R_{rr} - \frac{1}{2}g_{rr}R \\
&= -\partial_r^2\nu - (\partial_r\nu)^2 + \partial_r\nu\partial_r\lambda + \frac{2}{r}\partial_r\lambda + \frac{1}{2}e^{2\lambda}(-2e^{-2\lambda})[\partial_r^2\nu + (\partial_r\nu)^2 - \partial_r\nu\partial_r\lambda + \frac{2}{r}(\partial_r\nu - \partial_r\lambda) \\
&\quad + \frac{1}{r^2}(1 - e^{2\lambda})] \\
&= \frac{2}{r}\partial_r\nu + \frac{1}{r^2}(1 - e^{2\lambda}). \qquad \text{(A.15)}
\end{aligned}
$$

$$
\begin{aligned}
G_{\theta\theta} &= R_{\theta\theta} - \frac{1}{2} g_{\theta\theta} R \\
&= e^{-2\lambda}[r\partial_r\lambda - r\partial_r\nu - 1] + 1 - \frac{1}{r^2}(-2e^{-2\lambda})[\partial_r^2\nu + (\partial_r\nu)^2 - \partial_r\nu\partial_r\lambda + \frac{2}{r}(\partial_r\nu - \partial_r\lambda) \\
&\quad + \frac{1}{r^2}(1 - e^{2\lambda})] \\
&= r^2 e^{-2\lambda}[\partial_r^2\nu + (\partial_r\nu)^2 - \partial_r\nu\partial_r\lambda + \frac{1}{r}(\partial_r\nu - \partial_r\lambda)]. \qquad \text{(A.16)}
\end{aligned}
$$

$$
\begin{aligned}
G_{\phi\phi} &= R_{\phi\phi} - \frac{1}{2} g_{\phi\phi} R \\
&= \sin^2\theta\{e^{-2\lambda}[r\partial_r\lambda - r\partial_r\nu - 1] + 1\} - \frac{1}{2} r^2 \sin^2(\theta)(-2e^{-2\lambda})[\partial_r^2\nu + (\partial_r\nu)^2 - \partial_r\nu\partial_r\lambda \\
&\quad + \frac{2}{r}(\partial_r\nu - \partial_r\lambda) + \frac{1}{r^2}(1 - e^{2\lambda})] \\
&= e^{-2\lambda}\sin^2(\theta)[r\partial_r\lambda - r\partial_r\nu - 1 + e^{2\lambda}] + r^2\sin^2(\theta)e^{-2\lambda}[\partial_r^2\nu + (\partial_r\nu)^2 - \partial_r\nu\partial_r\lambda + \frac{2}{r}(\partial_r\nu - \partial_r\lambda) \\
&\quad - \frac{1}{r^2}(1 - e^{2\lambda})] \\
&= e^{-2\lambda}\sin^2(\theta)[r\partial_r\lambda - r\partial_r\nu - 1 + e^{2\lambda} + r^2\partial_r^2\nu + r^2(\partial_r\nu)^2 - r^2\partial_r\nu\partial_r\lambda + 2r\partial_r\lambda + 1 - e^{2\lambda}] \\
&= e^{-2\lambda}\sin^2(\theta)[r\partial_r\nu - \partial_r\lambda + r^2\partial_r^2\nu + r^2(\partial_r\nu)^2 - r^2\partial_r\nu\partial_r\lambda]. \qquad \text{(A.17)}
\end{aligned}
$$

Bibliography

[1] Amir H Abbassi. General Birkhoff's theorem. *arXiv preprint gr-qc/0103103*, 2001.

[2] B. P. Abbott and Others. Observation of gravitational waves from a binary black hole merger. *Physical Review Letters*, 116:061102, Feb 2016.

[3] Benjamin P Abbott, Rich Abbott, TDea Abbott, Fausto Acernese, Kendall Ackley, Carl Adams, Thomas Adams, Paolo Addesso, Rana X Adhikari, Vaishali B Adya, et al. Gw170817: observation of gravitational waves from a binary neutron star inspiral. *Physical Review Letters*, 119(16):161101, 2017.

[4] Miguel Alcubierre. *Introduction to 3+ 1 numerical relativity*, volume 140. OUP Oxford, 2008.

[5] Miguel Alcubierre, Gabrielle Allen, Bernd Brügmann, Gerd Lanfermann, Edward Seidel, Wai-Mo Suen, and Malcolm Tobias. Gravitational collapse of gravitational waves in 3d numerical relativity. *Physical Review D*, 61(4):041501, 2000.

[6] Miguel Alcubierre and Bernd Brügmann. Simple excision of a black hole in 3+ 1 numerical relativity. *Physical Review D*, 63(10):104006, 2001.

[7] Miguel Alcubierre, Bernd Brügmann, Peter Diener, Michael Koppitz, Denis Pollney, Edward Seidel, and Ryoji Takahashi. Gauge conditions for long-term numerical black hole evolutions without excision. *Physical Review D*, 67(8), April 2003.

[8] Lars Andersson. On the relation between mathematical and numerical relativity. *Classical and Quantum Gravity*, 23(16):S307, July 2006.

[9] Peter Anninos, Joan Massó, Edward Seidel, Wai-Mo Suen, and John Towns. Three-dimensional numerical relativity: The evolution of black holes. *Physical Review D*, 52(4):2059, 1995.

[10] Miguel Aparicio Resco, Álvaro de la Cruz-Dombriz, Felipe J. Llanes Estrada, and Víctor Zapatero Castrillo. On neutron stars in $f(R)$ theories: Small radii, large masses and large energy emitted in a merger. *Physics of the Dark Universe*, 13:147–161, September 2016.

[11] Richard Arnowitt, Stanley Deser, and Charles W Misner. Republication of: The dynamics of general relativity. *General Relativity and Gravitation*, 40:1997–2027, 2008.

[12] Uri M. Ascher, Robert M. M. Mattheij, and Robert D. Russell. Numerical solution of boundary value problems for ordinary differential equations. In *Classics in applied mathematics*, 1995.

[13] Artyom V Astashenok, Sergei D Odintsov, and Álvaro de la Cruz-Dombriz. The realistic models of relativistic stars in $f(R) = R + \alpha R^2$ gravity. *Classical and Quantum Gravity*, 34(20):205008, September 2017.

[14] K. E. Atkinson. *An Introduction to Numerical Analysis*. Wiley, 2nd edition, 1989.

[15] Luca Baiotti and Luciano Rezzolla. Binary neutron star mergers: a review of einstein's richest laboratory. *Reports on Progress in Physics*, 80(9):096901, 2017.

[16] Dinshaw S Balsara, Deepak Bhoriya, Chi-Wang Shu, and Himanshu Kumar. Efficient alternative finite difference weno schemes for hyperbolic systems with non-conservative products. *Communications on Applied Mathematics and Computation*, 2024.

[17] James M Bardeen and Tsvi Piran. General relativistic axisymmetric rotating systems: Coordinates and equations. *Physics Reports*, 96(4):205–250, 1983.

[18] James M Bardeen, Kip S Thorne, and David W Meltzer. A catalogue of methods for studying the normal modes of radial pulsation of general-relativistic stellar models. *Astrophysical Journal, vol. 145, p. 505*, 145:505, 1966.

[19] T W Baumgarte, Z B Etienne, Y T Liu, K Matera, N Ó Murchadha, S L Shapiro, and K Taniguchi. Equilibrium initial data for moving puncture simulations: the stationary 1 + log slicing. *Classical and Quantum Gravity*, 26(8):085007, April 2009.

[20] Thomas W. Baumgarte and Stuart L. Shapiro. Numerical integration of einstein's field equations. *Physical Review D*, 59(2), December 1998.

[21] Thomas W Baumgarte and Stuart L Shapiro. *Numerical relativity: solving Einstein's equations on the computer*. Cambridge University Press, 2010.

[22] Emanuele Berti, Vitor Cardoso, and Andrei O Starinets. Quasinormal modes of black holes and black branes. *Classical and Quantum Gravity*, 26(16):163001, July 2009.

[23] Nigel T Bishop. Linearized solutions of the einstein equations within a bondi–sachs framework, and implications for boundary conditions in numerical simulations. *Classical and Quantum Gravity*, 22(12):2393, 2005.

[24] Jose Luis Blázquez-Salcedo, Daniela D. Doneva, Jutta Kunz, and Stoytcho S. Yazadjiev. Radial perturbations of the scalarized einstein-gauss-bonnet black holes. *Physical Review D*, 98:084011, Oct 2018.

[25] Carles Bona and Joan Masso. Hyperbolic evolution system for numerical relativity. *Physical Review Letters*, 68:1097–1099, 03 1992.

[26] Carles Bona, Joan Masso, Edward Seidel, and Joan Stela. New formalism for numerical relativity. *Physical Review Letters*, 75(4):600, 1995.

[27] Hermann Bondi. Gravitational waves in general relativity. *Nature*, 186(4724):535–535, 1960.

[28] Hermann Bondi, M Gr J Van der Burg, and AWK Metzner. Gravitational waves in general relativity, vii. waves from axi-symmetric isolated system. *Proceedings of the Royal Society of London. Series A. Mathematical and Physical Sciences*, 269(1336):21–52, 1962.

[29] Bernd Brügmann. Fundamentals of numerical relativity for gravitational wave sources. *Science*, 361(6400):366–371, 2018.

[30] Annette Burden, Richard Burden, and J. Faires. *Numerical Analysis, 10th ed.* 01 2016.

[31] Juan Calderón Bustillo, Paul D. Lasky, and Eric Thrane. Black-hole spectroscopy, the no-hair theorem, and gw150914: Kerr versus occam. *Physical Review D*, 103(2), January 2021.

[32] M. Campanelli, C. O. Lousto, P. Marronetti, and Y. Zlochower. Accurate evolutions of orbiting black-hole binaries without excision. *Physical Review Letters*, 96:111101, Mar 2006.

[33] Zhoujian Cao. New method for characteristic evolutions in numerical relativity. *International Journal of Modern Physics D*, 22(08):1350042, 2013.

[34] Zhoujian Cao and Xiaokai He. Generalized bondi-sachs equations for characteristic formalism of numerical relativity. *Physical Review D—Particles, Fields, Gravitation, and Cosmology*, 88(10):104002, 2013.

[35] Sean M Carroll. An introduction to general relativity: spacetime and geometry. *Addison Wesley*, 101:102, 2004.

[36] Sean M Carroll. *Spacetime and geometry*. Cambridge University Press, 2019.

[37] Joan Centrella, John G. Baker, Bernard J. Kelly, and James R. van Meter. Black-hole binaries, gravitational waves, and numerical relativity. *Reviews of Modern Physics*, 82:3069–3119, Nov 2010.

[38] S Chandrasekhar. Dynamical instability of gaseous masses approaching the schwarzschild limit in general relativity. *Physical Review Letters*, 12(4):114, 1964.

[39] Subrahmanyan Chandrasekhar. On algebraically special perturbations of black holes. *Proceedings of the Royal Society of London. A. Mathematical and Physical Sciences*, 392(1802):1–13, 1984.

[40] Subrahmanyan Chandrasekhar and Steven Detweiler. The quasi-normal modes of the schwarzschild black hole. *Proceedings of the Royal Society of London. A. Mathematical and Physical Sciences*, 344(1639):441–452, 1975.

[41] G Chanmugam. Radial oscillations of zero-temperature white dwarfs and neutron stars below nuclear densities. *Astrophysical Journal, Part 1, vol. 217, Nov. 1, 1977, p. 799-808.*, 217:799–808, 1977.

[42] Cecilia Chirenti, Gibran H de Souza, and Wolfgang Kastaun. Fundamental oscillation modes of neutron stars: Validity of universal relations. *Physical Review D*, 91(4):044034, 2015.

[43] Sam R Dolan and Adrian C Ottewill. On an expansion method for black hole quasinormal modes and regge poles. *Classical and Quantum Gravity*, 26(22):225003, October 2009.

[44] Daniela D Doneva and Stoytcho S Yazadjiev. Stability of scalarized black holes in einstein-gauss-bonnet gravity. *Physical Review Letters*, 120(13):131103, 2018.

[45] V. Dzhunushaliev and V. Folomeev. On the linear stability of polytropic fluid spheres in R^2 gravity. *International Journal of Geometric Methods in Modern Physics*, 17(11):2050165, September 2020.

[46] Ray d'Invemo. *Introducing Einstein's relativity*. Oxford University Press, 1992.

[47] Chagpar Z Fatemah. *General Relativity: The Core Concepts and Its Significance in Astrophysics*. PhD thesis, University of Nairobi, 2009.

[48] Valeria Ferrari and Bahram Mashhoon. New approach to the quasinormal modes of a black hole. *Physical Review D*, 30(2):295, 1984.

[49] Apratim Ganguly, Radouane Gannouji, Rituparno Goswami, and Subharthi Ray. Neutron stars in the starobinsky model. *Physical Review D*, 89(6), March 2014.

[50] Jordi Gaset and Arnau Mas. A variational derivation of the field equations of an action-dependent einstein-hilbert lagrangian. *arXiv preprint arXiv:2206.13227*, 2022.

[51] Abhirup Ghosh, Richard Brito, and Alessandra Buonanno. Constraints on quasinormal-mode frequencies with ligo-virgo binary–black-hole observations. *Physical Review D*, 103(12), June 2021.

[52] Edward N Glass and Lee Lindblom. The radial oscillations of neutron stars: Erratum. *Astrophysical Journal Supplement v. 71, p. 173*, 71:173, 1989.

[53] Marcelo Gleiser and Richard Watkins. Gravitational stability of scalar matter. *Nuclear Physics B*, 319(3):733–746, 1989.

[54] Joshua N Goldberg, Alan J MacFarlane, Ezra T Newman, Fritz Rohrlich, and EC George Sudarshan. Spin-s spherical harmonics and their application to molecular scattering theory. *Journal of Mathematical Physics*, 8(11):2155–2161, 1967.

[55] R. Gómez, L. Lehner, R. L. Marsa, and J. Winicour. Moving black holes in 3d. *Physcal Review D*, 57:4778–4788, Apr 1998.

[56] Eric Gourgoulhon. Simple equations for general relativistic hydrodynamics in spherical symmetry applied to neutron star collapse. *Astronomy and Astrophysics (ISSN 0004-6361), vol. 252, no. 2, Dec. 1991, p. 651-663.*, 252:651–663, 1991.

[57] Eric Gourgoulhon. 3+ 1 formalism and bases of numerical relativity. *arXiv preprint gr-qc/0703035*, 2007.

[58] Markus Heusler. *Black Hole Uniqueness Theorems*. Cambridge Lecture Notes in Physics. Cambridge University Press, 1996.

[59] Changqing Hu and Chi-Wang Shu. Weighted essentially non-oscillatory schemes on triangular meshes. *Journal of Computational Physics*, 150(1):97–127, 1999.

[60] José Luis Jaramillo, Juan Antonio Valiente Kroon, and Eric Gourgoulhon. From geometry to numerics: interdisciplinary aspects in mathematical and numerical relativity. *Classical and Quantum Gravity*, 25(9):093001, 2008.

[61] Pascual Jordan, Jürgen Ehlers, and Wolfgang Kundt. Republication of: Exact solutions of the field equations of the general theory of relativity. *General Relativity and Gravitation*, 41:2191–2280, 2009.

[62] Kostas D Kokkotas and Bernd G Schmidt. Quasi-normal modes of stars and black holes. *Living Reviews in Relativity*, 2:1–72, 1999.

[63] Kokkotas, K. D. and Ruoff, J. Radial oscillations of relativistic stars*. *A and A*, 366(2):565–572, 2001.

[64] R. A. Konoplya and Alexander Zhidenko. Quasinormal modes of black holes: From astrophysics to string theory. *Reviews of Modern Physics*, 83(3):793–836, July 2011.

[65] Edward W Leaver. An analytic representation for the quasi-normal modes of Kerr black holes. *Proceedings of the Royal Society of London. A. Mathematical and Physical Sciences*, 402(1823):285–298, 1985.

[66] Luis Lehner. Numerical relativity: a review. *Classical and Quantum Gravity*, 18(17):R25, 2001.

[67] Georgios Lioutas, Andreas Bauswein, Theodoros Soultanis, Rüdiger Pakmor, Volker Springel, and Friedrich K Röpke. General relativistic moving-mesh hydrodynamics simulations with arepo and applications to neutron star mergers. *arXiv preprint arXiv:2208.04267*, 2022.

[68] Hongya Liu and Bahram Mashhoon. On the spectrum of oscillations of a Schwarzschild black hole. *Classical and Quantum Gravity*, 13(2):233, 1996.

[69] Carlos O Lousto and James Healy. Study of the intermediate mass ratio black hole binary merger up to 1000: 1 with numerical relativity. *Classical and Quantum Gravity*, 40(9):09LT01, 2023.

[70] Thomas Mädler. Simple, explicitly time-dependent and regular solutions of the linearized vacuum Einstein equations on a null cone. *arXiv preprint arXiv:1212.3316*, 2012.

[71] Thomas Mädler and Jeffrey Winicour. Bondi-Sachs formalism. *arXiv preprint arXiv:1609.01731*, 2016.

[72] Charles W. Misner, Kip S. Thorne, and John Archibald Wheeler. *Gravitation*. W. H. Freeman and Company, San Francisco, CA, 1973.

[73] Vincent Moncrief. Gravitational perturbations of spherically symmetric systems. i. the exterior problem. *Annals of Physics*, 88(2):323–342, 1974.

[74] Bishop Mongwane. Characteristic formulation for metric f (R) gravity. *Physical Review D*, 96(2):024028, 2017.

[75] Hans-Peter Nollert. Quasinormal modes: the characteristic 'sound' of black holes and neutron stars. *Classical and Quantum Gravity*, 16(12):R159, dec 1999.

[76] Christian David Ott. Stellar iron core collapse in 3+ 1 general relativity and the gravitational wave signature of core-collapse supernovae. *Ph. D. Thesis*, 2007.

[77] Oscar M Pimentel, FD Lora-Clavijo, and Guillermo A González. Ideal magnetohydrodynamics with radiative terms: energy conditions. *Classical and Quantum Gravity*, 34(7):075008, 2017.

[78] W. H. Press, S. A. Teukolsky, W. T. Vetterling, and B. P. Flannery. *Numerical Recipes: The Art of Scientific Computing*. Cambridge University Press, 3rd edition, 2007.

[79] William H Press. Long wave trains of gravitational waves from a vibrating black hole. *Astrophysical Journal, vol. 170, p. L105*, 170:L105, 1971.

[80] Juan M.Z. Pretel, Sergio E. Jorás, and Ribamar R.R. Reis. Strongest constraint in $f(R) = R + \alpha R^2$ gravity: stellar stability. *Journal of Cosmology and Astroparticle Physics*, 2020(11):048–048, November 2020.

[81] Alfio Quarteroni, Riccardo Sacco, and Fausto Saleri. *Numerical Mathematics*, volume 37. 01 2007.

[82] Ambrish M Raghoonundun. *Properties of Exact Analytic*. PhD thesis, UNIVERSITY OF CALGARY, 2009.

[83] Tullio Regge and John A. Wheeler. Stability of a schwarzschild singularity. *Physical Review*, 108:1063–1069, Nov 1957.

[84] Christian Reisswig. *Binary black hole mergers and novel approaches to gravitational wave extraction in numerical relativity*. PhD thesis, Hannover: Gottfried Wilhelm Leibniz Universität Hannover, 2010.

[85] Luciano Rezzolla and Olindo Zanotti. *Relativistic hydrodynamics*. Oxford University Press, 2013.

[86] Johannes Ruoff. New approach to the evolution of neutron star oscillations. *Physical Review D*, 63(6), February 2001.

[87] Rainer K Sachs. Gravitational waves in general relativity viii. waves in asymptotically flat space-time. *Proceedings of the Royal Society of London. Series A. Mathematical and Physical Sciences*, 270(1340):103–126, 1962.

[88] Rainer K Sachs. On the characteristic initial value problem in gravitational theory. *Journal of Mathematical Physics*, 3(5):908–914, 1962.

[89] Mark A. Scheel, Michael Boyle, Tony Chu, Lawrence E. Kidder, Keith D. Matthews, and Harald P. Pfeiffer. High-accuracy waveforms for binary black hole inspiral, merger, and ringdown. *Physical Review D*, 79:024003, Jan 2009.

[90] Bernard Schutz. *A First Course in General Relativity*. Cambridge University Press, 3 edition, 2022.

[91] Jing Shi, Changqing Hu, and Chi-Wang Shu. A technique of treating negative weights in weno schemes. *Journal of Computational Physics*, 175(1):108–127, 2002.

[92] Masaru Shibata. *Numerical relativity*, volume 1. World Scientific, 2015.

[93] Chi-Wang Shu. High-order finite difference and finite volume weno schemes and discontinuous galerkin methods for cfd. *International Journal of Computational Fluid Dynamics*, 17(2):107–118, 2003.

[94] Chi-Wang Shu and Stanley Osher. Efficient weighted essentially non-oscillatory schemes for hyperbolic conservation laws. *Journal of Computational Physics*, 83(1):32–78, 1989.

[95] Ulrich Sperhake. Non-linear numerical schemes in general relativity, 2002.

[96] Kalin V. Staykov, Daniela D. Doneva, Stoytcho S. Yazadjiev, and Kostas D. Kokkotas. Gravitational wave asteroseismology of neutron and strange stars in R^2 gravity. *Physical Review D*, 92(4), August 2015.

[97] Josef Stoer, Roland Bulirsch, R Bartels, Walter Gautschi, and Christoph Witzgall. *Introduction to numerical analysis*, volume 1993. Springer, 1980.

[98] Ting-Ting Sun, Zi-Yue Zheng, Huan Chen, G Fiorella Burgio, and Hans-Josef Schulze. Equation of state and radial oscillations of neutron stars. *Physical Review D*, 103(10):103003, 2021.

[99] Marcus Thierfelder, Sebastiano Bernuzzi, and Bernd Brügmann. Numerical relativity simulations of binary neutron stars. *Physical Review D*, 84(4), August 2011.

[100] HM Väth and G Chanmugam. Radial oscillations of neutron stars and strange stars. *Astronomy and Astrophysics (ISSN 0004-6361), vol. 260, no. 1-2, p. 250-254.*, 260:250–254, 1992.

[101] CV Vishveshwara. Scattering of gravitational radiation by a schwarzschild black-hole. *Nature*, 227(5261):936–938, 1970.

[102] Robert M Wald. General relativity. *Press, Chicago, USA*, 10, 1984.

[103] Sam Walters. How Einstein got his field equations. *arXiv preprint arXiv:1608.05752*, 2016.

[104] David Wands. Extended gravity theories and the einstein–hilbert action. *Classical and Quantum Gravity*, 11(1):269, 1994.

[105] Galina Weinstein. Einstein's 1916 derivation of the field equations. *arXiv preprint arXiv:1310.6541*, 2013.

[106] J Winicour. Newtonian gravity on the null cone. *Journal of Mathematical Physics*, 24(5):1193–1198, 1983.

[107] Jeffrey Winicour. Characteristic evolution and matching. *Living Reviews in Relativity*, 12(1):3, 2009.

[108] Jeffrey Winicour. Characteristic evolution and matching. *Living Reviews in Relativity*, 15:1–99, 2012.

[109] Hwei-Jang Yo, Thomas W Baumgarte, and Stuart L Shapiro. Improved numerical stability of stationary black hole evolution calculations. *Physical Review D*, 66(8):084026, 2002.

[110] James W York Jr. Kinematics and dynamics of general relativity. *Sources of gravitational radiation*, pages 83–126, 1979.

[111] Frank J Zerilli. Effective potential for even-parity regge-wheeler gravitational perturbation equations. *Physical Review Letters*, 24(13):737, 1970.

[112] Ying-Tao Zhang and Chi-Wang Shu. Eno and weno schemes. In *Handbook of Numerical Methods for Hyperbolic Problems*, pages 105–120. Elsevier, 2016.